An Analysis of the Alice Arm Crash Program Data - Summer 1981

P. S. Rambold and D. J. Stucchi

Institute of Ocean Sciences
Department of Fisheries and Oceans
Sidney, B.C. V8L 4B2

1983

Canadian Technical Report of Hydrography and Ocean Sciences No. 25

Canada

Canadian Technical Report of Hydrography and Ocean Sciences

These reports contain scientific and technical information of a type that represents a contribution to existing knowledge but which is not normally found in the primary literature. The subject matter is generally related to programs and interests of the Ocean Science and Surveys (OSS) sector of the Department of Fisheries and Oceans.

Technical Reports may be cited as full publications. The correct citation appears above the abstract of each report. Each report will be abstracted in Aquatic Sciences and Fisheries Abstracts. Reports are also listed in the Department's annual index to scientific and technical publications.

Technical Reports are produced regionally but are numbered and indexed nationally. Requests for individual reports will be fulfilled by the issuing establishment listed on the front cover and title page. Out of stock reports will be supplied for a fee by commercial agents.

Regional and headquarters establishments of Ocean Science and Surveys ceased publication of their various report series as of December 1981. A complete listing of these publications and the last number issued under each title are published in the *Canadian Journal of Fisheries and Aquatic Sciences*, Volume 38: Index to Publications 1981. The current series began with Report Number 1 in January 1982.

Rapport technique canadien sur l'hydrographie et les sciences océaniques

Ces rapports contiennent des renseignements scientifiques et techniques qui constituent une contribution aux connaissances actuelles mais que l'on ne trouve pas normalement dans les revues scientifiques. Le sujet est généralement rattaché aux programmes et intérêts du service des Sciences et Levés océaniques (SLO) du ministère des Pêches et des Océans.

Les rapports techniques peuvent être considérés comme des publications à part entière. Le titre exact figure au-dessus du résumé du chaque rapport. Les résumés des rapports seront publiés dans la revue Résumés des sciences aquatiques et halieutiques et les titres figureront dans l'index annuel des publications scientifiques et techniques du Ministère.

Les rapports techniques sont produits à l'échelon régional mais sont numérotés et placés dans l'index à l'échelon national. Les demandes de rapports seront satisfaites par l'établissement auteur dont le nom figure sur la couverture et la page de titre. Les rapports épuisés seront fournis contre rétribution par des agents commerciaux.

Les établissements des Sciences et Levés océaniques dans les régions et à l'administration centrale ont cessé de publier leurs diverses séries de rapports depuis décembre 1981. Vous trouverez dans l'index des publications du volume 38 du *Journal canadien des sciences halieutiques et aquatiques*, la liste de ces publications ainsi que le dernier numéro paru dans chaque catégorie. La nouvelle série a commencé avec la publication du Rapport n° 1 en janvier 1982.

Canadian Technical Report of Hydrography and Ocean Sciences No. 25

1983

AN ANALYSIS OF THE ALICE ARM CRASH PROGRAM DATA - SUMMER 1981

by

P.S. Rambold and D.J. Stucchi

Institute of Ocean Sciences
Department of Fisheries and Oceans
Sidney, B.C. V8L 4B2

Copyright Minister of Supply and Services Canada - 1983

Cat. No. FS 97-18/25 ISSN 0711-6764

Correct citation for this publication:

Rambold, P.S. and D.J. Stucchi. 1983. An analysis of the Alice Arm crash program data - Summer 1981.
Can. Tech. Rep. Hydrogr. Ocean Sci: 25: 66p.

TABLE OF CONTENTS

	Page
ABSTRACT	iv
ACKNOWLEDGEMENTS	v
INTRODUCTION	1
THE CRASH PROGRAM DATA	1
ANALYSIS OF THE VARIATIONS IN THE FJORD'S MASS FIELD	4
Fresh Water Input	4
Wind Effects	6
Tides	7
Outside Forcing	10
MODEL OF ESTUARINE FLOW	12
CONCLUSIONS AND RECOMMENDATIONS	14
REFERENCES	16
FIGURES	17
TABLES	28
APPENDIX A: Calculation of two layer representation	32
APPENDIX B: Plots of two layer representation.	33
APPENDIX C: Twenty five hour time series plots of FWC from September 1982.	52
APPENDIX D: Cross spectra between Q19 and N08, Q19 and 013, and 013 and N08.	55
APPENDIX E: Temperature-salinity diagrams from Q19.	58

ABSTRACT

Rambold, P.S. and D.J. Stucchi. An analysis of the Alice Arm crash program data - Summer 1981. Can. Tech. Rep. Hydrogr. Ocean Sci. 25: 66p.

From June 23 to September 12, 1981, more than eleven hundred vertical profiles of temperature, salinity and light transmission were taken in Alice Arm, B.C. This large data set - the crash program - was analyzed to determine what local or external forces were affecting the stratification and circulation in this fjord. The crash program data suffers from two major limitations, an instrument related problem and the aliasing of the tidal signals. Local run-off and winds do not appear to influence the fjord significantly except for one extreme run-off event which noticeably altered the fjord's stratification. Tidal mixing is significant, as a fortnightly signal was detected in the data and the changes in stratification were consistent with increased vertical mixing after spring tides. An intermediate water renewal was observed to occur in Alice Arm just after deep water renewal began in Observatory Inlet. The majority of the variance in the fjord's mass field is unexplained because of the limitations in the data and possibly because Alice Arm is forced from outside - Observatory Inlet - where observations were lacking. An existing model of fjord circulation was tested on Alice Arm but it was found to be unsuitable.

Key words: fjord circulation, tidal mixing, water exchange, Alice Arm, B.C.

RÉSUMÉ

Rambold, P.S. and D.J. Stucchi. An analysis of the Alice Arm crash program data - Summer 1981. Can. Tech. Rep. Hydrogr. Ocean Sci. 25: 66p.

Entre le 23 juin et le 12 septembre 1982, plus de onze cents profils verticaux de température, de salinité et de transmission de lumière ont été obtenus dans le bras Alice (C.-B.). On a analysé cet ensemble imposant de données - dans le cadre du programme intensif - pour déterminer quelles forces locales ou extérieures influent sur la stratification et la circulation dans ce fjord. Deux limites importantes affectent les données du programme intensif, soit un problème lié aux instruments et le repliement des signaux de marée. L'écoulement et les vents au niveau local ne semblent pas avoir une grande influence sur le fjord à l'exception d'un écoulement extrême qui a modifié de façon sensible la stratification du fjord. Le mélange des marées est important puisqu'un signal bimensuel a été décelé dans les donnés et les changements dans la stratification coïncidaient avec l'accroissement du brassage vertical après les marées du printemps. Un renouvellement des eaux intermédiaires a été observé dans le bras Alice juste après que le renouvellement des eaux profondes ait commencé dans l'inlet Observatory. Le majeure partie de la variance dans le champ de masse du fjord n'est pas expliquée en raison des limitations dans les données et peut-être parce que le bras Alice subit des contraintes de l'extérieur - l'inlet Observatory - où les observations font défaut. Un modèle illustrant la circulation dans les fjords a été verifié dans le bras Alice, mais celiu-ci s'est révélé inadéquat.

Mot cles: circulation dans ce fjord, mélange des marées, éxchange d'eau, le bras Alice, C.-B.

ACKNOWLEDGEMENTS

We thank Amax of Canada Ltd., and Dobrocky Seatech, Ltd. for providing us with tidal height and anemometer measurements from Alice Arm.

INTRODUCTION

Alice Arm, a fjord on the northern British Columbia coast (see Figure 1) became the centre of considerable controversy in 1981, subsequent to the Kitsault Mine being granted a permit to discharge mine tailings into the fjord at depth. The federal government instituted a monitoring program - the crash program - to be undertaken by the Institute of Ocean Sciences (IOS), Department of Fisheries and Oceans. The data set resulting from the crash program is somewhat unique in the study of fjord oceanography to date, as it represents a continuous daily sampled time series of vertical water properties over a period of several months. The main objective of this study is to examine the relationship between the changes in the fjord's mass field and the factors that are responsible for these changes.

Alice Arm is a small (16 km), narrow (1.4 km), deep (385m) fjord which connects with Observatory Inlet and Hastings Arm over a complex sill region (Figure 2). The sill region is approximately 5 km long, ranging in depth from 25 to 115m with an average depth of about 70m. The sill region is constricted at its northern end near Alice Rock (42m) and further south at Liddle Channel (25m) and Davies Passage. The sill region connects directly with both Hastings Arm and Observatory Inlet with a 55m sill separating Observatory Inlet from Hastings Arm and a 60m sill dividing Observatory Inlet from Portland Inlet (Figure 2). Communication to more oceanic waters is via Observatory and Portland Inlets to Chatham Sound and eventually Dixon Entrance (Figure 1).

The analysis of the crash program data set is divided into three parts. The first will describe the crash program data set, how it was parameterized and its limitations. The next part will deal with the relationships between the fjord's mass field and local run-off, winds, tides and outside forcing. In the third part an existing model of fjord circulation will be examined for its relevancy to a fjord like Alice Arm. The report will conclude with summary of results and recommendations.

THE CRASH PROGRAM DATA

In June, 1981, at the request of the Minister of the Department of Fisheries and Oceans, scientists from IOS began a three month long sampling program of water characteristics in Alice Arm. During the course of the survey in excess of 1100 conductivity, temperature, salinity and light transmission profiles were obtained. As the object of the survey was the delineation and monitoring of the suspended tailings plume the majority of the profiles were taken near the tailings outfall at the head of the fjord. Shown in Figure 3 is the station location grid used. Stations are identified

by a notation consisting of a letter and a number, starting with the letter A to the north and the number 1 to the east. Listed in Table 1 are the days on which profiles were obtained at each station. It is evident from Table 1 that several stations were sampled more frequently than others; these are N08, M09, N14, O13, P12 and Q19 all within a few kilometres of the tailing discharge point (Figure 3). The subsequent analysis will involve these six stations as they received the best coverage.

A Guildline Instruments digital CTD (conductivity, temperature and depth) together with a Seatech Transmissometer were used to measure vertical profiles of temperature, salinity and light transmission. These measurements were obtained from the contract vessel Bastion City. Details of the processing of these data, a comprehensive index and guides for the access programs are given by Nicoll and Stucchi (1982).

This report is primarily concerned with the variation of 2 days or longer in the upper part (0 to 100m) of the water column. There are numerous shorter term variations which will not be resolvable in this data set, such as: diurnal wind effects, internal waves and seiches. The mass field of the fjord is represented by a two layer system and its associated properties. The two layer representation of the observed density profile is determined using the objective method of Freeland and Farmer (1980). The method consists of using the density profile to compute the first internal wave speed and the potential energy of the profile and then constructing a two layer representation that conserves both of the above properties. The details of this procedure are left to Appendix A. The relevant parameters describing the two layer system are upper layer sigma-t, upper layer thickness, potential energy and the first internal mode wave speed. In addition the fresh water content (FWC) of the top 50m of the water column is calculated from the actual observed profile as follows

$$FWC = \int_0^{50} \left(1 - \frac{S(z)}{S_{ref}}\right) dz$$

where S_{ref} is the salinity at some reference depth and S(z) is the salinity profile. This is equivalent to partitioning the top 50m into two layers, the bottom layer of salinity S_{ref}, and the top layer of fresh water. The FWC is essentially the thickness of this top fresh water layer. The results of the two layer representation and FWC calculations are plotted in Appendix B, Figures B1 to B18. Before we begin with the analysis of these results it is important to comment upon two problems with this data set. The first is an instrumental problem and the second, more serious one, is that of aliasing the tidal signals.

The inaccuracies in the data due to limitations in the Guildline CTD are primarily caused by the unpredictable and coarse response of the pressure sensor in the top few metres of the water column. As a result, the vertical profiles of salinity, temperature and light transmission are not reliable in the top 4 metres of the water column. A clear sign of this problem is that the recorded starting depths of the profiles are erratic and often 2 or 3 metres below the surface although the instrument was invariably at the surface when the profile commenced. This instrumental problem obviously introduces an error into the FWC calculation since the vertical gradient in salinity is largest in the top few metres and the contribution to FWC appreciable. If it is assumed that the error is no larger than the contribution to FWC from the top 4 metres of the water column, then at most the FWC values are in error by 20 to 30%. In fact, the error is probably considerably less because the contribution from the top few metres of the profile is not excluded.

A second, more serious difficulty in the crash program data is the potential aliasing problem. Because the samples were taken at a rate of about one sample per day there is a certain danger that higher frequency signals (primarily tides) are being aliased into the data. Tides and diurnal winds which affect the fjord at frequencies greater than 0.5 cycles/day will be aliased into the measured signal at lower frequencies.

Some idea of the amplitude of the tidal signal can be gained by examining two 25 hour time series taken on September 1st and 2nd, 1982, (one year later). One time series was obtained at the head of the fjord near station F06 and the other was obtained near the sill near station W65. Time series obtained during the crash program were not used because they were at most only 6 hours in length. Figures C1 and C2 in Appendix C show the variation in FWC at stations F06 and W65 over a 25 hour period. The variation in FWC near the head (F06) is of order $3m^3$, comparable to variations which occur in the daily sampled series for the three month period (Figures B3, B6, B9, B12, B15 and B18). The FWC variation near the sill is somewhat smaller. Thus it would appear to be difficult to establish whether any long period variation which exists in the three month series is real or is simply an artifact of the shorter period variations.

An indication of the degree to which the time series have been contaminated by aliasing may be obtained from the coherence between the different stations for the parameters characterizing the fjord's mass field, i.e. FWC, upper layer density and thickness, etc. Given that the calculated phase speed of the first mode internal wave is in the range 0.8 to 1.4m s^{-1}, the time for a signal to propagate between the most distant of the frequently

sampled stations (i.e. 2.1 km separation between Q19 and NO8) varies from 25 to 44 minutes. The time scales of the forcing of the fjord are much longer, ranging from 12 hours to many days. Thus, variations in the fjord's mass field are expected to be coherent and in phase over a distance of 2 km. The loss of coherence in the measured signal between stations could imply that the aliased tidal signal was significantly contaminating the time series. However, it could be argued that because the stations were sampled close together in time (within a few hours) then the aliasing of the tidal signal would be systematic. This argument is plausible for the closely spaced stations, but not for the most distant stations, where sampling occurred at significantly different times. Cross spectra were computed for FWC, upper layer depth, upper layer density and first mode phase speed between the most distant stations (Q19 and NO8) and between two pairs of stations about 1 km apart (Q19 and O13, O13 and NO8). The results which are plotted in Appendix D, Figures D1 and D2, reveal that for the stations furthest apart (Q19 and NO8) coherence squared (hereafter coherence) is significant (at 95% level) only for upper layer density, and then only at frequencies below 0.133 cycles/day. The phases of the significant coherence estimates are close to zero. Most of the variance in the parameters is located at frequencies lower than 0.167 cycles/day. Between stations Q19 and O13, significant coherence is generally found for all parameters at frequencies lower than 0.167 cycles/day, with the associated phase close to zero. A more complicated relationship is indicated between O13 and NO8. Upper layer density is coherent with zero phase across most of the spectrum yet upper layer depth shows little significant coherence. FWC and phase speed show significant coherence at the high frequency end and in the middle of the spectrum. The results of this exercise are ambiguous. The significant coherence for upper layer density between the most distant stations suggests that aliasing has not completely destroyed the measured time series. Yet the lack of coherence for the other parameters indicates aliasing is severe. Despite the difficulties mentioned above we will continue with the analysis.

ANALYSIS OF THE VARIATIONS IN THE FJORD'S MASS FIELD

Fresh Water Input

A major component of the circulation in the fjord is that driven by run-off, i.e. estuarine circulation. The input of fresh water, usually at the head, forms a thin brackish layer which moves seaward driven by pressure gradient produced by the inflow. As the surface layer moves seaward, it is mixed with and entrains seawater from below. There are a number of theories or models of estuarine flow (see review by Farmer and Freeland, 1983) which describe the thickness, salinity and development of the surface brackish layer. A number of conditions and factors control the brackish layer, of

which run-off is one. Thus it is not unreasonable to expect that there be some relationship between the variation in the character of the brackish layer (as represented by FWC, upper layer depth or upper layer density) and the local run-off.

A number of rivers flow into Alice Arm, most of which enter the fjord at or near the head. The largest of these rivers is the Kitsault, which drains a land area of 454 km^2, 57% of the total drainage for Alice Arm (793 km^2). Other important inflows are: the Illiance River (131 km^2), Lime Creek (40 km^2) and Roundy Creek (21 km^2). A total of 83% of the drainage into Alice Arm occurs within 4 km of the head of the fjord. The Kitsault River was gauged 1981 by the Water Resources Branch, of the Water Survey of Canada. For the purpose of this study, it will be assumed that the total drainage into Alice Arm is twice that of the Kitsault River, and that all fresh water enters at the head of the fjord.

The run-off to Alice Arm is characterized by a large, broad peak from late May to the end of June due to snow melt and in the fall there are large, short-lived run-off events associated with storms. Run-off reaches a minimum in late winter because most of the precipitation is retained in the watershed in the form of snow and ice. The daily run-off for the Kitsault River (Amax, 1981) coincident with the crash program data is shown in Figure 4. The period covered is from late June to early September, i.e. after the snow melt peak, to the beginning of the fall rain storms. The run-off data is dominated by the intense ($200m^3\ s^{-1}$), but short-lived run-off peak from September 8 to 11. Otherwise the run-off values average about $30m^3\ s^{-1}$ with several minor events apparent in the data.

A comparison of the run-off data (Figure 4) with the FWC, upper layer sigma-t, upper layer depth, and phase speed, on the whole, reveals no correlation, except for an apparent surface layer response to the large run-off event of September 8 to 11. From September 10 to 11 the FWC increases sharply from about 4 to $9m^3$, Figures B3, B6, B12 and B15. Upper layer sigma-t decreases suddenly and the upper layer depth increases at the same time (Figures B1, B4, B7, B10 and B13). The phase speed of the first mode internal wave also increases sharply to approximately $1.2m\ s^{-1}$. (Figures B2, B5, B11 and B14.)

The generally poor correlation may be explained in two ways: 1) the FWC time series (also upper layer depth and upper layer sigma-t time series) are not accurate representations of these quantities because of the inherent instrumental and aliasing problems discussed earlier, and/or, 2) local run-off - during the survey period - may be of lesser importance than other processes (i.e. tides, winds, exchange with Observatory Inlet), in

determining the stratification of the upper layers. A comparison of the fresh water input to the tidal prism (surface area of fjord times the tidal range) gives an indication of the relative importance of these driving forces. Table 2 lists the ratio of local freshwater input to the tidal prism at various times for Alice Arm and for several Alaskan fjords. The September run-off event which was observed to influence the fjord was about 8% of tidal prism, while the events of July and August which had no observed impact on the FWC were about 3 times smaller at 2.7% of the tidal prism. Similarly, low ratios (~2%) are observed in Endicott Arm and Boca de Quadra where local run-off is reported to have little influence on the circulation (Nebert and Burrell, 1982).

It is difficult to determine the extent to which these factors account for the generally poor correlation between the variation in the fjord's mass field and local run-off. However, despite the instrument and sampling problems the fjord responded to the large run-off event in September. Unfortunately, this is a rather isolated event occurring at the very end of the data set so it is not possible to make any generalizations as to the circulation patterns in Alice Arm during high run-off. It can be expected however that during these periods of high run-off the contribution to the circulation by the fresh water input is significant and may well become the primary driving force of the upper layer circulation.

Wind Effects

Local winds may influence the upper layers of a fjord in several ways. One way is by imparting energy to the surface layers causing vertical mixing to occur. Stigebrandt (1981) developed a model (to be discussed in more detail in the next section) for the effects of wind mixing on the thickness of the upper layer. Under certain conditions the model predicts that the upper layer depth is proportional to the wind speed cubed. Another way in which the wind affects the upper layer was described and modeled by Farmer and Osborn (1976) for Alberni Inlet. It was found that the upper layer near the head of Alberni Inlet, in response to strong up-inlet winds, underwent a rapid deepening followed by a slow relaxation over several days. The inlet responded in a manner analogous to a heavily damped harmonic oscillator.

The wind data from Alice Arm were obtained near sea level at the tailings outfall mixing chamber, about 2.5 km from the head of the fjord (see Figure 3). The wind speed and direction for July and August are plotted in Figure 5. These data indicate that the summer winds are primarily diurnal in character, with the strongest (~ 6m s^{-1}) winds directed up-inlet during the day (sea breeze) and weaker, more variable down-inlet winds occurring at night. There are three events (July 18-21, July 25-27 and July 29-31) during

which up-inlet winds persist for several days. Overall winds are directed up-inlet and speeds seldom exceed 7m s^{-1}. Because the anemometer is located at the side of the inlet, the wind data collected may not accurately represent the winds found at mid-channel. Winds measured at the side of the inlet are probably lower and more turbulent than those at mid-channel.

A comparison of upper layer depth (see Figures B1, B4, B7, B10, B13 and B16) with wind speed cubed (Figure 6) shows no correlation between these two variables. Also strong up-inlet winds do not appear to produce the rapid deepening of the upper layer and its subsequent slower relaxation. The largest wind event of the summer which occurs from July 18 to 21, appears to have no effect on the depth of the upper layer. In short, the local winds do not appear to have any discernable effect on the FWC, upper layer depth or upper layer density. The reasons for this apparent lack of wind effect may be 1) instrument and aliasing problems are obscuring the actual wind response of the fjord, or 2) the local winds in Alice Arm during the summer are not strong enough to produce significant responses in the upper layers of the fjord. As mentioned earlier, measured wind speeds rarely exceed 7m s^{-1} and peak dirunal wind speeds fall in the range 3 to 6m s^{-1}. These are by most standards, weak winds. For example, the wind events in Alberni Inlet that had noticeable effects on the pycnocline were typically 10 to 15m s^{-1}, more than twice as large as those observed in Alice Arm. In summary, wind effects in Alice Arm during the summer were probably slight and produced no obviously correlated signal in the density field.

Tides

The input of energy from the tides to the vertical mixing processes will of course affect the stratification and circulation of the upper layers of the fjord. The energy from the tides is extracted by three mechanisms, 1) boundary friction, 2) generation of internal waves and other internal disturbances, and 3) tidal jets. The barotropic tidal currents are in general small in Alice Arm, however significant currents are expected in the sill region particularly at Alice Rock and Liddle Channel. The sectionally averaged barotropic tidal current U_T defined as

$$U_T = \frac{A}{Am} \frac{d\zeta}{dt}$$

where A is the surface area of the fjord, Am is the cross-sectional area at the sill, and ζ is the tidal elevation. The sectionally averaged tidal currents, U_T at these constrictions attain maxima of 1.1m s^{-1} at Liddle Channel 0.6m s^{-1} at Alice Rock. The sill region is geometrically complex,

ranging in depth from 25 to 115m with a number of constrictions and sills as mentioned above. Its overall length, which is about 5 km, is comparable to the tidal excursion there. Stratified water entering the sill region will be mixed vertically to varying degrees and it will also mix with remnant water in the sill region from the preceding tide. On the flood tide the resultant mixture will enter Alice Arm and contribute to the stratification of the upper layers. The degree of mixing in the sill region will depend upon the competition between the flux of buoyancy to the sill region and the production of turbulence by boundary friction in the sill region. The latter will vary appreciably because of the neap-spring cycle in the tidal flow.

Internal waves may be generated at the sill or over the sloping bottom at the head of a fjord. Stigebrandt (1980) suggested that internal waves of tidal frequency can be generated by flow over a sill if the densimetric Froude number, F_d, is less than critical, i.e. $F_d < 1$. The densimetric Froude number is defined as the ratio of the maximum sectionally averaged tidal current, U_T, over the sill, to the phase speed, C_i, of an internal wave. During the summer, Alice Arm stratification is such that F_d is generally less than critical, thus internal wave generation is possible according to Stigebrandt (1980). In Stigebrandt's model the flux of energy from the barotropic tide to the internal tide is proportional to the amplitude squared of the surface tide. Blackford (1978) in his model demonstrated that not only is the amplitude of internal waves generated at the tidal frequency directly proportional to the tidal flow, U_T, across the sill, but also that internal waves at twice the forcing frequency would be generated with their amplitude proportional to U_T^2. In both the above mentioned models of internal wave generation the amount of energy in the internal waves is dependent upon the amplitude of the surface tide. Some of this energy will eventually be made available for mixing. However, even though the details of this conversion are not clearly understood, the flow of energy from the barotropic tide to the internal waves to mixing and dissipation is expected to vary with the neap-spring cycle in the surface tides.

The mixing associated with a turbulent jet on the lee side of a sill could be significant to the stratification in the upper layers. However, Stigebrandt (1980) indicates a jet will be formed only when F_d is supercritical, and for Alice Arm during the summer months F_d is generally less than one.

Within Alice Arm, tides act as standing waves, so that all parts of the fjord experience the same tidal signal at any given time. Tides in Alice Arm are of mixed type, mainly semi-diurnal. The three largest amplitude constituents are M_2 at 2.0m, S_2 at 0.7m, and K_1 at 0.5m. The neap-spring

variation in the tidal flow across the sill is represented by the root mean square of the sectionally averaged tidal current through Liddle Channel and Davies Passage calculated as follows

$$U_{Trms} = \frac{A}{Am}\left[\frac{1}{T}\int_{o}^{T}\left(\frac{d\zeta}{dt}\right)^2 dt\right]^{\frac{1}{2}}$$

where T is the averaging period, chosen to be 24 hours for this calculation. The tidal height data, used in the computation was collected by Amax of Canada Ltd. with a bottom mounted pressure gauge adjacent to the tailings outfall mixing chamber. The area of the fjord, A, is $2.2 \times 10^7 m^2$ and the cross-sectional area, Am, at Liddle Channel and Davies Passage at mean sea level is $1.23 \times 10^4 m^2$. The neap-spring variation in U_{Trms} is plotted in Figure 7.

The parameters that describe the character of the upper layers such as FWC, upper layer depth, upper layer sigma-t, potential energy, etc., were examined for fortnightly variations. Visual inspection established the existence of significant correlation between upper layer density at Q19 (Figure B1) and the neap-spring variation in the tides (Figure 7). A cross-spectral analysis between the fortnightly tidal signal (Figure 7) and those characteristics of the surface waters of the fjord mentioned earlier was undertaken at all stations. The results of the analysis which are shown in Table 3 reveal that at the fortnightly frequency upper layer sigma-t was significantly coherent (at 95% level) with the fortnightly tidal signal, at all stations. The upper layer sigma-t lagged the fortnightly signal by about 90^o or 3.7 days. The upper layer depth at 4 out of the 6 stations was also coherent with the fortnightly tidal variation, and the phasing was the same as for the upper layer density. None of the other characteristics was coherent with the fortnightly variation. The analysis reveals that the upper layer thickens and increases in density about 3 to 4 days after spring tides. This response is consistent with increased mixing between the upper and lower layers. However, it is not possible with these data to determine what mechanism is responsible for the mixing and where the mixing is occurring. The large phase lag of 3 to 4 days is curious, in that tidal mixing in the sill region and also the mixing resulting from the dissipation of energy contained in the internal wave field are both expected to be largest at the time of spring tides.

Two hypotheses are advanced to explain the large phase lag. The first is that the increased density and thickness of the upper layer results from the intrusion of a mixed water mass into Alice Arm. This mixed water mass is created by the intense mixing at the Observatory Inlet sill and subsequently

spreads (20 cm s^{-1}) up Observatory Inlet and into Alice Arm. The second hypothesis for the phase lag is that the effects of mixing (by whatever agent) on stratification are cumulative. Vertical mixing is most effective at peak tides, but once some mixing has taken place, subsequent mixing is facilitated because of the reduced stratification. As the amplitude of the tide decreases a balance point is reached between the stabilizing flux of buoyancy and the production of turbulence. At this point the cumulative effects of mixing attain a maximum (maximum upper layer sigma-t and maximum upper layer depth). An evaluation of these two hypotheses will await the analysis of moored instrument data from outside the fjord (i.e. Observatory Inlet) and in the Alice Arm sill region.

Outside Forcing

The stratification in Alice Arm may also be affected by the intrusion of waters from Observatory Inlet. The circulation of a fjord may be dominated by outside forcing as was shown to be the case in Alberni Inlet during the winter months (Stucchi, 1983). The wind induced fluctuations in the density field on the adjacent continental shelf forced Alberni Inlet to continually adjust to the changing conditions at its mouth. Similarly, the changing surface density field of Observatory Inlet may influence the stratification and circulation in Alice Arm.

The major source of fresh water to the region is the Nass River (~30 times the discharge of the Kitsault River) which enters at the junction of Observatory and Portland Inlets, about 50 km from Alice Arm (Figure 2). Only 5 km north of the mouth of the Nass River there is a major sill in Observatory Inlet. The tidal flow over the Observatory Inlet sill is known to be energetic and capable of producing internal waves, hydraulic jumps and other internal disturbances (Farmer and Freeland, 1983). The interaction between the large source of fresh water and the energetic tidal flow over the Observatory Inlet sill is anticipated to produce significant fluctuations in the density field that may well extend into Alice Arm. Deep water renewal and wind forcing may also produce changes in the density field in Observatory Inlet. Unfortunately, in the crash program data set, relatively few observations were obtained outside Alice Arm, consequently fluctuations in the outside conditions are poorly resolved. However longer term changes such as those brought about by deep water renewal were resolved.

During July and August deep water renewal occurred in Observatory Inlet as density was observed to increase over all but the top 20m of the water column(Figure 8). In Alice Arm starting about mid-July and continuing to the last week in August, the contours of sigma-t in the range 23.3 to 23.7 diverge (see Figure 9) suggesting that an inflow of water between 50 and 120m

occurred - an intermediate water renewal. On a temperature-salinity (TS) diagram (Figure 10) showing water properties from stations inside (station Q19) and outside (station XX) Alice Arm, on August 10, the near surface water (0 to 30m) of Observatory Inlet is clearly seen to be denser than most of the waters in Alice Arm. It is also evident from Figure 10 that Observatory Inlet waters are significantly warmer (0.5 to 1°C) than those of Alice Arm - a condition which appears to be true for the entire survey period.

The denser Observatory Inlet water in its passage through the Alice Arm sill region will be modified by mixing to varying degrees before it enters Alice Arm. Because the waters of Observatory Inlet are warmer than those of Alice Arm (Figure 10), intrusions of these warmer waters should be apparent as layers of higher temperature. Shown in Appendix E (Figures E1 to E8) is a series of TS diagrams approximately 10 days apart from a well sampled station (Q19) which clearly shows layers of higher temperatures. These higher temperature layers are present throughout Alice Arm with the thickest and warmest layers observed near the sill. Further down the fjord toward the head the layers decrease in thickness and temperature difference as they spread and mix with the resident waters. Furthermore, these higher temperature layers are observed over the entire survey period, though they are most intense during the intermediate water renewal period.

The effect that intermediate water renewal has on FWC is described in the following simple model. On the flood tide dense water from outside is drawn into Alice Arm undergoing some mixing in its transit over the sill region. Upon entering the fjord the modified Observatory Inlet water descends to a depth of corresponding density and spreads out along that density surface. On the ebb tide, the less dense surface (above sill level) waters are preferentially removed. The general circulation pattern is shown in Figure 11. The net effect is that the FWC of the fjord will decrease as the upper layers are removed to accommodate the influx below sill level. In a general sense the observation of FWC and upper layer density are consistent with the model. FWC values show a trend to decreasing values at about the same time as intermediate water renewal commences. Also, FWC values are generally lower during the renewal period (Figures B3, B6, B9, B12, B15 and B18). Upper layer density values increase in general during the renewal period (Figures B1, B4, B7, B10, B13 and B16). An accurate time history of the volumes of the influx to the intermediate layers cannot be obtained from the data, consequently it is not possible to examine the correlation between the variations in FWC or upper layer density and the intensity of the intermediate water renewal.

MODEL OF ESTUARINE FLOW

There have been a number of models developed to describe the nature of estuarine flow such as those of Rattray (1967), Long (1975) and Stigebrandt (1981). Because of its simplicity, the model of Stigebrandt (1981) will be briefly described and tested for its suitability to Alice Arm.

Stigebrandt identifies two types of fjord based on the condition of hydraulic control at the mouth. In a normal N fjord the upper layer thickness is small compared to the depth of the sill, a situation that occurs when local run-off is small and the sill deep. In an overmixed O fjord the upper layer thickness is a significant fraction of the total sill depth, a condition that occurs in shallow silled fjords and those with substantial mixing. The model which Stigebrandt (1981) developed applies to N fjords only.

The model is layered, assumes steady state and does not include tidal, frictional or rotational effects. It is based upon hydraulic control at the mouth of the fjord, i.e. the upper layer velocity equals the speed of the interfacial wave. The critical condition is defined in terms of the densimetric Froude number

$$F_d = \frac{u_1^2}{g' h_1} = 1$$

where u_1, h_1 refer to the upper layer velocity and depth, and $g' = g(\rho_2 - \rho_1)/\rho_2$ is the reduced gravity with ρ_1 and ρ_2 the densities of the upper and lower layers. Mixing is introduced through a mixing parameter

$$P = \frac{S_2}{S_2 - S_1}$$

where S_1 and S_2 are the salinities of the upper and lower layers. Using the conservation of volume and salinity an expression for the depth of the upper layer at the mouth of the fjord is derived. Additionally, Stigebrandt incorporates the effect of wind mixing within the fjord and derives the contribution to the upper layer thickness. The expression for the upper layer depth is

$$h_1 = \frac{\gamma W^3 A}{Q_F g \beta S_2} + \phi \left(\frac{Q_F^2}{g \beta S_2 B_m^2} \right)^{1/3}$$

where Q_F is the fresh water inflow, W is the wind velocity, A is the surface area of the fjord, B_m the fjord width at the mouth, β a constant relating salinity to density, γ and ϕ constants. The first term in the above expression is the contribution to the upper layer thickness from wind mixing in the fjord. The second term is the contribution from the hydraulic control of flow at the mouth. As the fresh water input to the fjord increases wind mixing effects are reduced, and the wind's contribution to the layer depth reduced while the components due to hydraulic control at the mouth increase. The classification of Alice Arm as an N or O fjord using Figure 2 in Stigebrandt (1981) gives ambiguous results. If the mixing parameter, P, is used to locate the fjord on the line of constant estuarine Froude number, F_e, then the observations indicate that Alice Arm is clearly an N fjord. However, using the relative depth

$$\eta = \frac{h_2}{h_2 + h_1}$$

of the lower layer in the constriction together with the lines of constant F_e indicate that Alice Arm is an O fjord.

A fundamental assumption of the model is that of hydraulic control at the mouth, i.e. $F_d = 1$. In the presence of strong tidal flow over the sill the assumption may not hold as the flow will be primarily barotropic. The upper layer velocity at the mouth (from equation (6) in Stigebrandt (1981)) of the fjord is given by

$$U_{1m} = \left(\frac{Q_F g \beta S_2}{B_m} \right)^{1/3} .$$

The flow through the mouth will be barotropic when $U_T > U_{1m}$. Using the following values for the fjord parameters

$B_m = 900m$ (Liddle Channel - Davies Passage)

$\beta = 8 \times 10^{-4}$ $(^o/oo)^{-1}$

$S_2 = 30$ $(^o/oo)$

the calculated upper layer velocities for normal and peak run-off conditions Q_F = 80 and 400m^3 s^{-1} are 0.28 and 0.47m s^{-1} respectively. The maxima of the sectionally averaged tidal velocities for large and average tides are 1.1 and 0.8m s^{-1} respectively. Flow through the mouth will be barotropic most of the time except near slack water. The assumption of hydraulic control at the mouth is not possible most of the time. Thus the model does not appear to be applicable as the fundamental condition of hydraulic control is not satisfied and, in addition, it is not clear that Alice Arm is an N fjord.

Stigebrandt (1977) showed that the two layer transport capacity of a constriction can be increased by the fluctuating barotropic currents. For the situation in which hydraulic control exists (i.e. $U_{1m} > U_T$) the time mean transport, $\bar{q}_1$, through the constriction for the upper layer is

$$\bar{q}_1 = \frac{1}{4} B_m H_m (g' H_m)^{\frac{1}{2}}$$

However when $U_T > U_{1m}$, Stigebrandt (1977) showed the

$$\bar{q}_1 = \frac{1}{4} B_m H_m (g' H_m)^{\frac{1}{2}} \left[\frac{2}{\pi}\theta_1 + \frac{2}{\pi} F \cos \theta_1\right]$$

where $F = U_T/U_{1m}$ and θ_1 = arc $\sin(F^{-1})$, and the transport capacity increases. For average tides, and average run-off and maximum run-off conditions the transport capacity is 1.93 and 1.28 times the transport capacity of the constriction when hydraulic control is present. The assumptions made by Stigebrandt (1977) in his two layer model of the transport capacity of the constriction are not completely satisfied in Alice Arm, specifically the condition that the length of the sill region is short compared to the tidal excursion. Because the length of the sill region is comparable to the tidal excursion, recirculation of water between Alice Arm and Observatory Inlet is expected to be significant and the calculated transport capacity of the constriction will be reduced.

CONCLUSIONS AND RECOMMENDATIONS

The crash program data set, although unique in a way, was not designed for the type of analysis undertaken in this report, because it suffers from two major limitations: 1) the inherent limitation of the CTD which made accurate measurements in the top five metres of the water column difficult, and 2) the aliasing of the tidal signal. The crash program was a monitoring

study designed specifically to monitor the suspended tailings plume near the outfall. Nevertheless, investigation of the relationships between the fluctuations in the fjord's mass field and its forcing has revealed the following results, subject to the limitations of the data:

1. Local run-off during the survey period does not appear to significantly influence the upper layers of the fjord except during extreme run-off conditions. Run-off during the survey period was generally low.

2. Local winds, which are relatively weak during the summer, do not appear to cause significant mixing or distortion of the upper layers.

3. A significant fortnightly variation was observed in both upper layer density and pycnocline depth. The increased upper layer density and thickness after periods of spring tides is consistent with increased vertical mixing at these times. It is not clear whether the tidal mixing is occurring over the Alice Arm sill or further out in Observatory Inlet.

4. After deep water renewal began in Observatory Inlet an intermediate water renewal occurred in Alice Arm. During the period of intermediate water renewal, mid-July to late August, FWC in the fjord generally decreased, consistent with the intermediate water renewal circulation. In large part the variance of the fjord's mass field is unexplained. This may be due to the problems in the crash program data and/or it may be that Alice Arm is forced primarily from outside (Observatory Inlet) where observations were absent.

5. The estuarine circulation model of Stigebrandt (1981) is not applicable to Alice Arm primarily because of the assumption of hydraulic control at the mouth.

Despite the limitations in the data, useful information was obtained from the analysis and valuable lessons learned. In future, long time series observations of the vertical structure of the fjord are best collected with moored instrumentation such as conductivity-temperature chains and current meters. A conductivity-temperature chain could obtain profiles with reasonable vertical resolution, over longer periods at frequencies high enough to avoid aliasing the tidal signals. Further studies in Alice Arm to understand the major forcing there should concentrate on a) the processes occurring in and around the sill region, and b) the forcing from outside Alice Arm i.e. Observatory Inlet.

REFERENCES

Amax of Canada, Ltd. 1981. Kitsault Mine effluent monitoring report. Prepared for Environment Canada, Vancouver, B.C.

Blackford, B.L. 1978. On the generation of internal waves by tidal flow over a sill - a possible nonlinear mechanism. J. Mar. Res., 36, 529-549.

Farmer, D.M. and H.J. Freeland. 1983. The physical oceanography of fjords. Prog. Oceanogr. Vol.12, No.2, 147-220.

Farmer, D.M. and T.R. Osborn. 1976. The influence of wind on the surface layer of a stratified inlet: Part I Observations. J. Phys. Oceanogr., 6, 931-940.

Freeland, H.J. and D.M. Farmer. 1980. Circulation and energetics of a deep, strongly stratified inlet. Can. J. Fish. Aquat. Sci., Vol. 37, 1398-1410.

Long, R.R. 1975. Circulations and density distribution in a deep, strongly stratified, two-layer estuary. J. Fluid Mech., 71, 529-540.

Nebert, D.L. and D.C. Burrell. 1982. Marine environmental studies in Boca de Quadra and Smeaton Bay: Physical oceanography, 1980. Inst. Mar. Sci., University of Alaska, Fairbanks. 57 pp.

Nicoll, M. and D.J. Stucchi. 1982. Alice Arm 1981 CTD data access guide. Can. Contract. Rep. Hydrogr. Ocean Sci: 5: 76 pp.

Rattray, M., Jr. 1967. Some aspects of the dynamics of circulations in fjords. "Estuaries", ed. G.H. Lauff, AAAC, Washington, D.C. 52-62.

Stigebrandt, A. 1976. Vertical diffusion driven by internal waves in a sill fjord. J. Phys. Oceanogr., 6, 486-495.

Stigebrandt, A. 1977. On the effects of barotropic current fluctuations on the two-layer transport capacity of a constriction. J. Phys. Oceanogr., 7, 118-122.

Stigebrandt, A. 1980. Barotropic and baroclinic response of a semi-enclosed basin to barotropic forcing from the sea. in "Fjord Oceanography", Freeland et al, eds., Nato Conf. Ser., Ser.IV: Marine Sciences, Plenum, 141-164.

Stigebrandt, A. 1981. A mechanism governing the estuarine circulation in deep, strongly stratified fjords. Est. Coast Mar. Sci. 13, 197-211.

Stucchi, D.J. 1983. Shelf-fjord exchange on the west coast of Vancouver Island. in "Coastal Oceanography: Physical Aspects", Gade et al, eds., Nato Conf. Ser., Marine Sciences, Plenum. (In press)

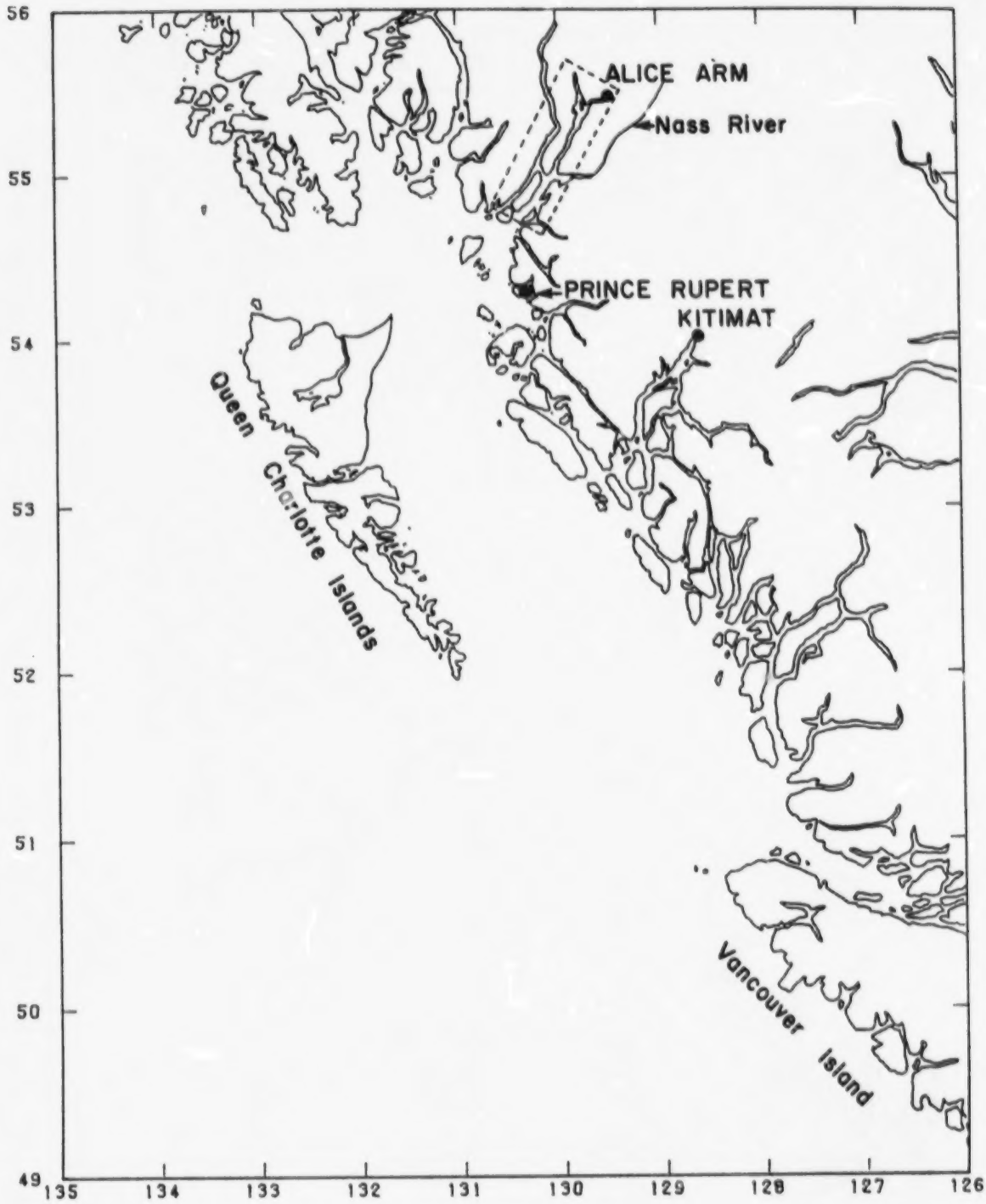

Figure 1. General location map.

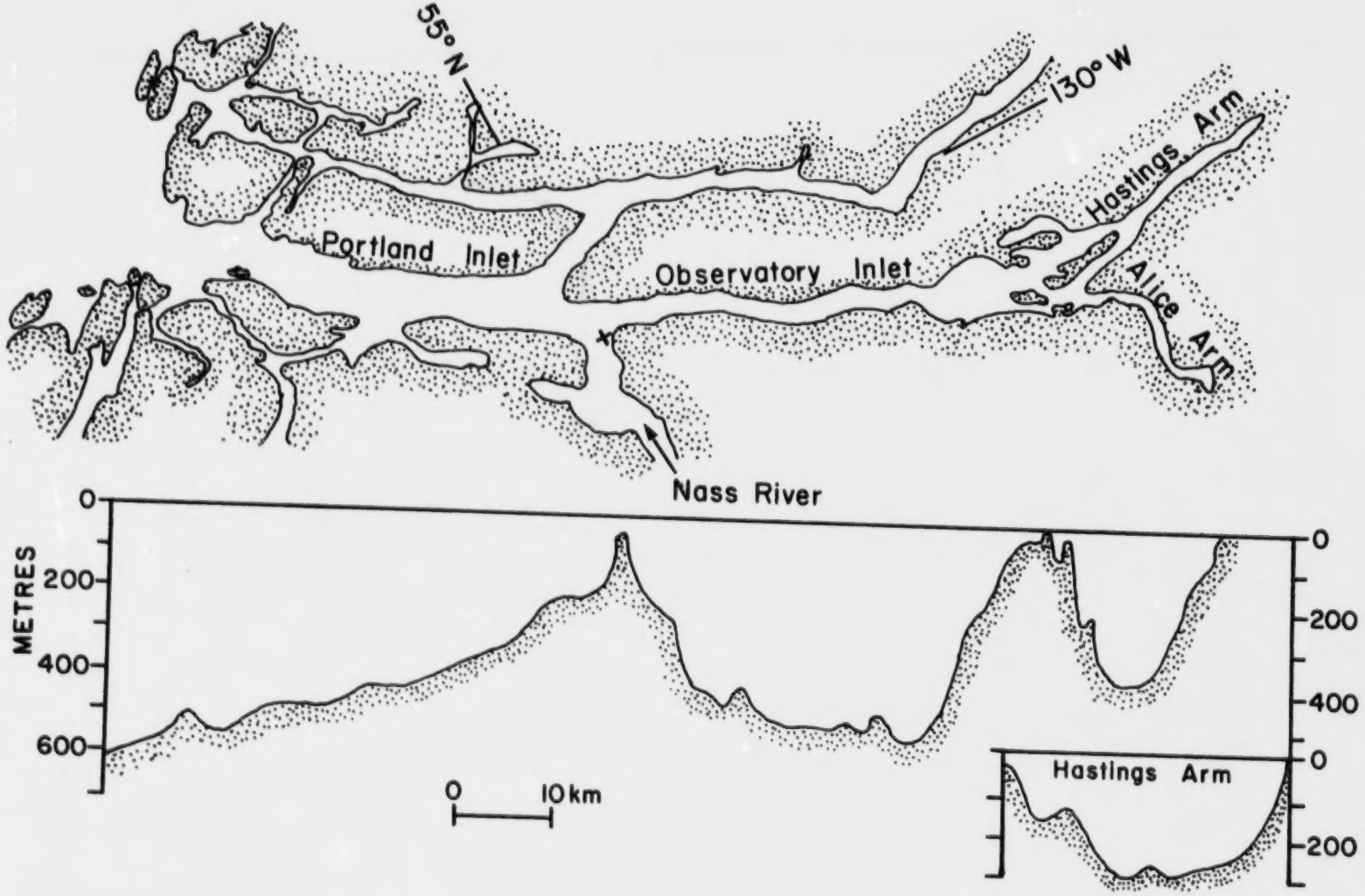

Figure 2. Plan view and longitudinal depth profile at Portland Inlet, Observatory Inlet, Alice Arm and Hastings Arm.

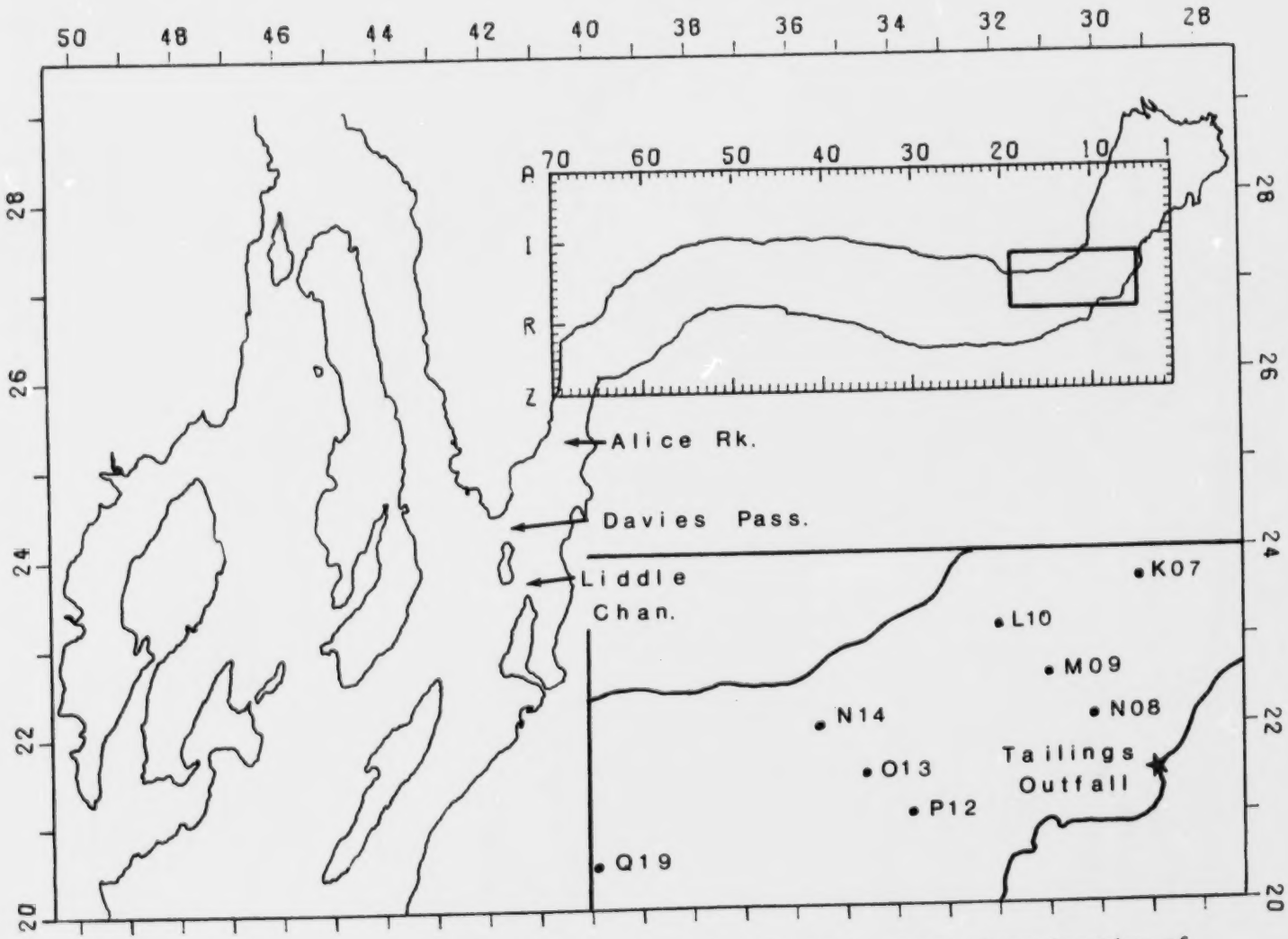

Figure 3. Alice Arm map showing crash program station grid. Inset shows location of most frequently sampled stations, also shown is the location of the tailings outfall.

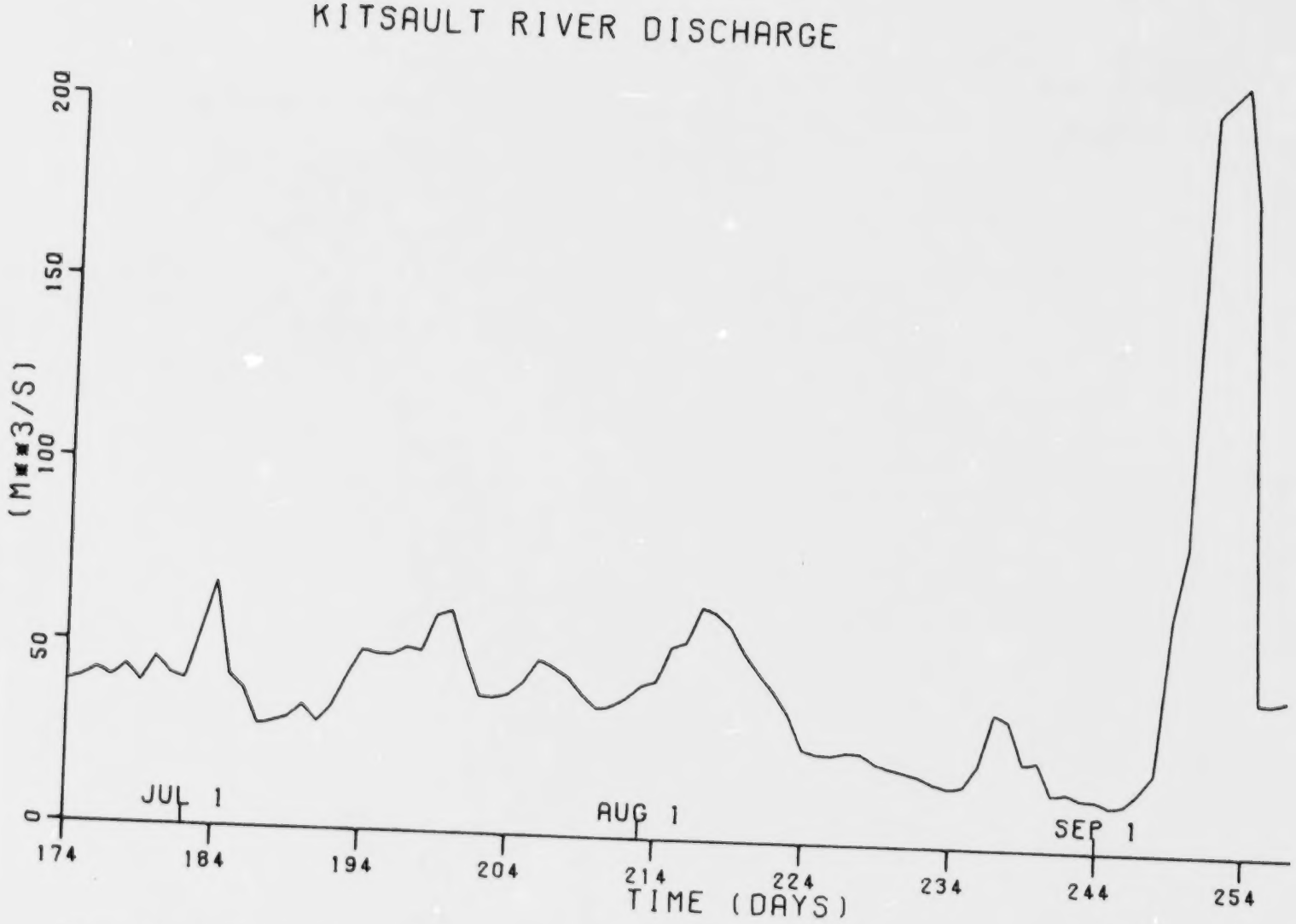

Figure 4. Kitsault River discharge.

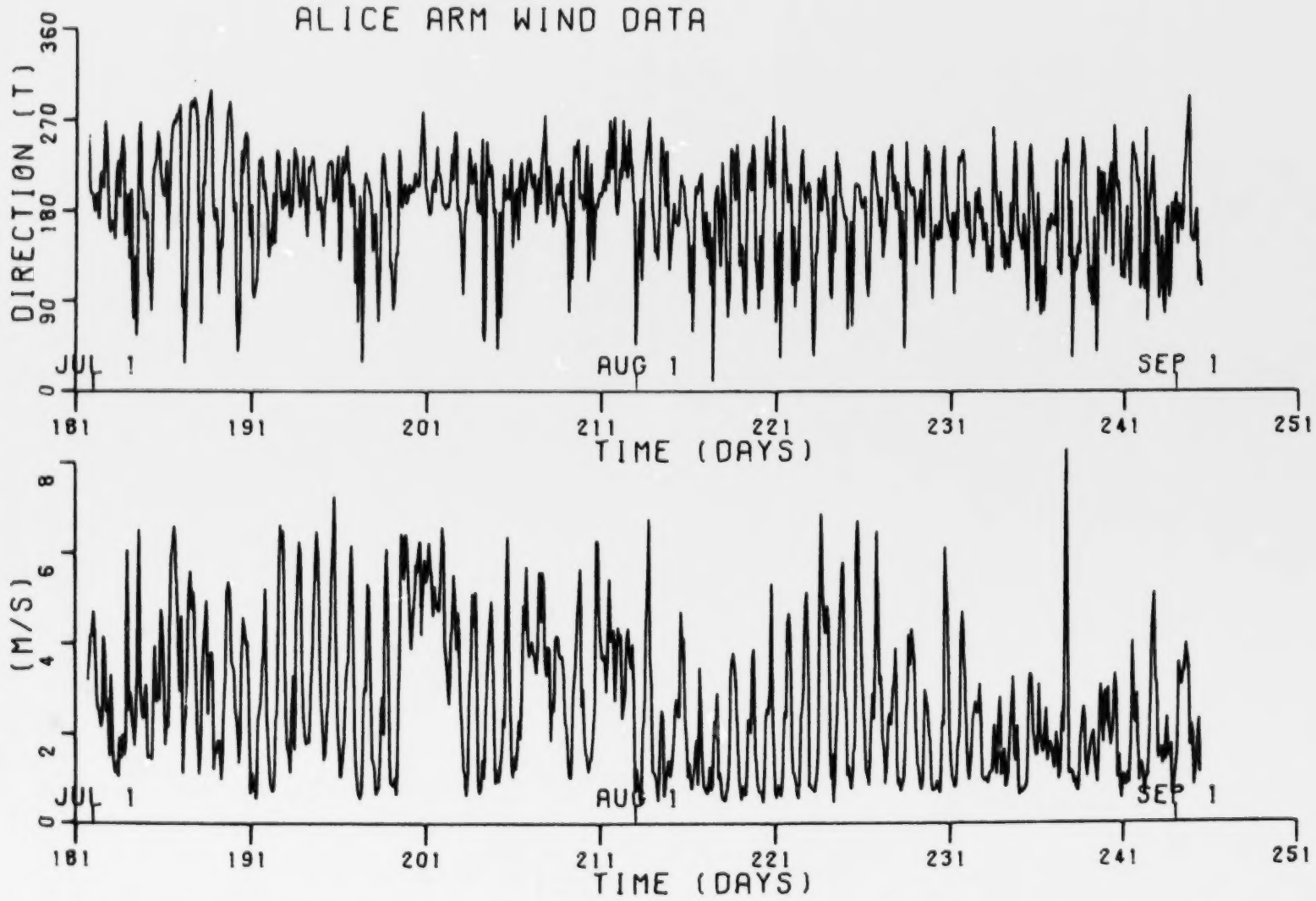

Figure 5. Wind speed and direction observations obtained near the tailings outfall from the end of June to beginning of September, 1981.

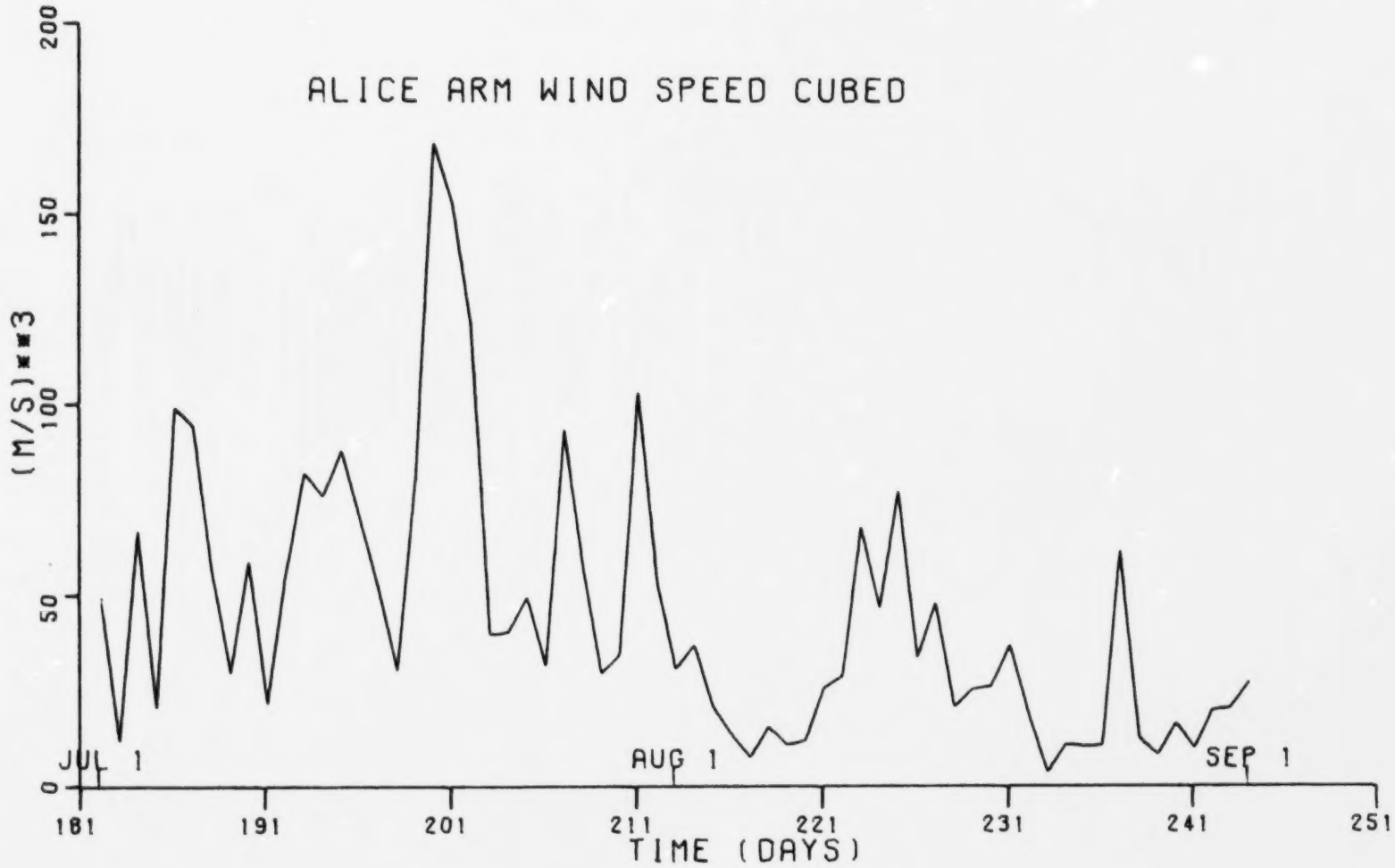

Figure 6. Plot of the daily average of the wind speed cubed from Alice Arm for July and August 1981.

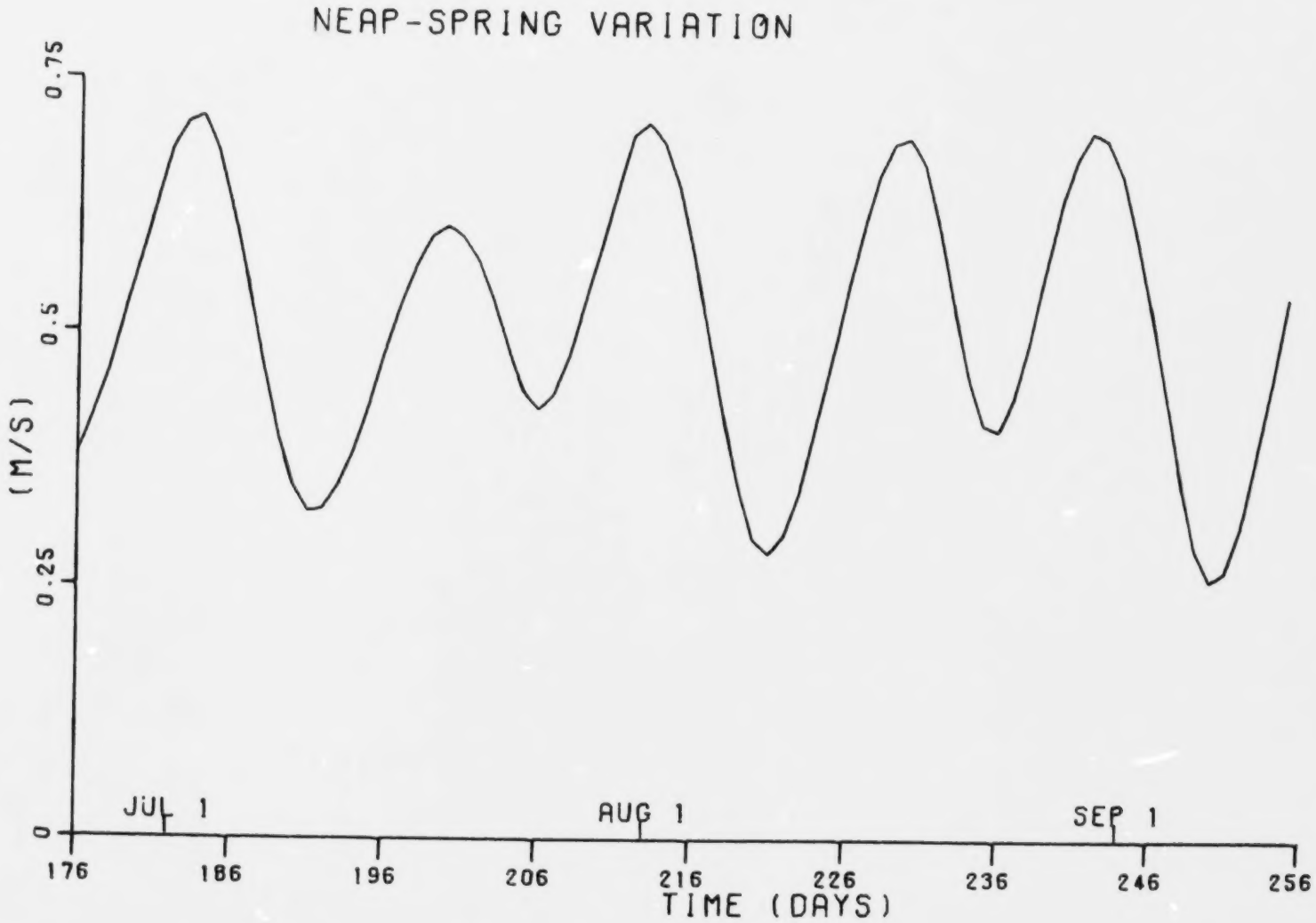

Figure 7. Neap-spring variation of tidal flow in Alice Arm during the crash program .

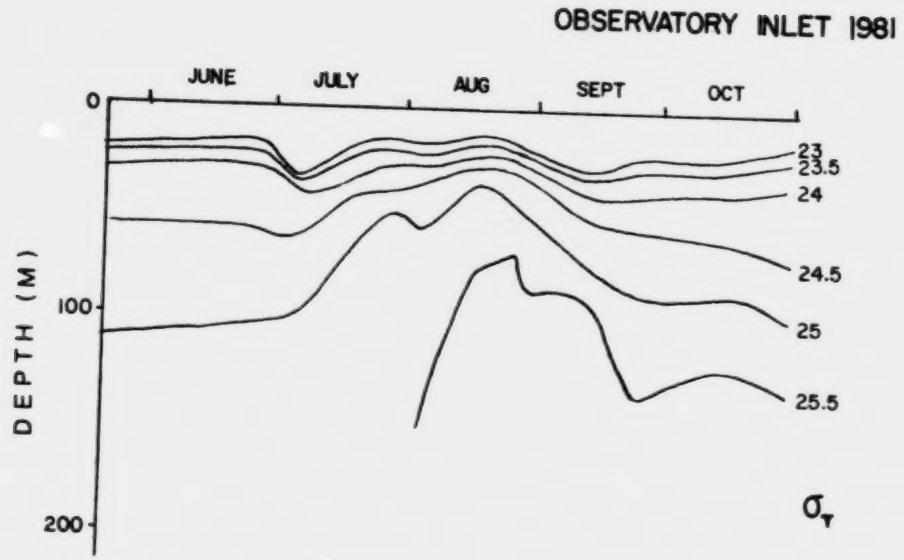

Figure 8. Depth-time plot of σ_T from a station at the northern end of Observatory Inlet.

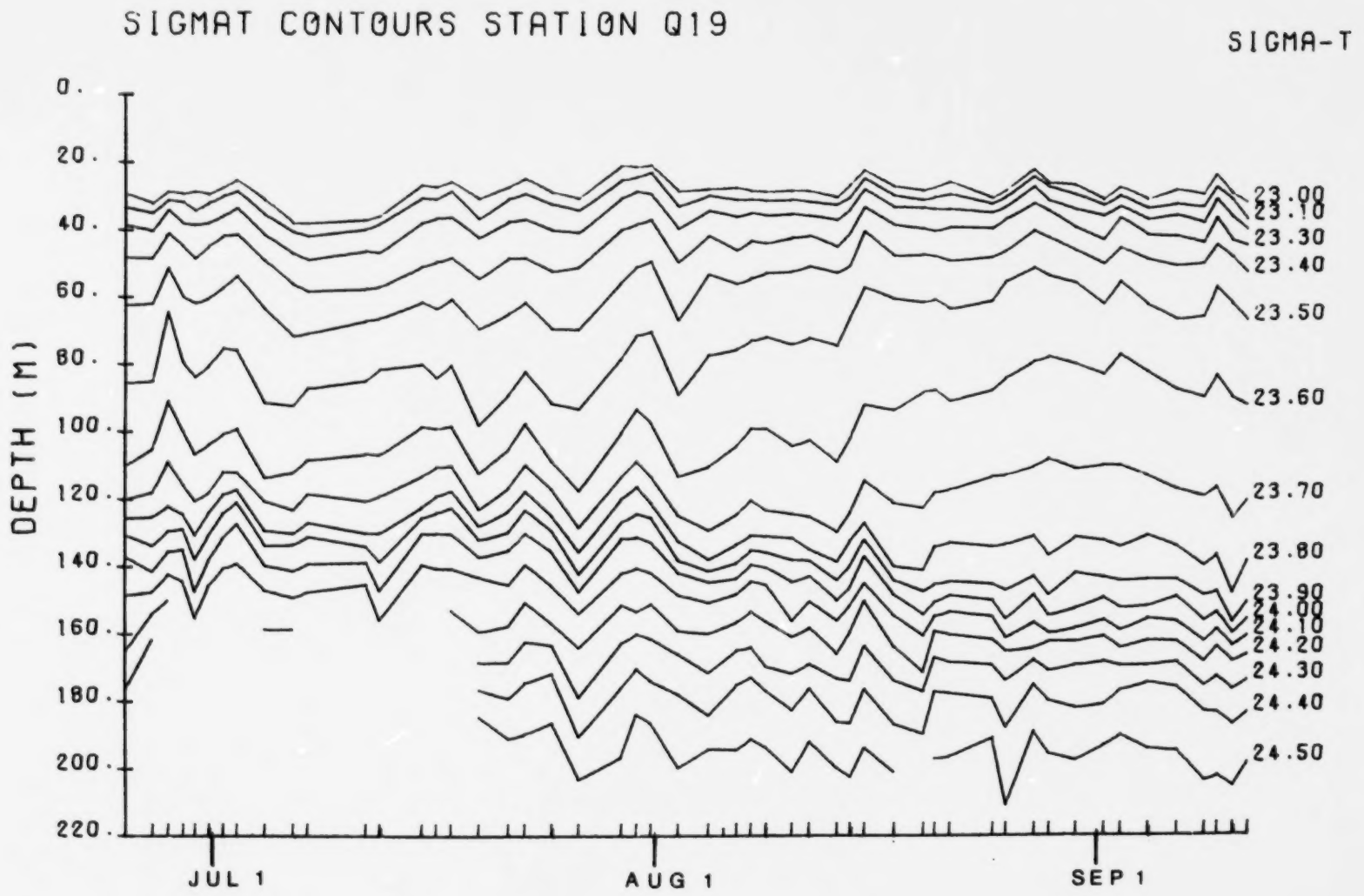

Figure 9. Depth-time plot of σ_T from station Q19 in Alice Arm.

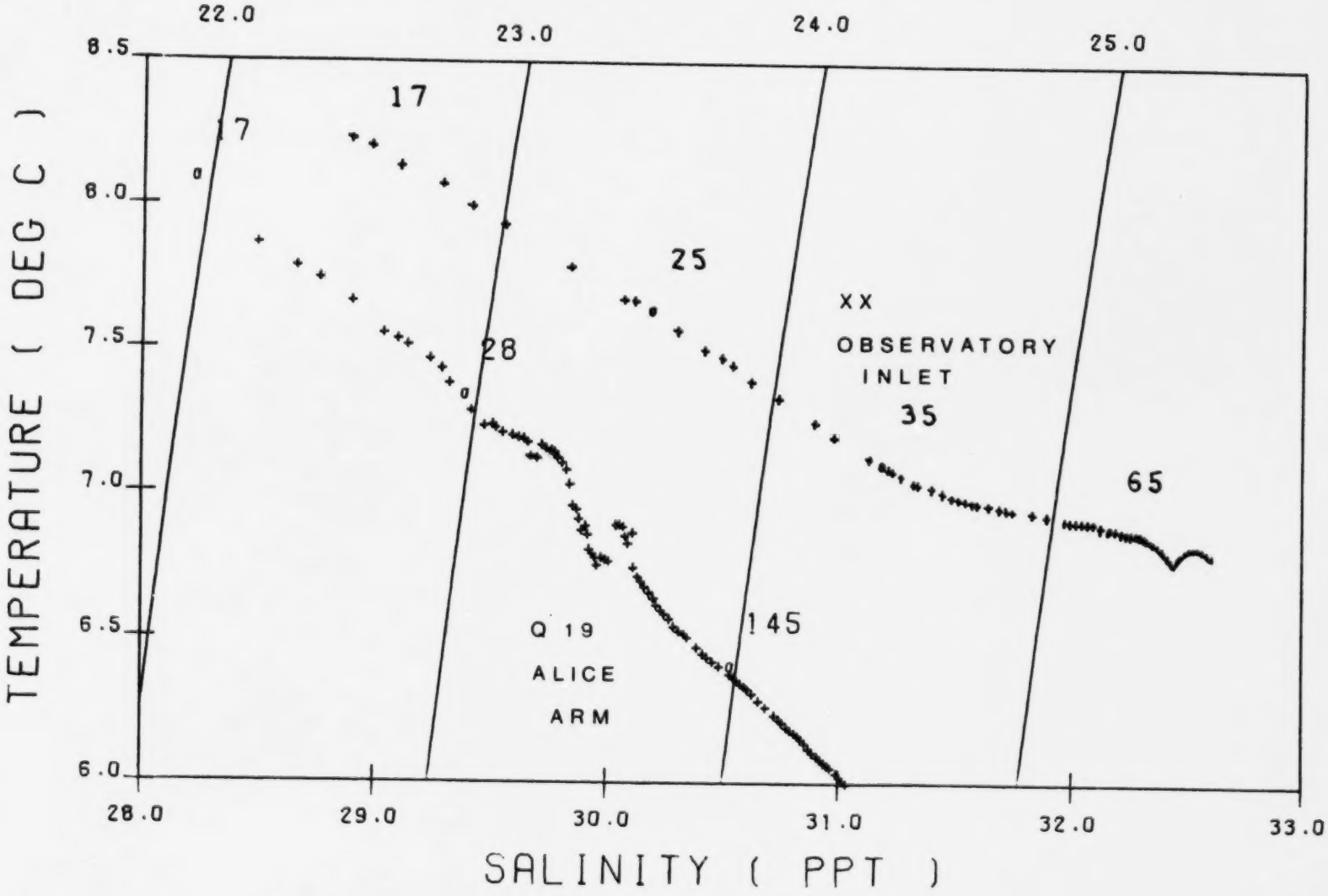

Figure 10. Temperature-salinity plot of station XX in Observatory Inlet and station Q19 in Alice Arm taken on August 10, 1981.

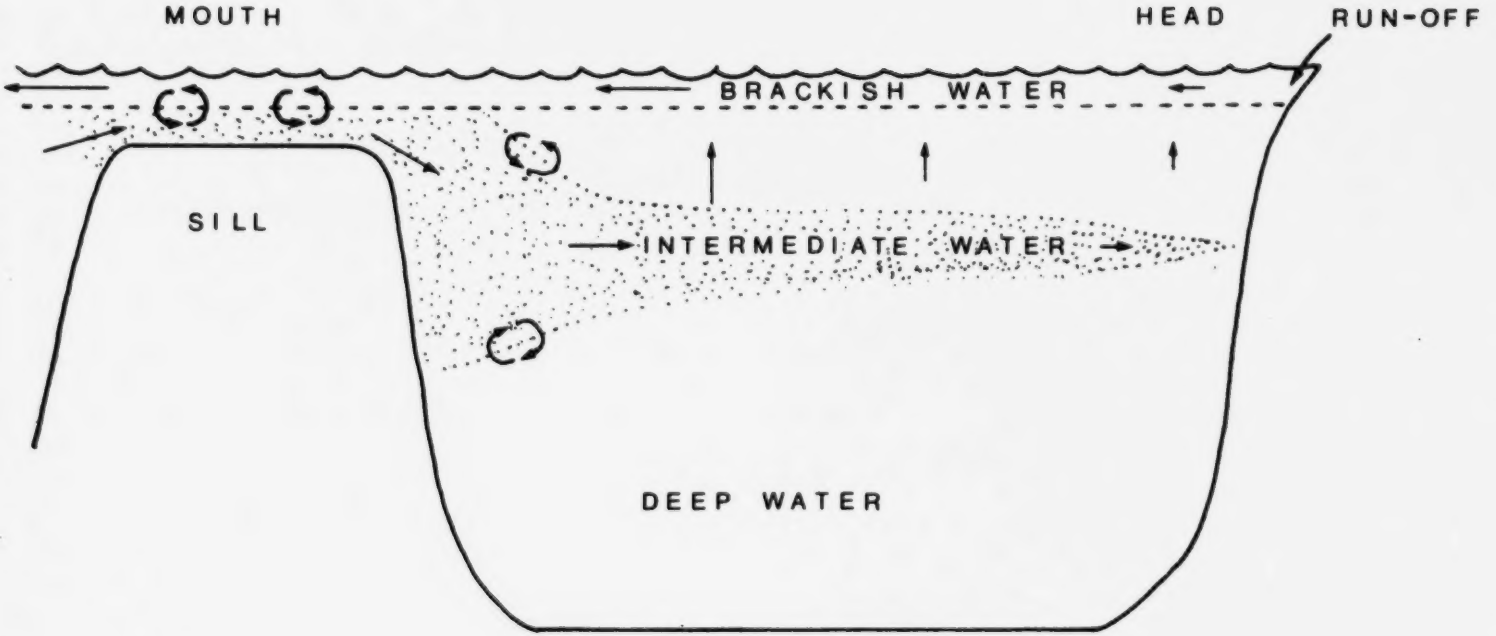

Figure 11. Idealized net circulation in a fjord during intermediate water renewal.

Table 1. Sampling statistics: * = more than 5 samples, X = 2 to 5 samples, 1 = 1 sample.

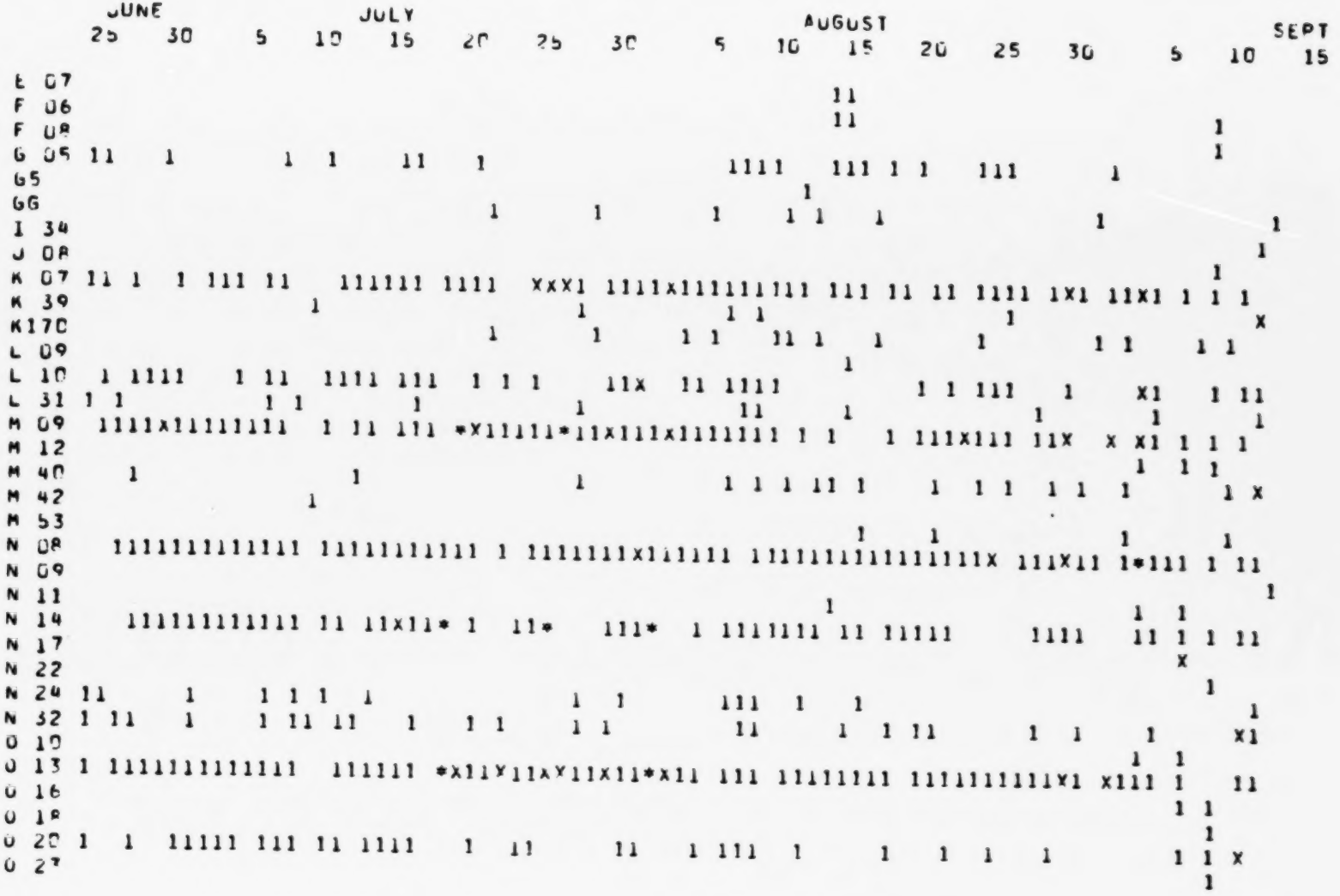

Table 1. (Continued) Sampling statistics

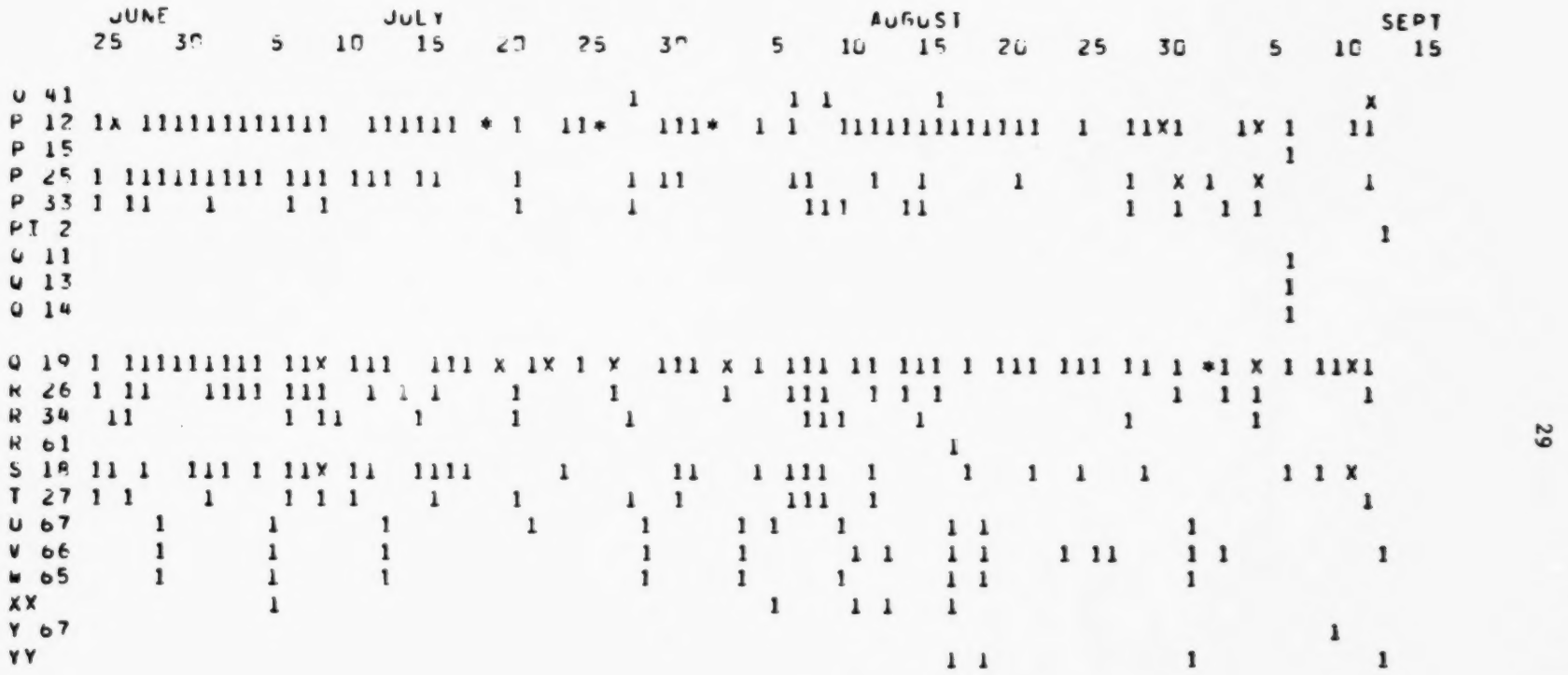

Table 2. Ratio of local fresh water input to tidal prism

	%
Alice Arm (1981)	
a) May-June melt	2.2
b) July-August maxima	2.7
c) September 8 to 11 event	8.0
Endicott Arm, Alaska*	2.0
Silver Bay, Alaska*	8.0
Boca de Quadra, Alaska*	1.8

*From Nebert and Burrell (1982)

Table 3. Coherence and phase between fortnightly variations shown in Figure 7 and upper layer sigma-t, and upper layer depth for all stations at frequency of 0.0667 cycles per hour (period of 15 days).

Station	Upper Layer Sigma-t		Upper Layer Depth		95% noise level
	Coherence	Phase	Coherence	Phase	
Q19	0.68	-93.1°	0.45	-84.8°	0.40
P12	0.49	-83.2	-	-	0.40
O13	0.51	-92.6	0.41	-102.1	0.40
N14	0.52	-80.7	0.50	-86.3	0.41
N08	0.50	-95.3	0.62	-43.6	0.40
M09	0.56	-94.4	-	-	0.42

APPENDIX A

Calculation of two layer representation

The objective method for determining the pycnocline depth developed by Freeland and Farmer (1980) involves calculating and conserving two parameters of the profile, the first mode internal wave speed C_1, and the potential energy χ. The speed of the first mode internal wave is found by solving the following differential equation:

$$\frac{d^2W_1}{dz^2} + W_1 N^2(z)/C_1^2 = 0 \qquad (1)$$

with boundary conditions $W_1(0) = W_1(H) = 0$

where $N^2(z)$ is the buoyancy frequency, $W_1(z)$ the amplitude of the first mode eigenfunction, and H is the total depth. Potential energy is calculated by integrating over the profile

$$\chi = \frac{1}{H^2} \int_0^H \sigma_T(z) z dz \qquad (2)$$

where $\sigma_T = 10^3(\rho-1)$. In a two layer system C_1^2 and χ are defined as follows

$$C_1^2 = g' (\sigma_2-\sigma_1) h (H-h)/H \qquad (3)$$

and $$\chi = \tfrac{1}{2} \left\{\sigma_1 h^2 + \sigma_2 (H^2-h^2)\right\} /H^2 \qquad (4)$$

where $g' = g/(\rho_2 \times 1000)$, h is the depth of the upper layer and σ_1 and σ_2 the density anomalies for the upper and lower layers. By setting σ_1 to a reasonable value, σ_2 and h could be computed from (3) and (4). The problem is to chose a reasonable value of σ_1; this is accomplished by starting with a 5m depth averaged value of σ_1. Values for σ_2 and h are calculated and a new value of σ_1 estimated by

$$\sigma_1 = \frac{1}{h} \int_o^h \sigma(z) dz. \qquad (5)$$

New values of σ_2 and h are calculated and the value of σ_1 recomputed. This iterative procedure was stopped when successive values of h differed by less than 5 cm. The iteration for h converged in less than 10 steps.

APPENDIX B

Time series plots of upper layer sigma-t and upper layer depth (Figures B1, B4, B7, B10, B13 and B16), phase speed of first mode internal wave and potential energy (Figures B2, B5, B8, B11, B14 and B17), and FWC (0 to 50m) (Figures B3, B6, B9, B12, B15 and B18) for stations Q19, N14, 013, P12, N08 and M09 during the summer of 1981.

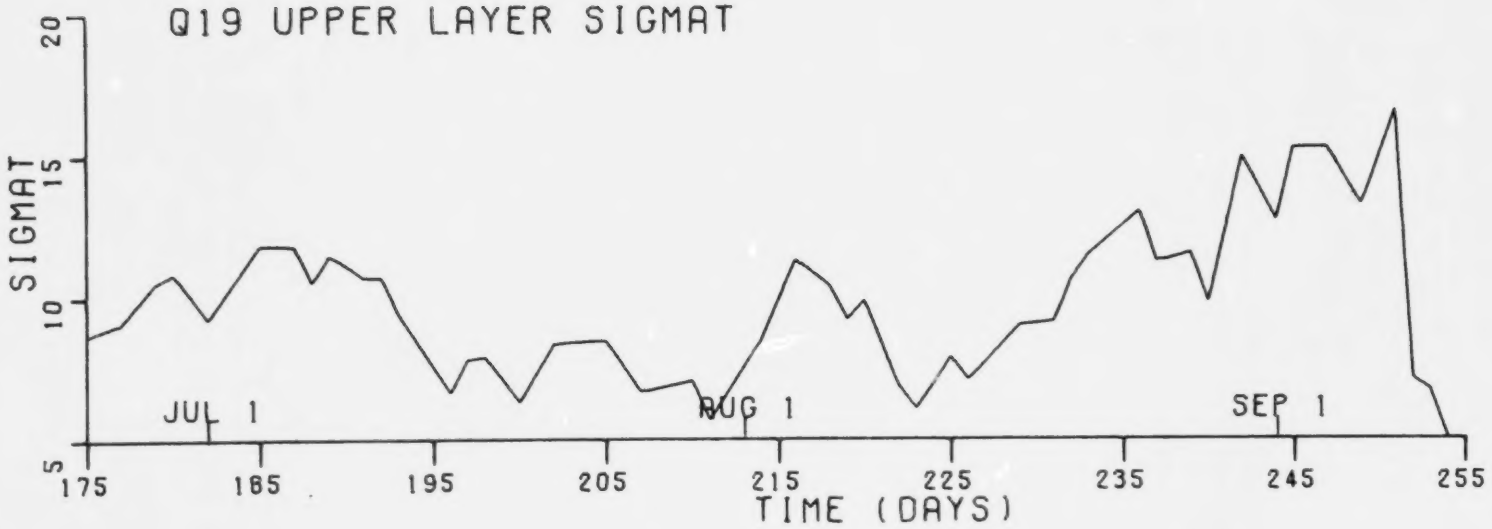
Q19 UPPER LAYER SIGMAT
SIGMAT
20
15
10
5
JUL 1
AUG 1
SEP 1
175
185
195
205
215
225
235
245
255
TIME (DAYS)

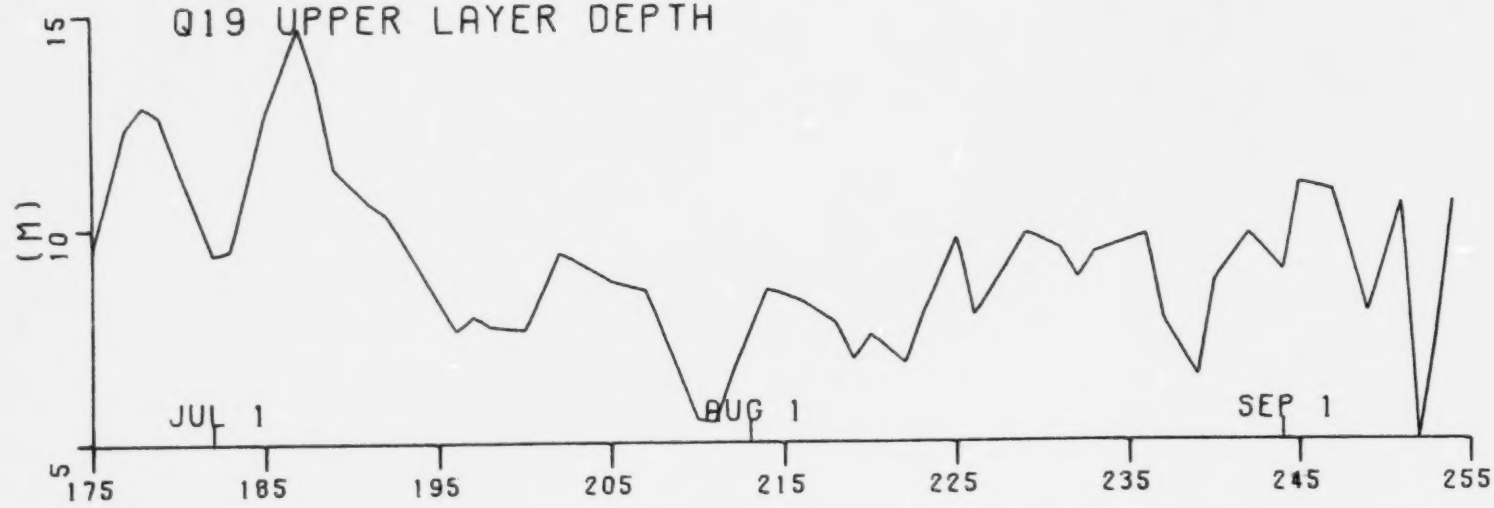
Q19 UPPER LAYER DEPTH
(M)
15
10
5
JUL 1
AUG 1
SEP 1
175
185
195
205
215
225
235
245
255

Figure B1

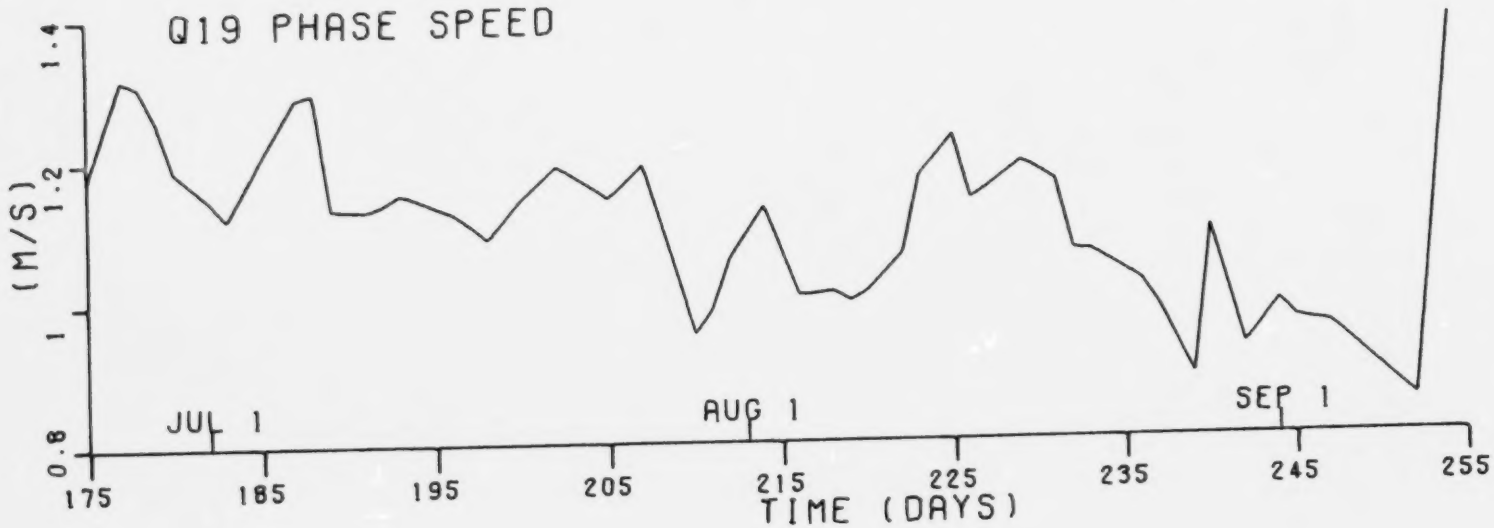
Q19 PHASE SPEED
(M/S)
1.4
1.2
1
0.8
JUL 1
AUG 1
SEP 1
175
185
195
205
215
225
235
245
255
TIME (DAYS)

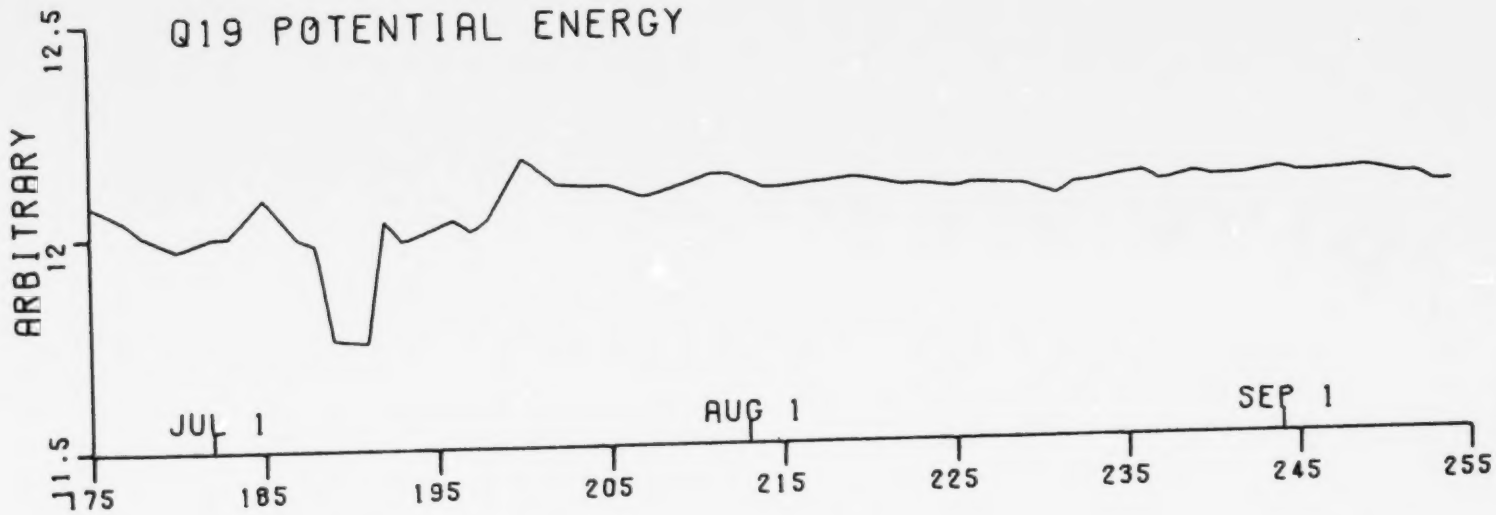
Q19 POTENTIAL ENERGY
ARBITRARY
12.5
12
11.5
JUL 1
AUG 1
SEP 1
175
185
195
205
215
225
235
245
255

Figure B2

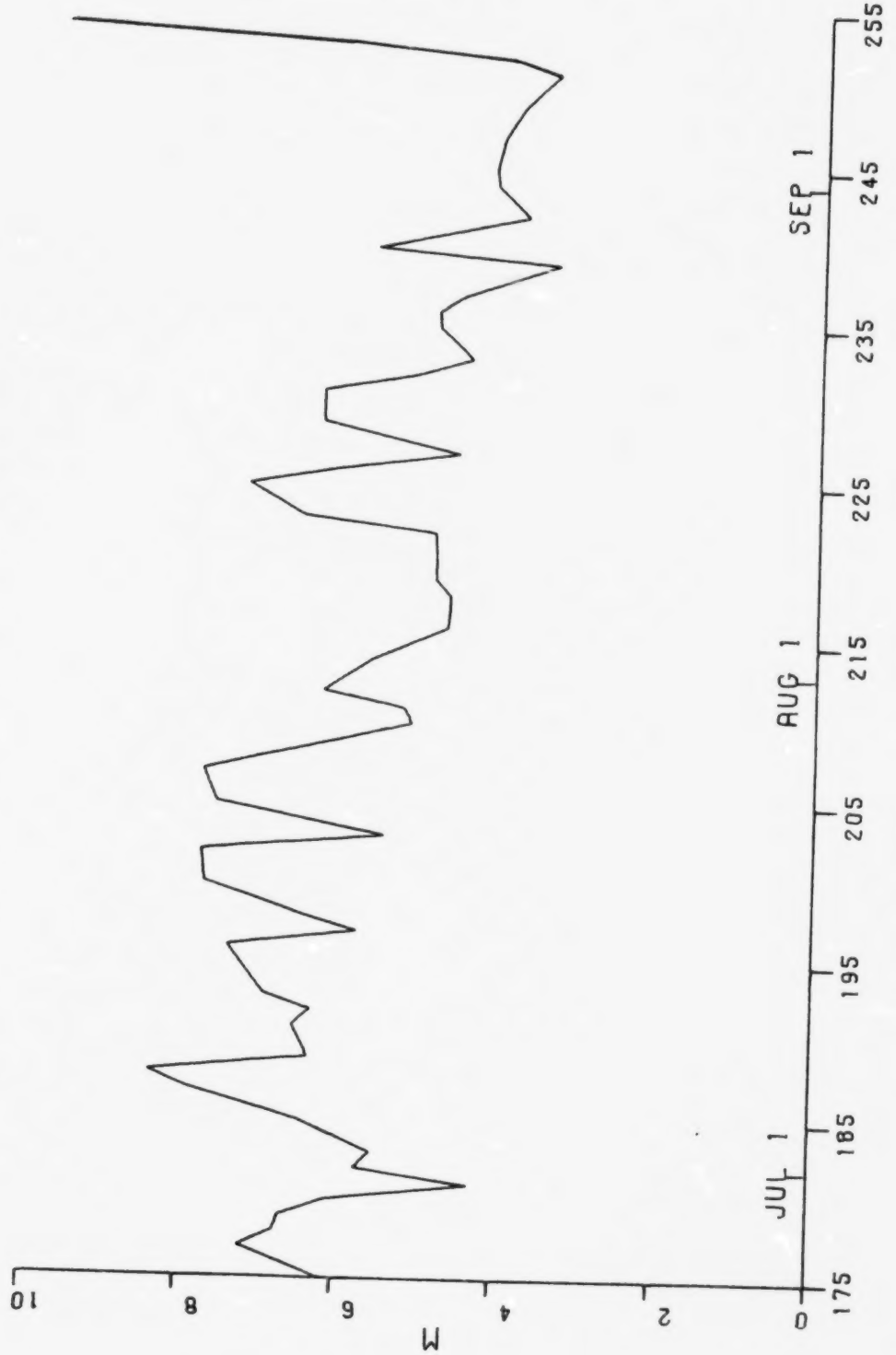
Q19 FRESH WATER CONTENT (0 TO 50 M)
M
0
2
4
6
8
10
175
185
195
205
215
225
235
245
255
JUL 1
AUG 1
SEP 1

Figure B3

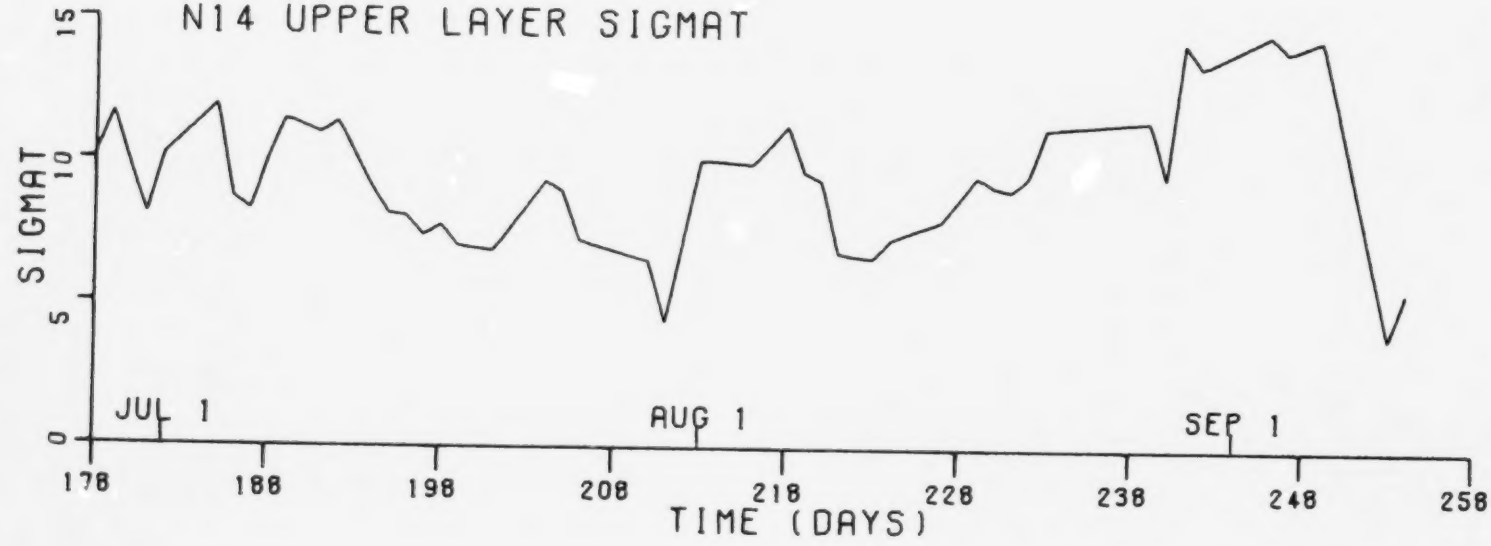
N14 UPPER LAYER SIGMAT
SIGMAT
15
10
5
0
JUL 1
AUG 1
SEP 1
178
188
198
208
218
228
238
248
258
TIME (DAYS)

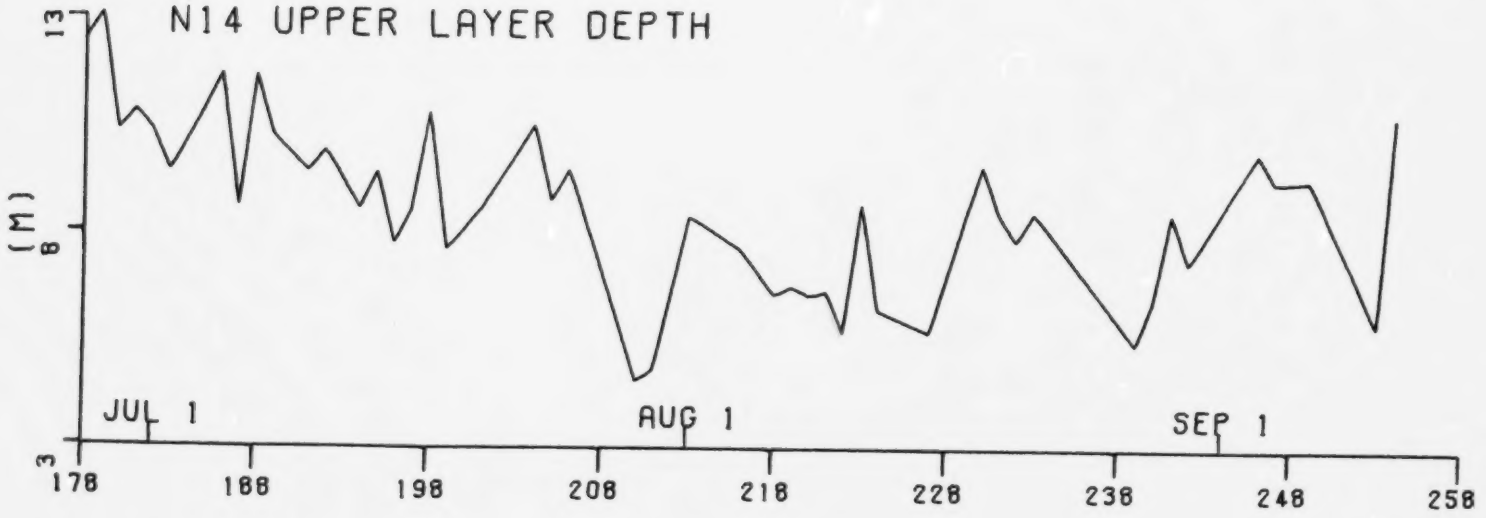
N14 UPPER LAYER DEPTH
(M)
13
8
3
JUL 1
AUG 1
SEP 1
178
188
198
208
218
228
238
248
258

Figure B4

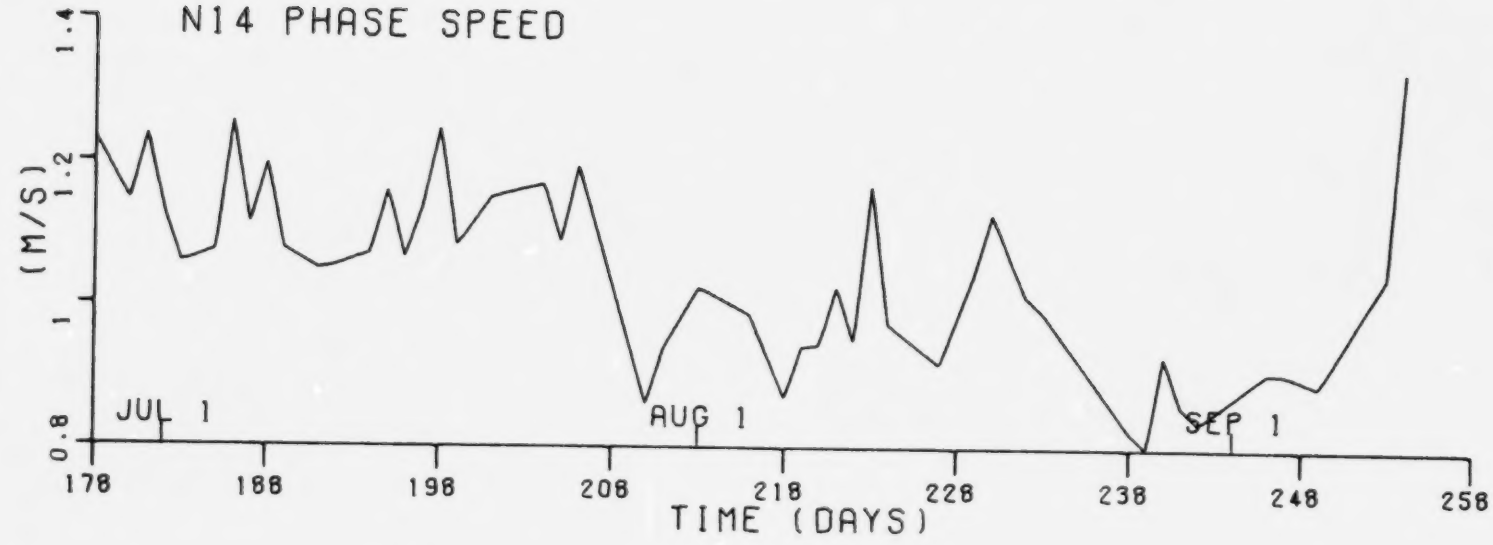
N14 PHASE SPEED
(M/S)
1.4
1.2
1
0.8
JUL 1
AUG 1
SEP 1
178
188
198
208
218
228
238
248
258
TIME (DAYS)

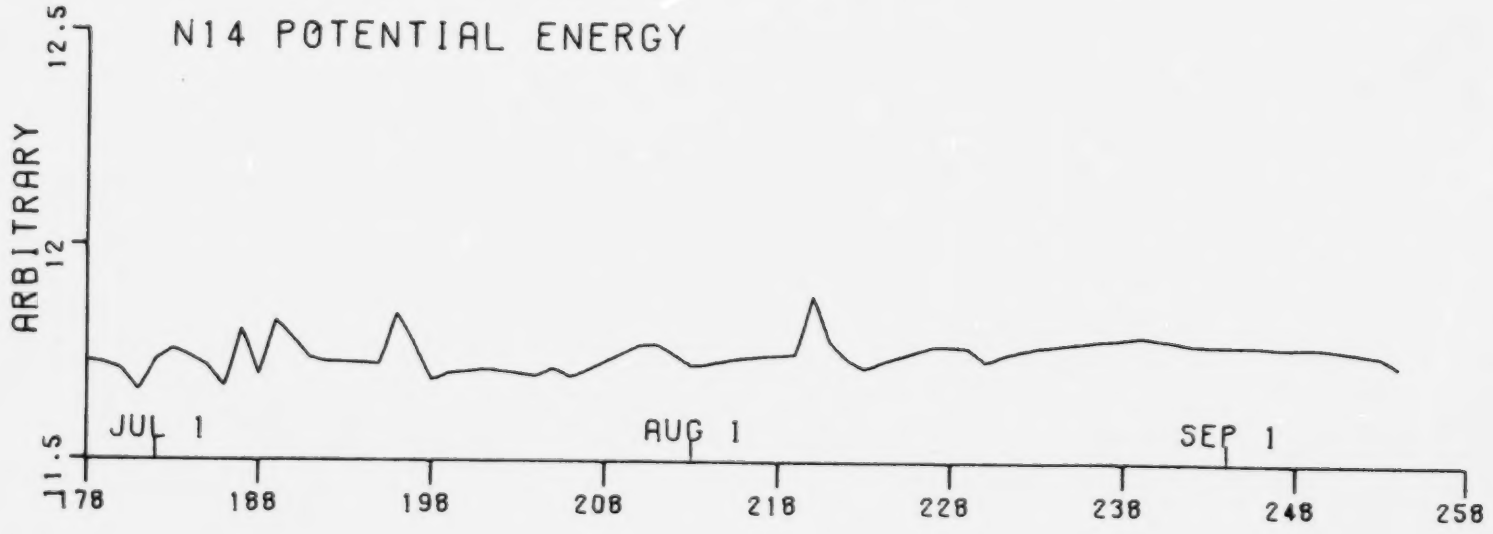
N14 POTENTIAL ENERGY
ARBITRARY
12.5
12
11.5
JUL 1
AUG 1
SEP 1
178
188
198
208
218
228
238
248
258

Figure B5

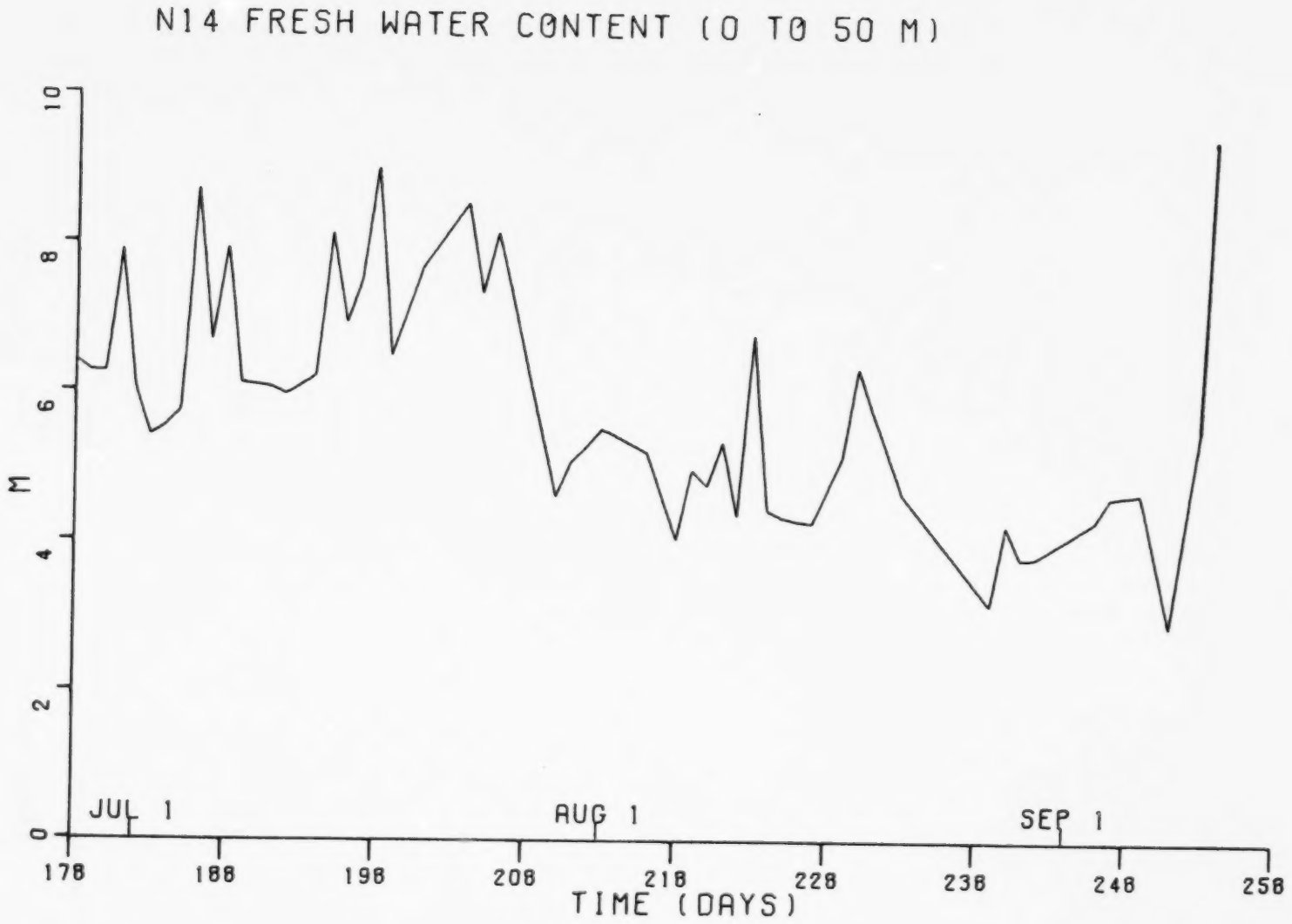
N14 FRESH WATER CONTENT (0 TO 50 M)
M
0
2
4
6
8
10
JUL 1
AUG 1
SEP 1
178
188
198
208
218
228
238
248
258
TIME (DAYS)

Figure B6

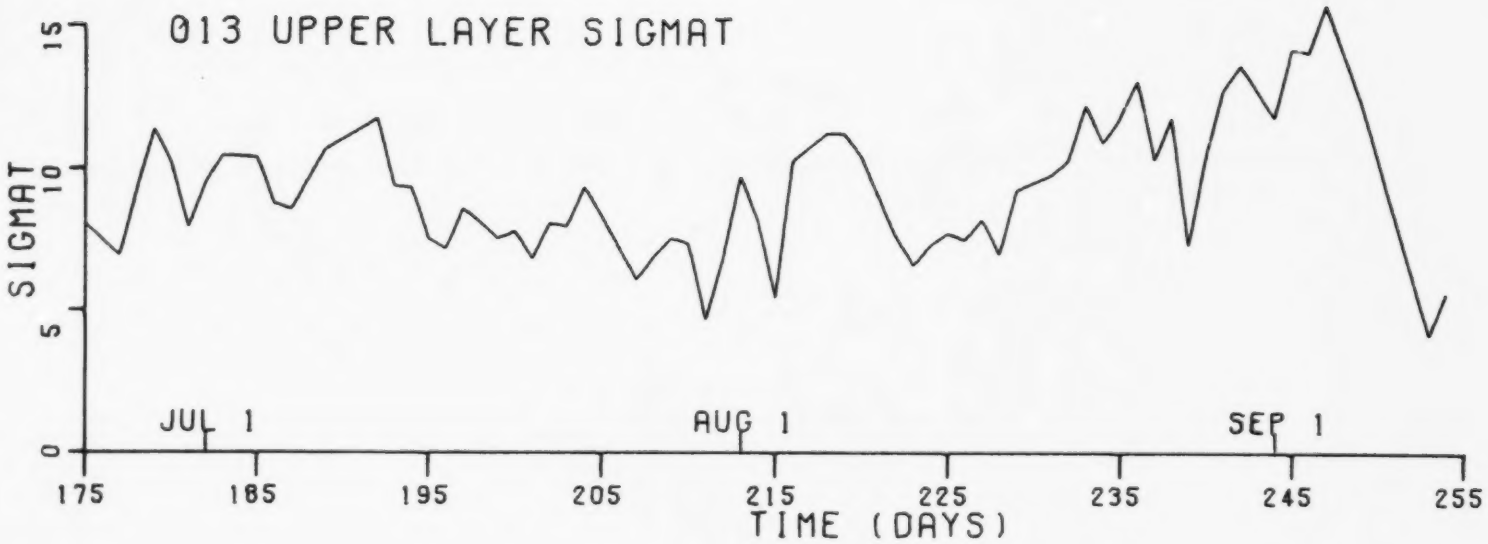
013 UPPER LAYER SIGMAT
SIGMAT
0
5
10
15
JUL 1
AUG 1
SEP 1
175
185
195
205
215
225
235
245
255
TIME (DAYS)

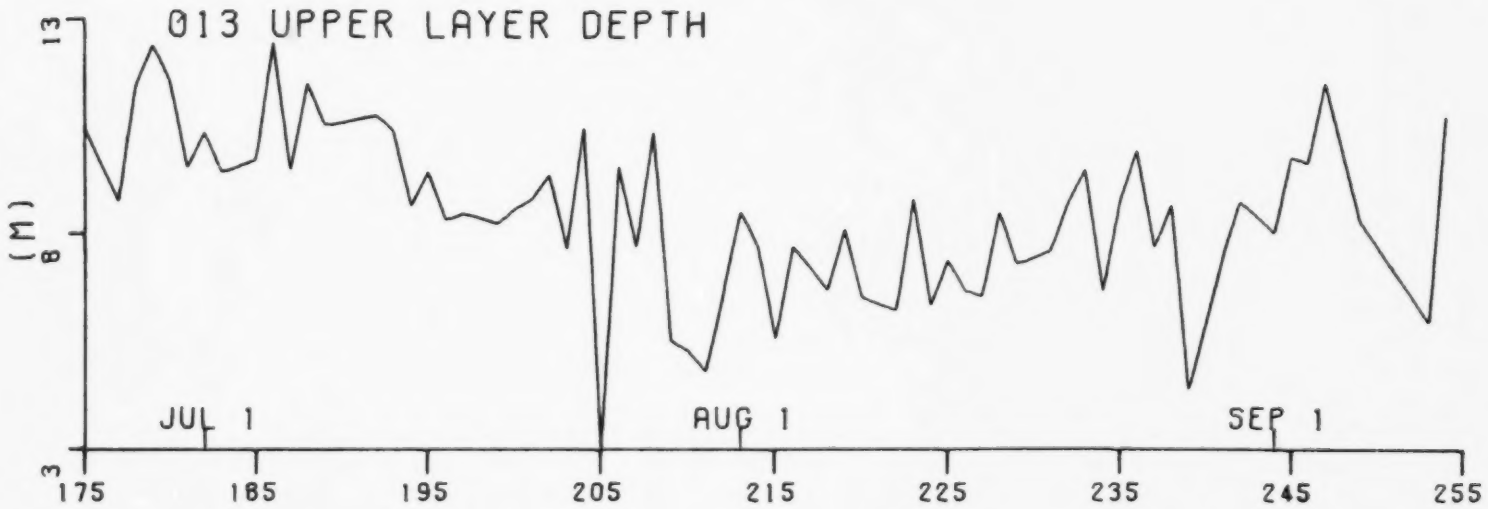
013 UPPER LAYER DEPTH
(M)
3
8
13
JUL 1
AUG 1
SEP 1
175
185
195
205
215
225
235
245
255

Figure B7

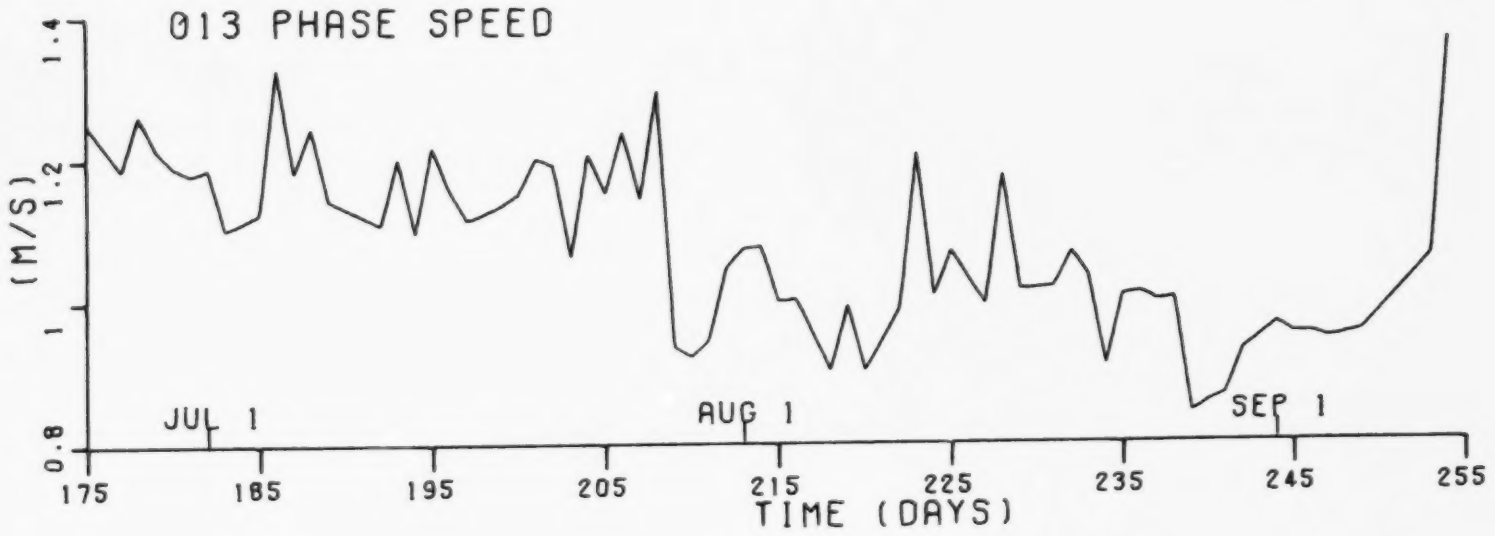
013 PHASE SPEED
(M/S)
1.4
1.2
1
0.8
JUL 1
AUG 1
SEP 1
175
185
195
205
215
225
235
245
255
TIME (DAYS)

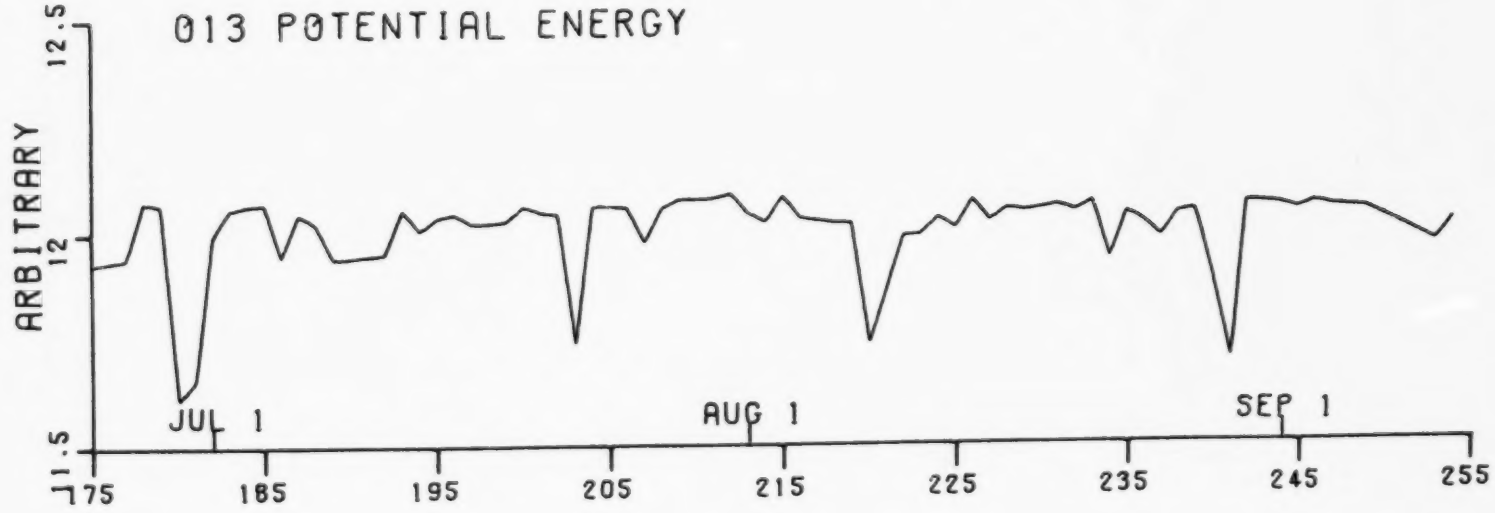
013 POTENTIAL ENERGY
ARBITRARY
12.5
12
11.5
JUL 1
AUG 1
SEP 1
175
185
195
205
215
225
235
245
255

Figure B8

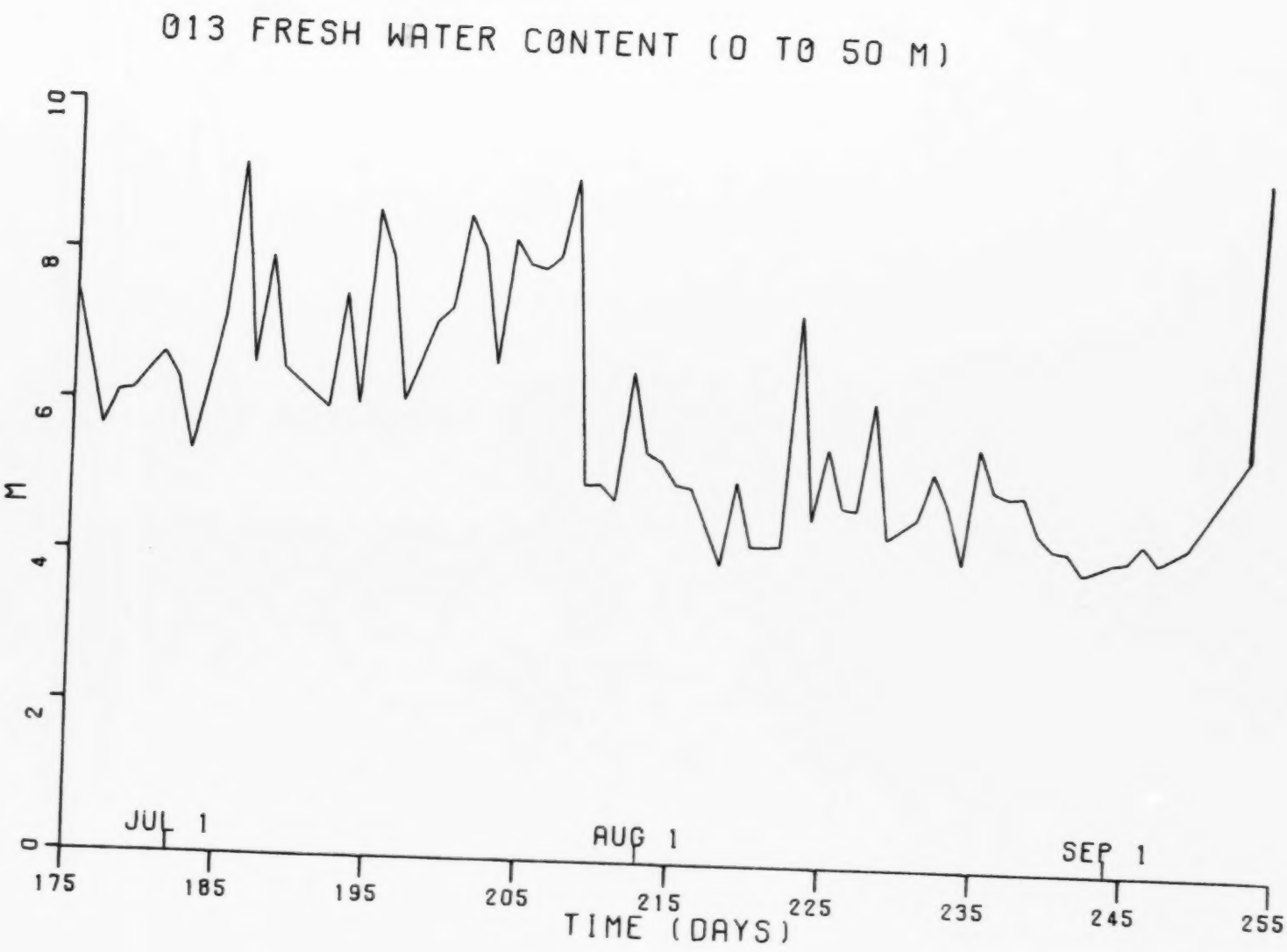
013 FRESH WATER CONTENT (0 TO 50 M)
M
0
2
4
6
8
10
JUL 1
AUG 1
SEP 1
175
185
195
205
215
225
235
245
255
TIME (DAYS)

Figure B9

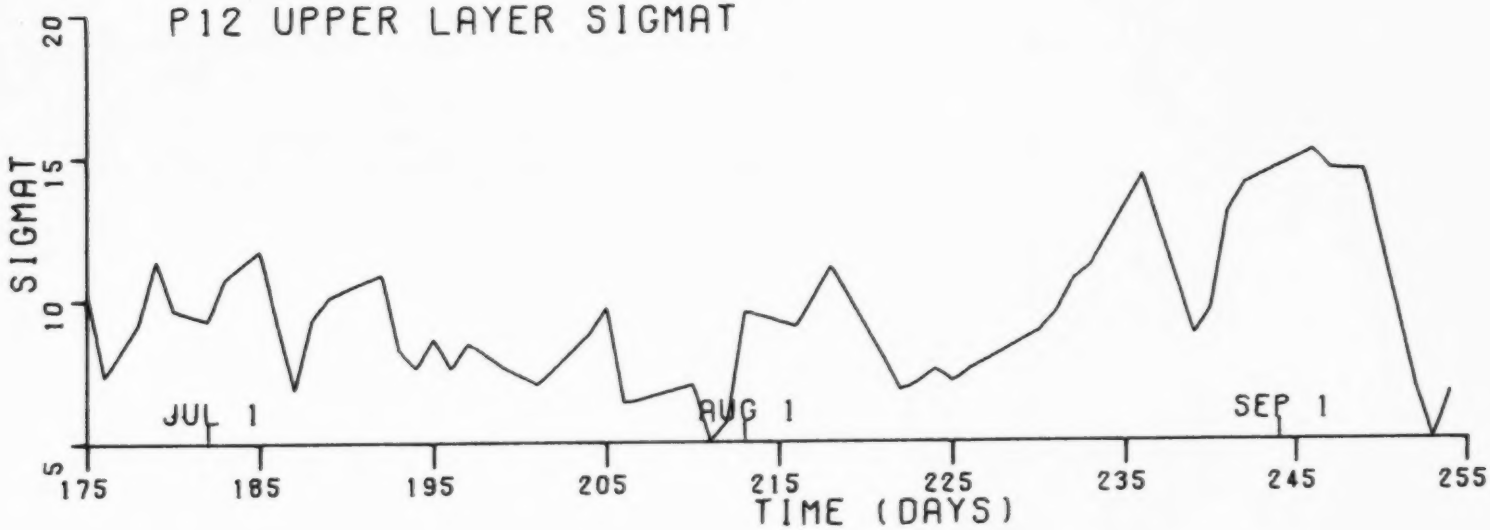
P12 UPPER LAYER SIGMAT
SIGMAT
20
15
10
5
JUL 1
AUG 1
SEP 1
175
185
195
205
215
225
235
245
255
TIME (DAYS)

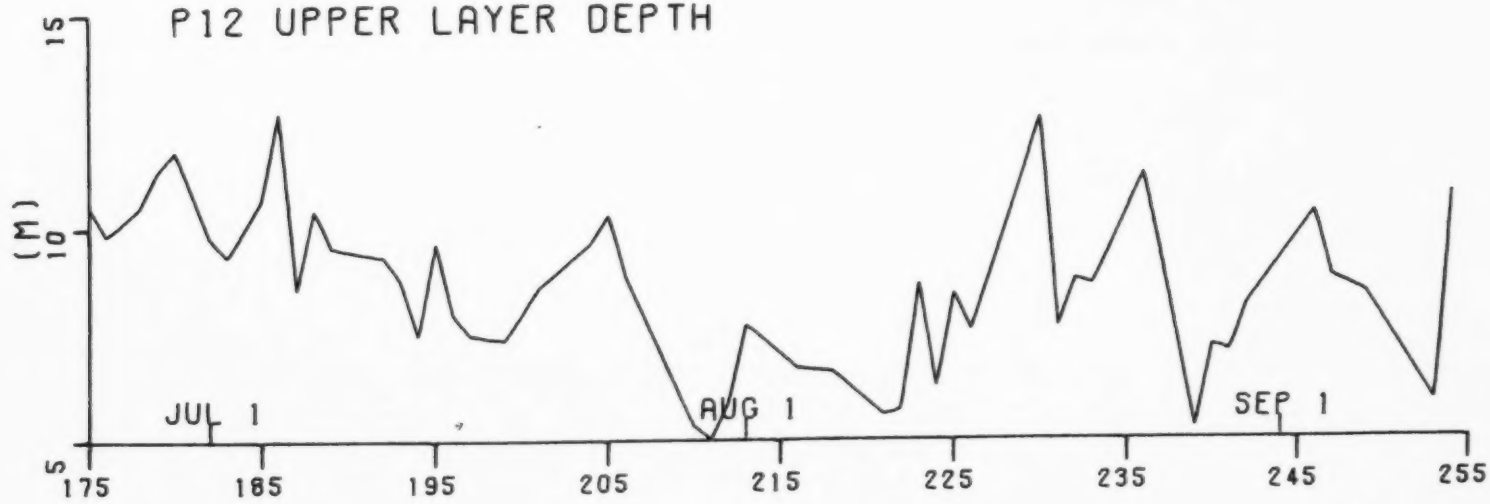
P12 UPPER LAYER DEPTH
(M)
15
10
5
JUL 1
AUG 1
SEP 1
175
185
195
205
215
225
235
245
255

Figure B10

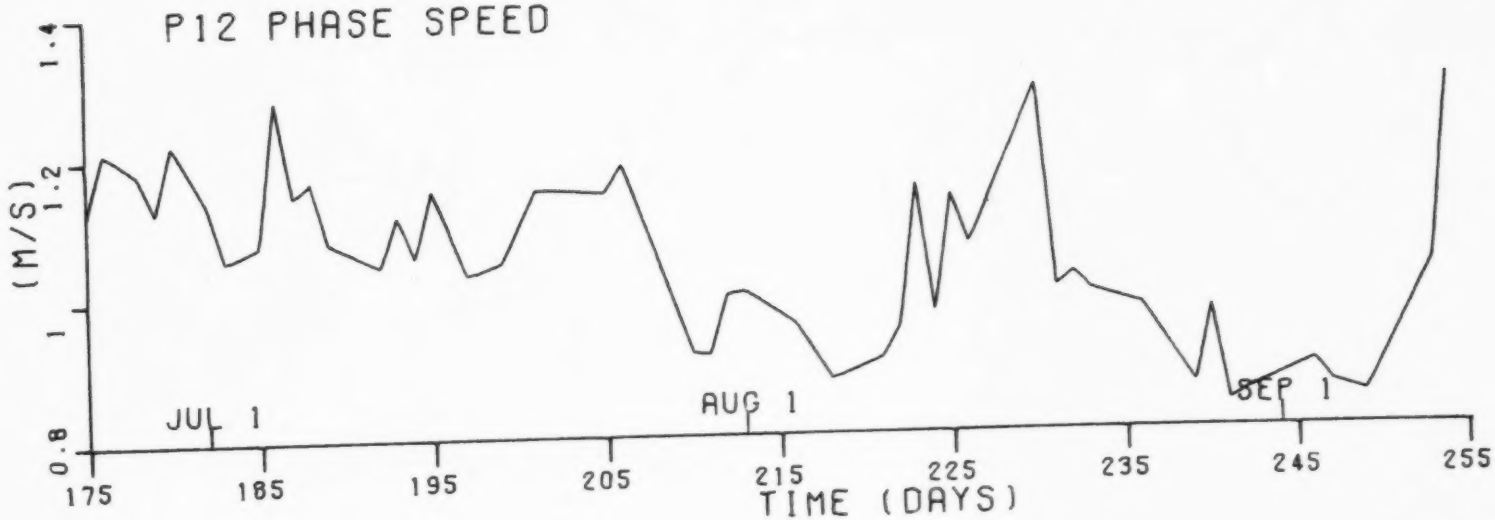
P12 PHASE SPEED
(M/S)
1.4
1.2
1
0.8
JUL 1
AUG 1
SEP 1
175
185
195
205
215
225
235
245
255
TIME (DAYS)

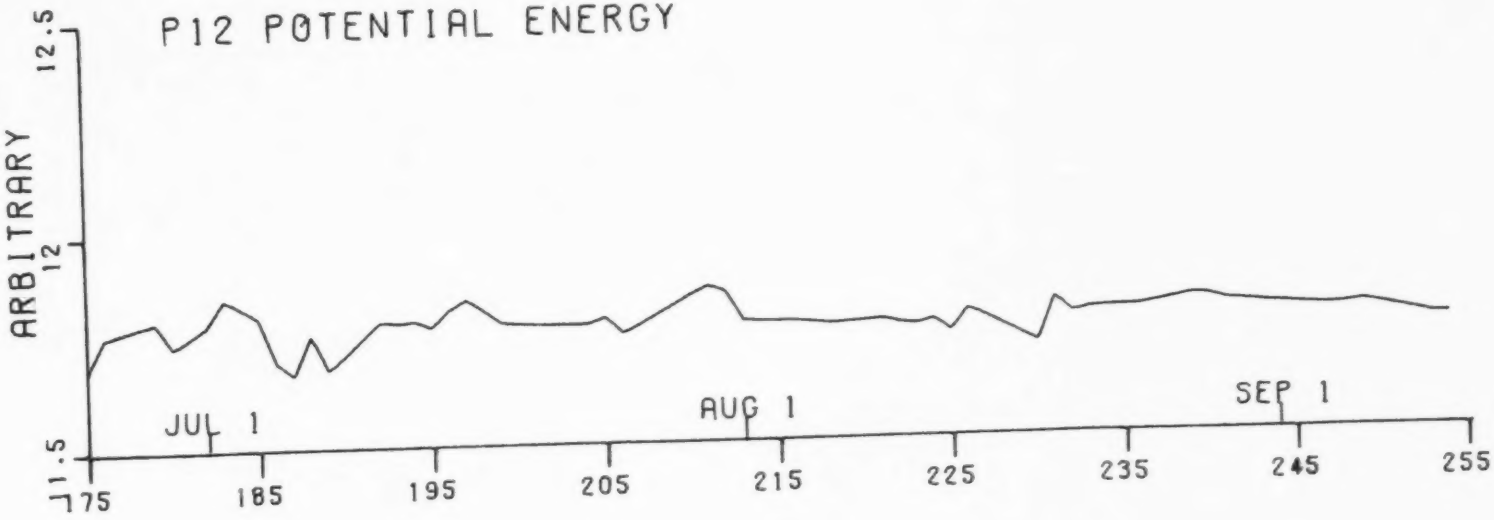
P12 POTENTIAL ENERGY
ARBITRARY
12.5
12
11.5
JUL 1
AUG 1
SEP 1
175
185
195
205
215
225
235
245
255

Figure B11

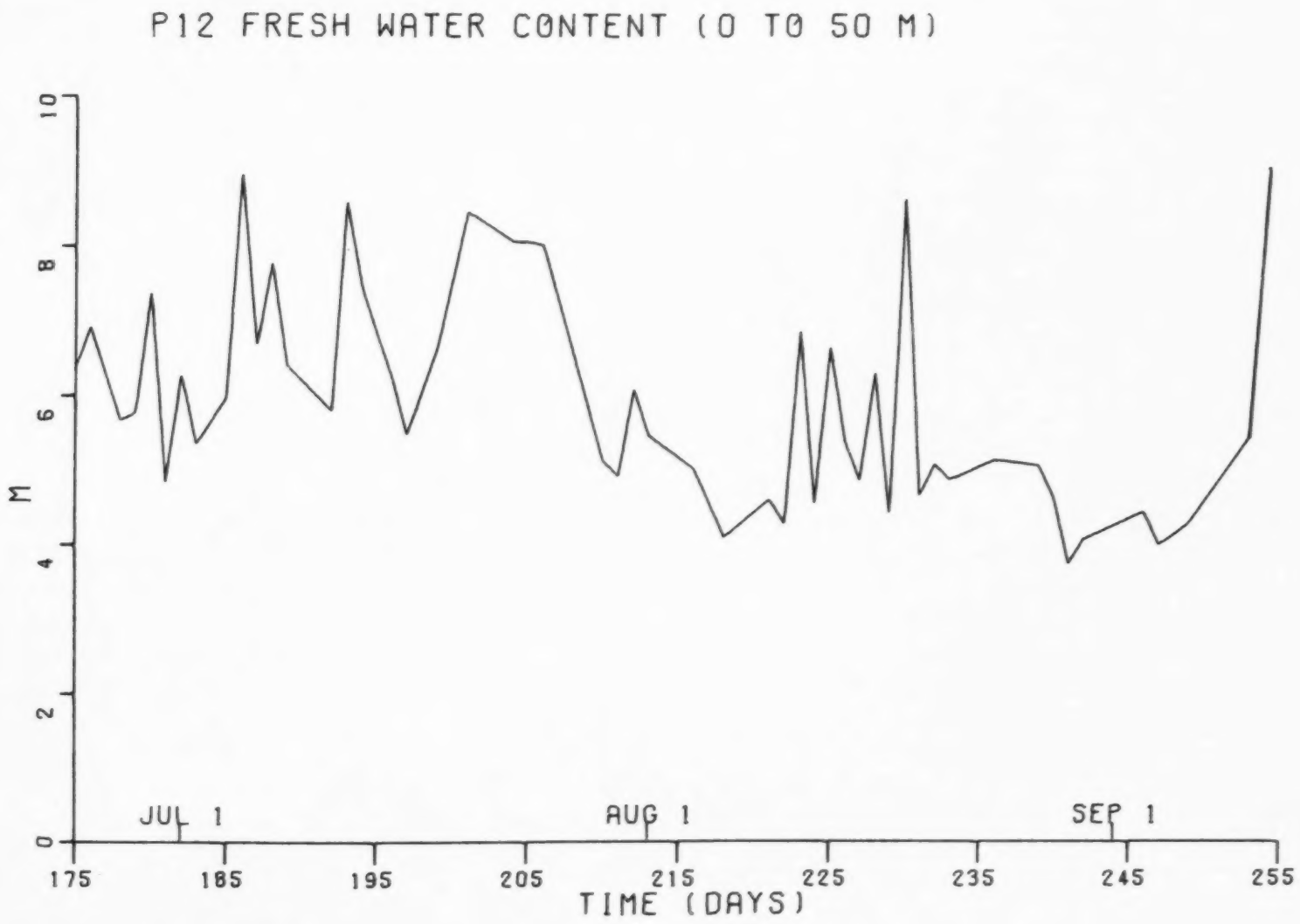
P12 FRESH WATER CONTENT (0 TO 50 M)
M
0
2
4
6
8
10
JUL 1
AUG 1
SEP 1
175
185
195
205
215
225
235
245
255
TIME (DAYS)

Figure B12

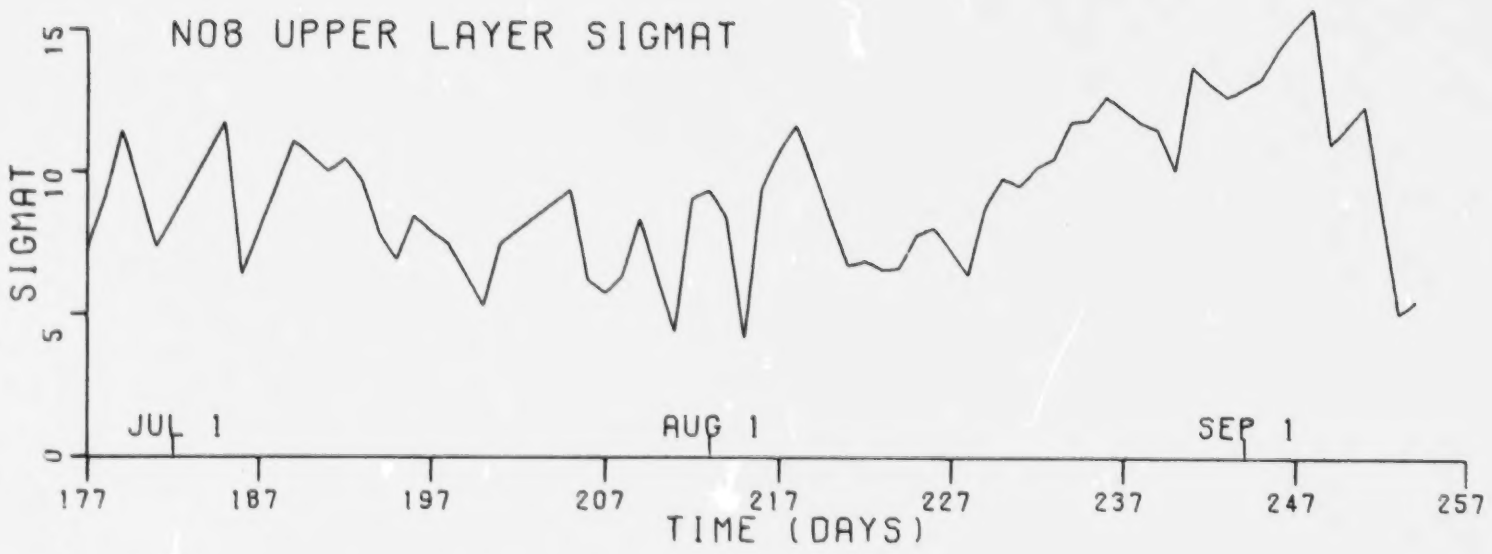
NOB UPPER LAYER SIGMAT
SIGMAT
15
10
5
0
JUL 1
AUG 1
SEP 1
177
187
197
207
217
227
237
247
257
TIME (DAYS)

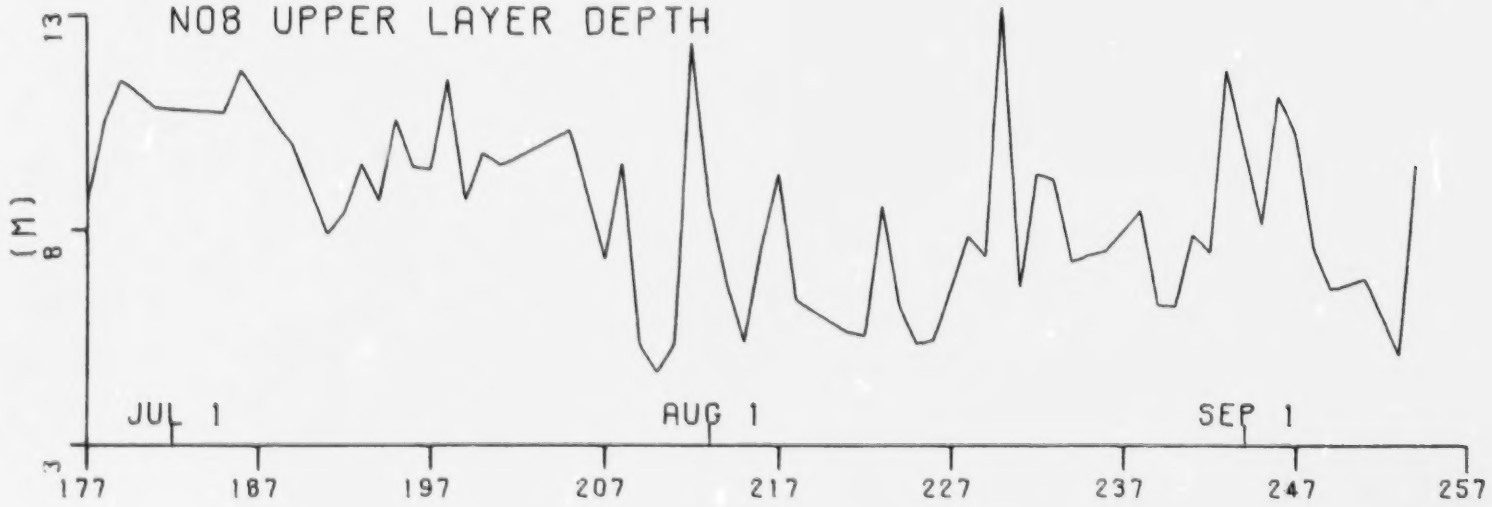
NOB UPPER LAYER DEPTH
(M)
13
8
3
JUL 1
AUG 1
SEP 1
177
187
197
207
217
227
237
247
257

Figure B13

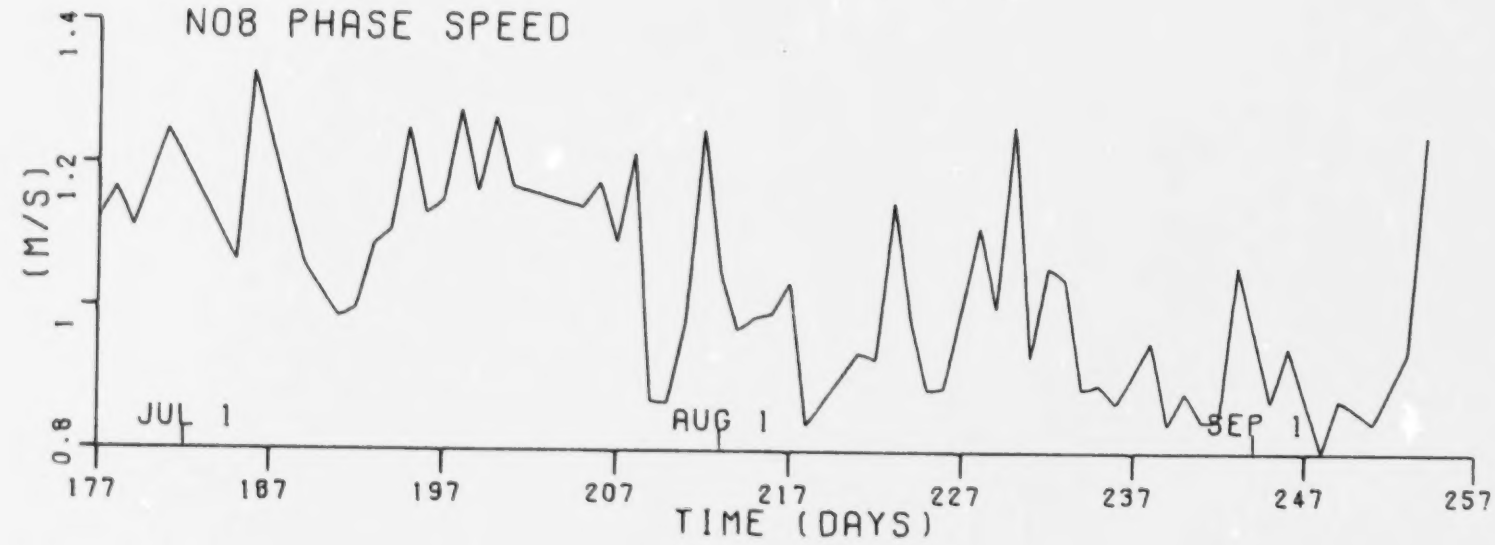
NO8 PHASE SPEED
(M/S)
1.4
1.2
1
0.8
JUL 1
AUG 1
SEP 1
177
187
197
207
217
227
237
247
257
TIME (DAYS)

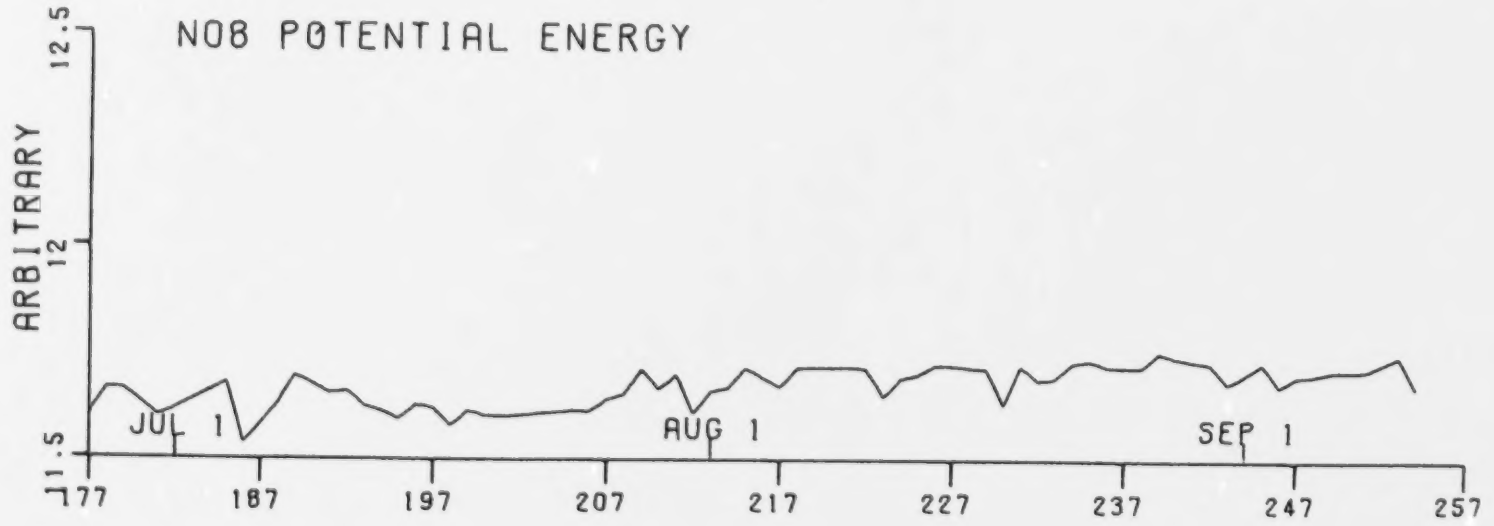
NO8 POTENTIAL ENERGY
ARBITRARY
12.5
12
11.5
JUL 1
AUG 1
SEP 1
177
187
197
207
217
227
237
247
257

Figure B14

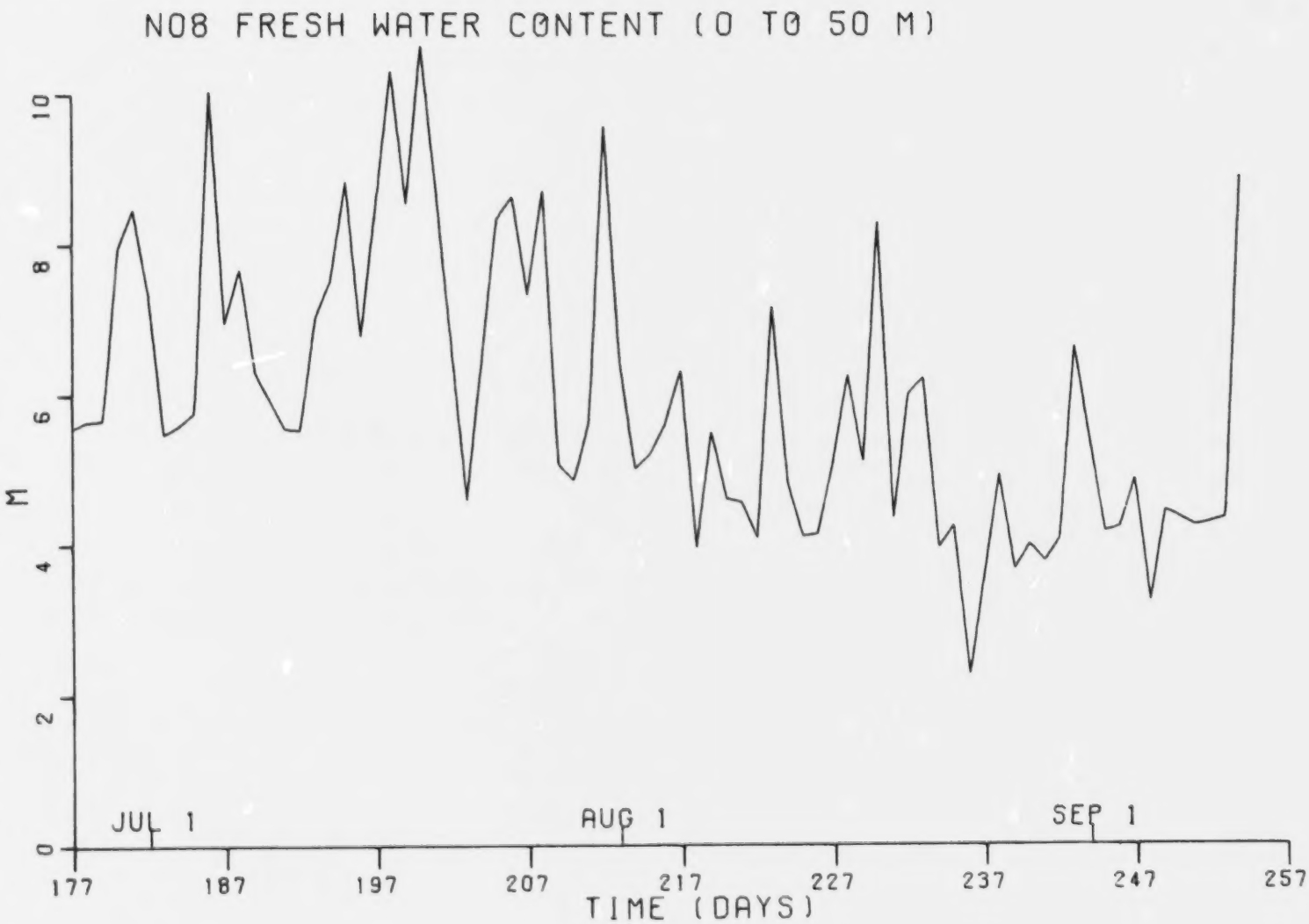
N08 FRESH WATER CONTENT (0 TO 50 M)
M
0
2
4
6
8
10
JUL 1
AUG 1
SEP 1
177
187
197
207
217
227
237
247
257
TIME (DAYS)

Figure B15

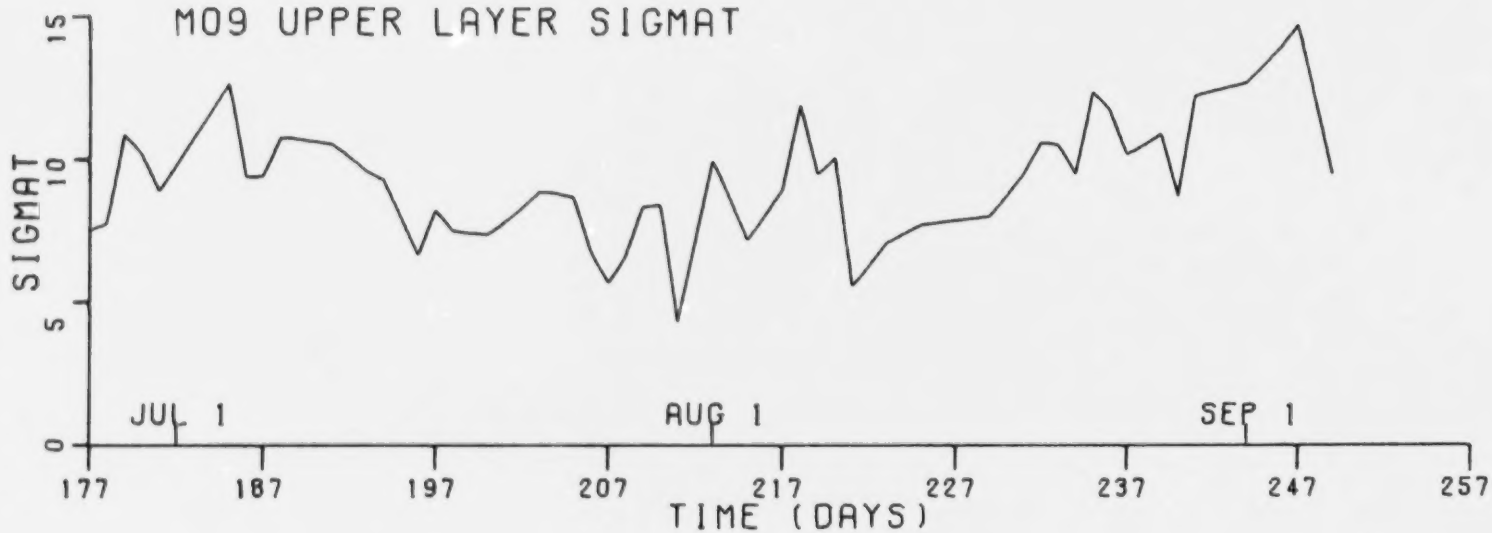
M09 UPPER LAYER SIGMAT
SIGMAT
0
5
10
15
JUL 1
AUG 1
SEP 1
177
187
197
207
217
227
237
247
257
TIME (DAYS)

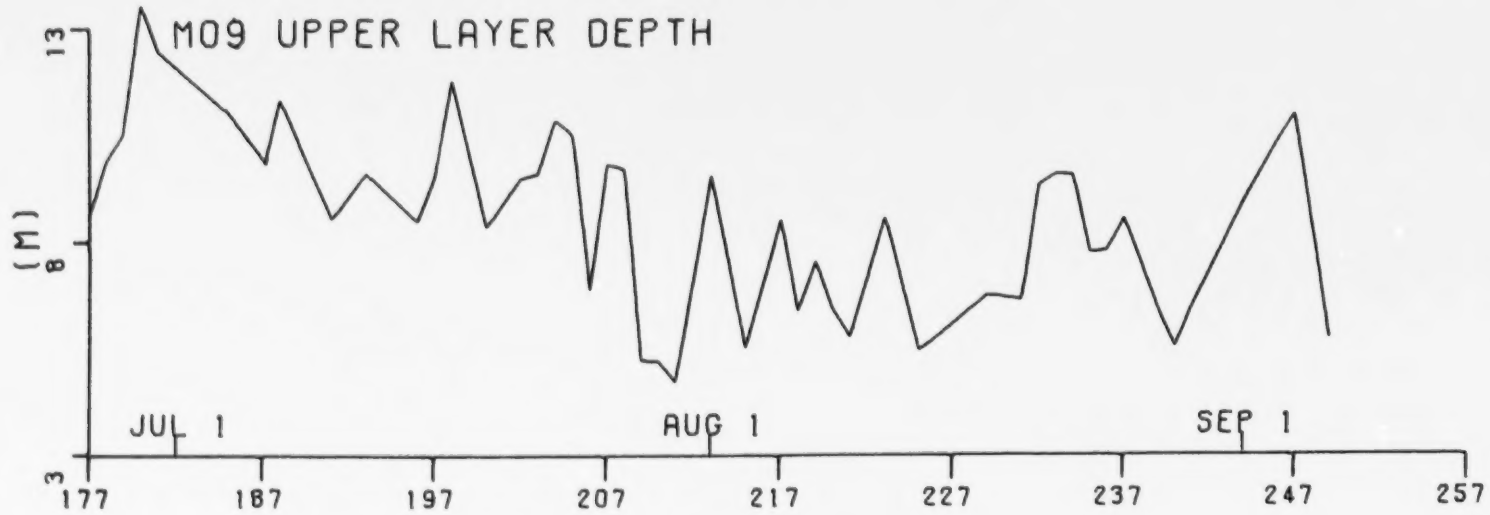
M09 UPPER LAYER DEPTH
(M)
3
8
13
JUL 1
AUG 1
SEP 1
177
187
197
207
217
227
237
247
257

Figure B16

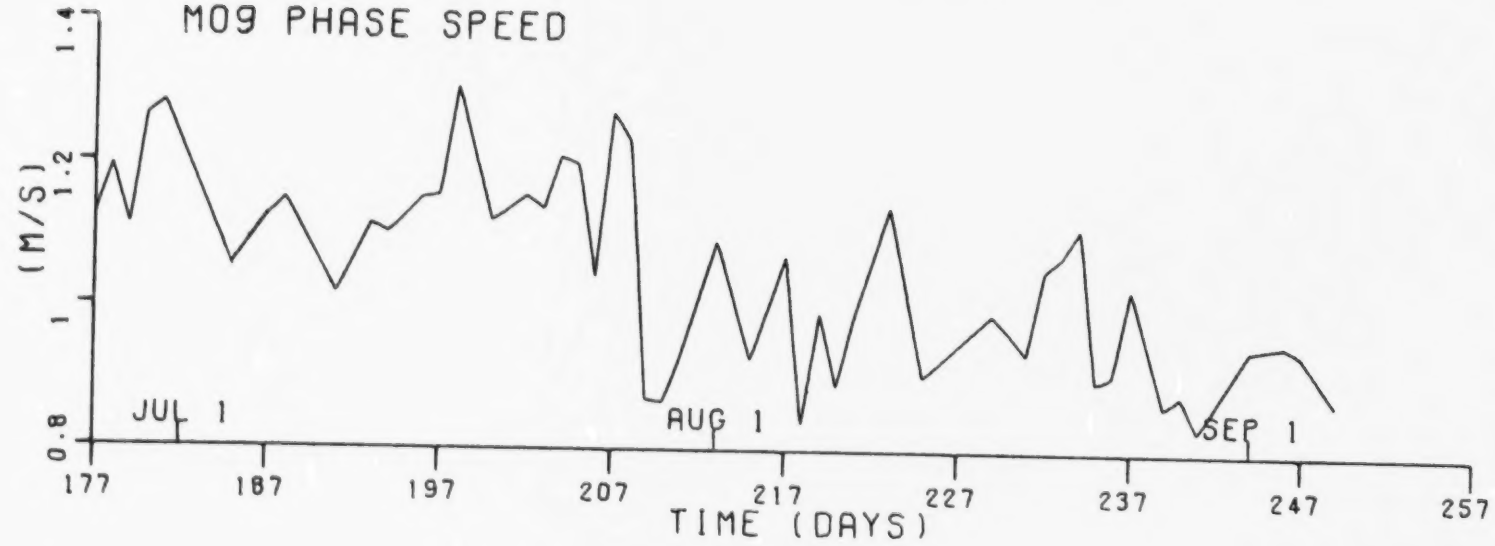
M09 PHASE SPEED
(M/S)
1.4
1.2
1
0.8
JUL 1
AUG 1
SEP 1
177
187
197
207
217
227
237
247
257
TIME (DAYS)

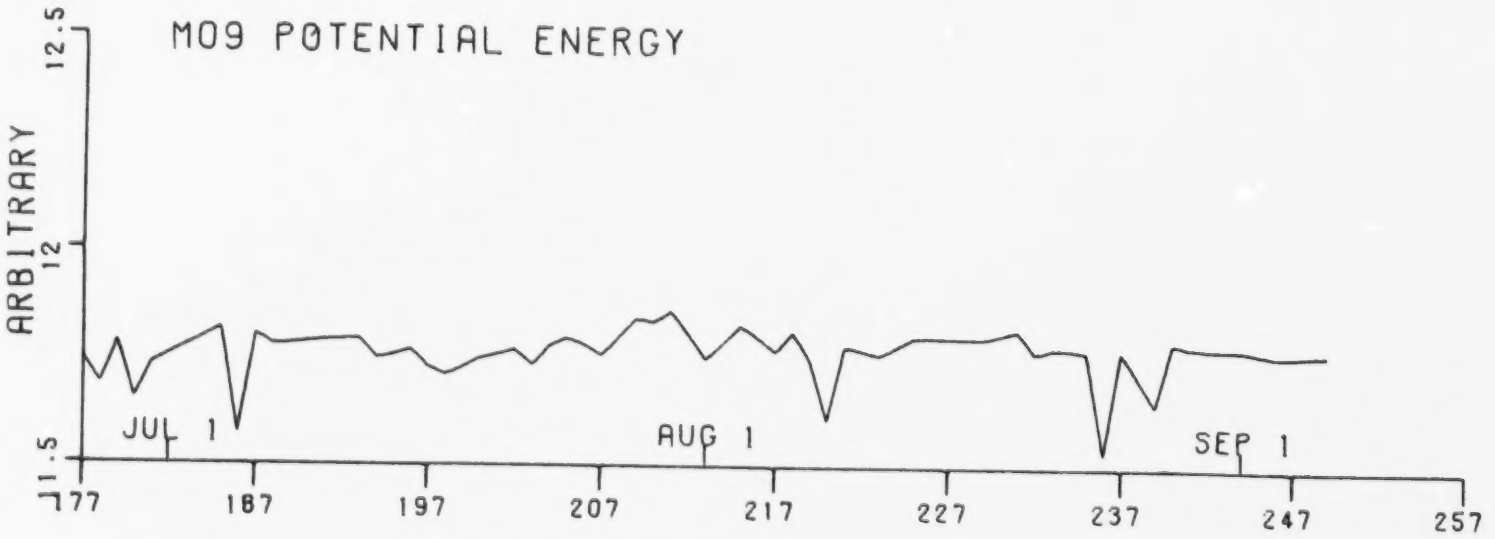
M09 POTENTIAL ENERGY
ARBITRARY
12.5
12
11.5
JUL 1
AUG 1
SEP 1
177
187
197
207
217
227
237
247
257

Figure B17

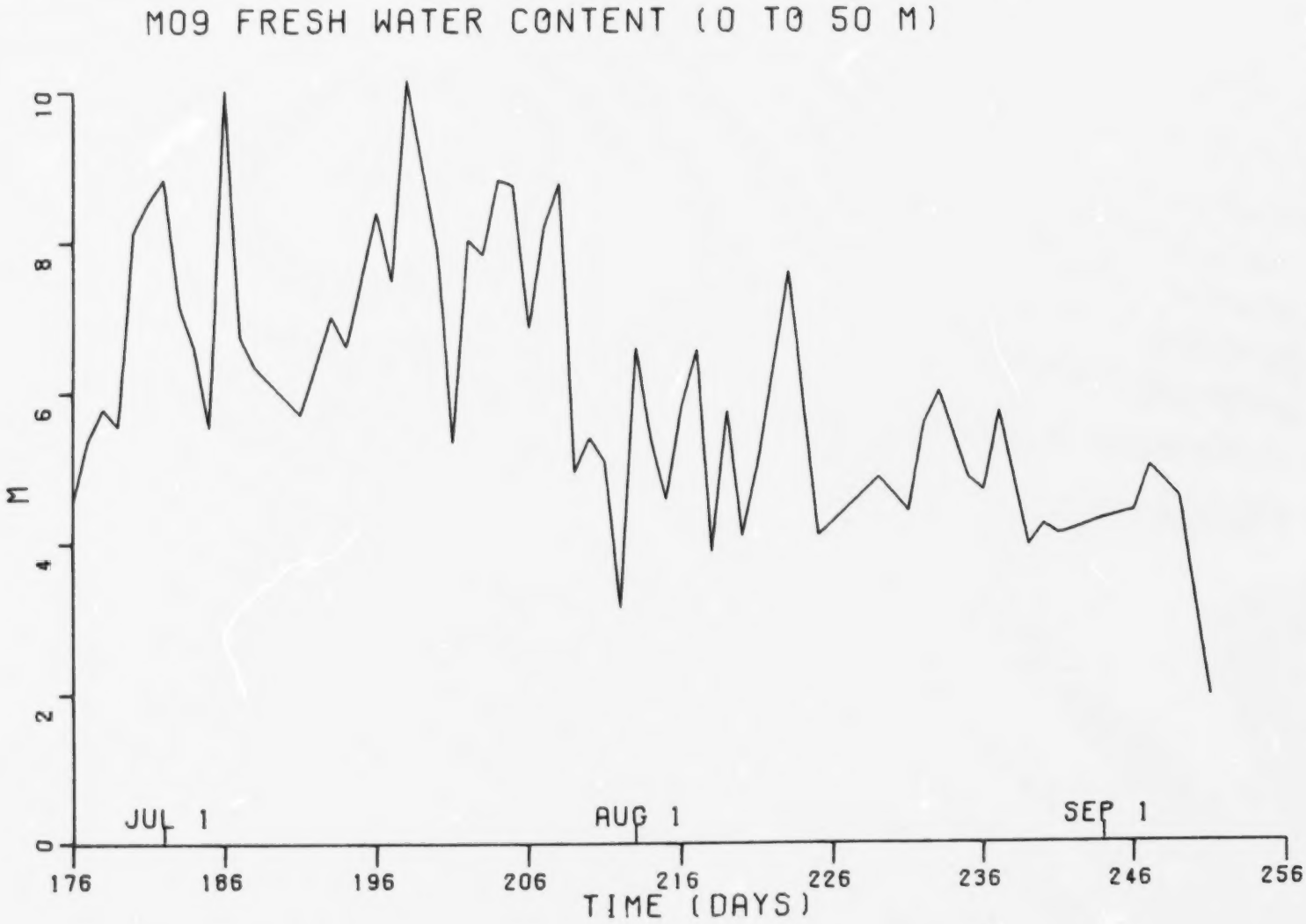
M09 FRESH WATER CONTENT (0 TO 50 M)
M
0
2
4
6
8
10
JUL 1
AUG 1
SEP 1
176
186
196
206
216
226
236
246
256
TIME (DAYS)

Figure B18

APPENDIX C

Twenty five hour time series plots of FWC (0 to 50m) from station F06, September 1, 1982 (Figure C1) and September 2, 1982 (Figure C2).

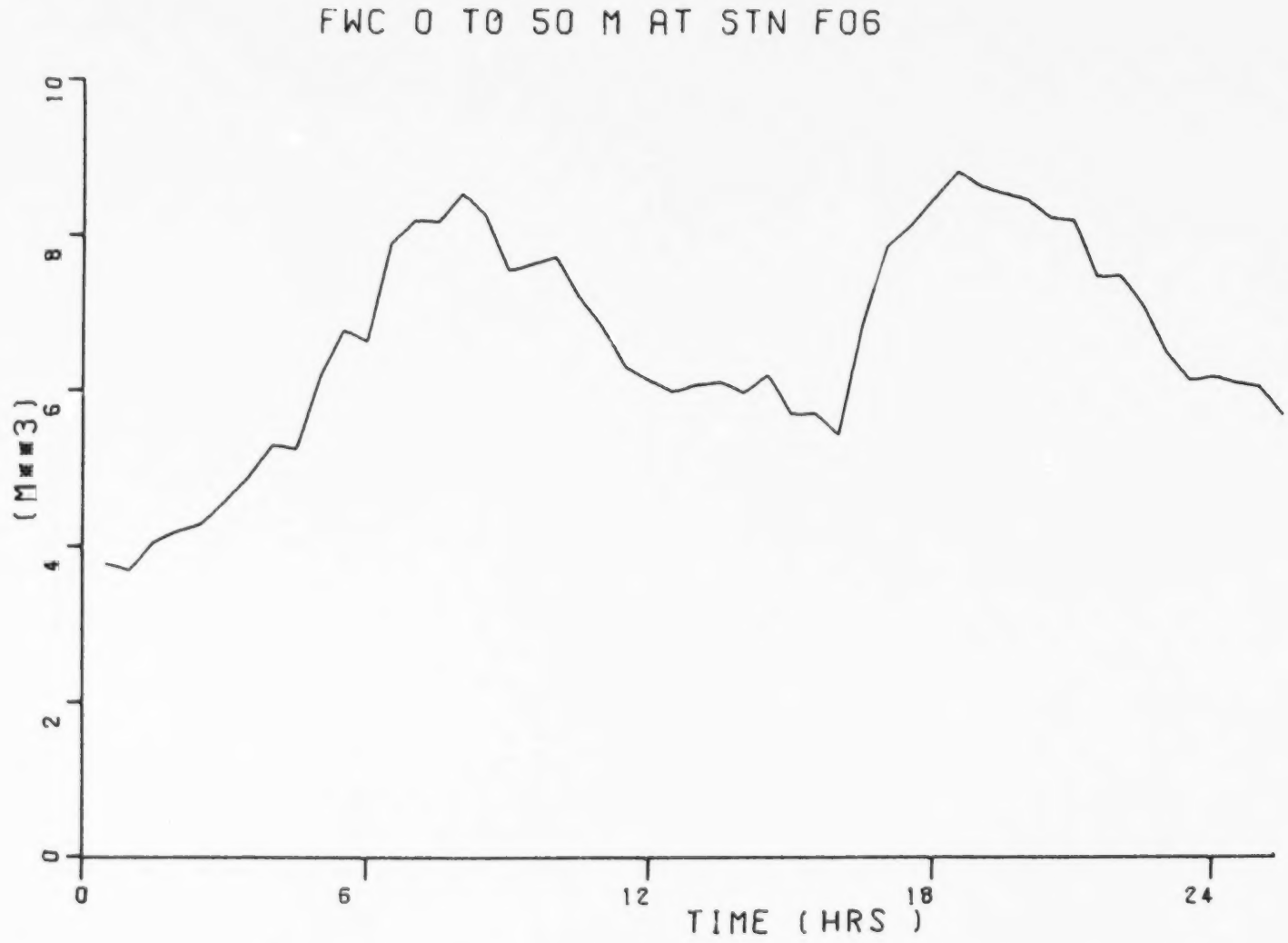

Figure C1. Twenty five hour time series plot of FWC at station F06, September 1, 1982.

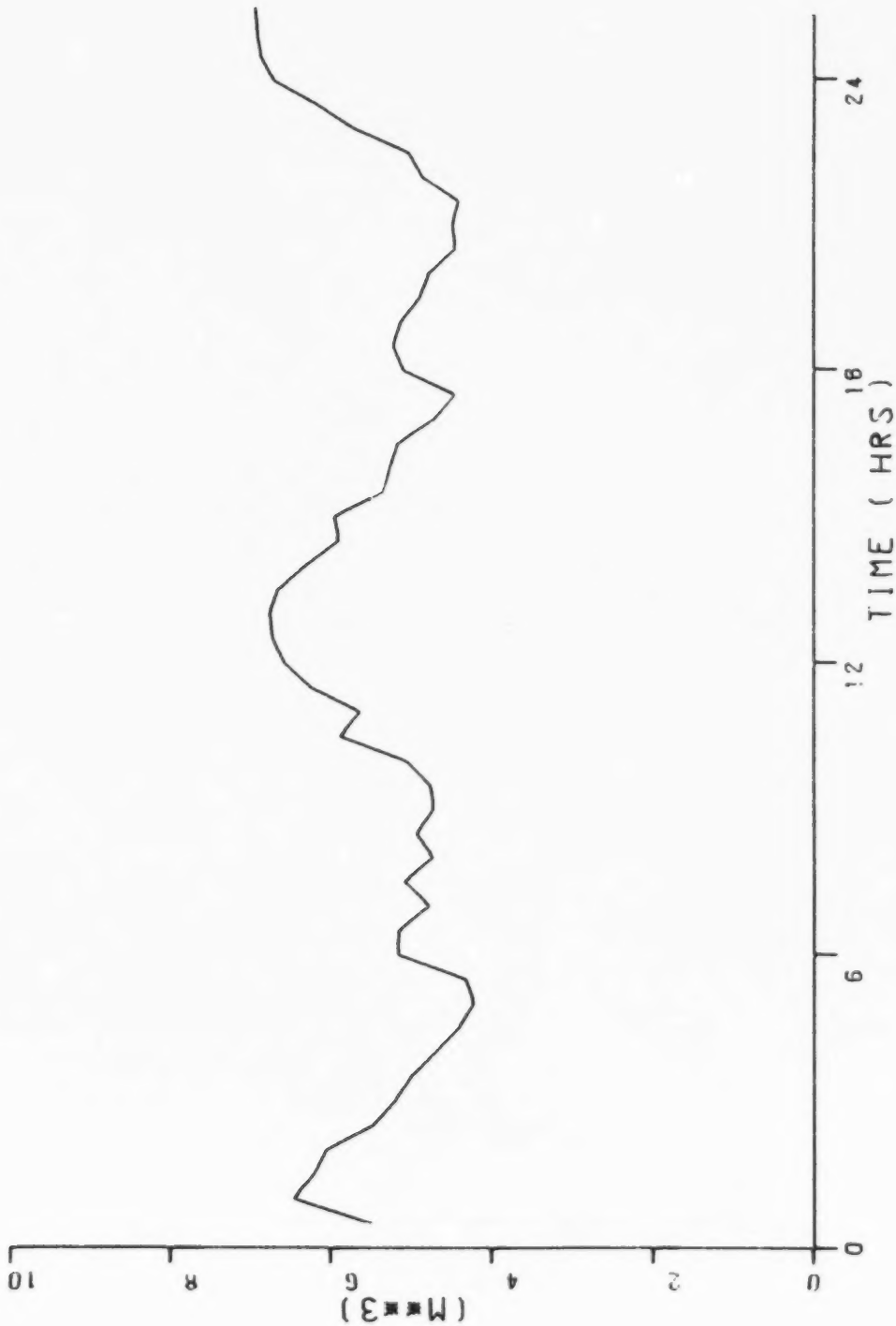

Figure C2. Twenty five hour time series plot of FWC at station W65, September 2, 1982.

APPENDIX D

Cross spectra between Q19 and N08, Q19 and 013, and 013 and N08 for FWC and upper layer depth (Figure D1), and for upper layer density and first mode internal wave speed (Figure D2). Coherence squared estimates are joined by solid lines, phase estimates are represented by "⊙" and the horizontal dashed line is the level of significance at 95%.

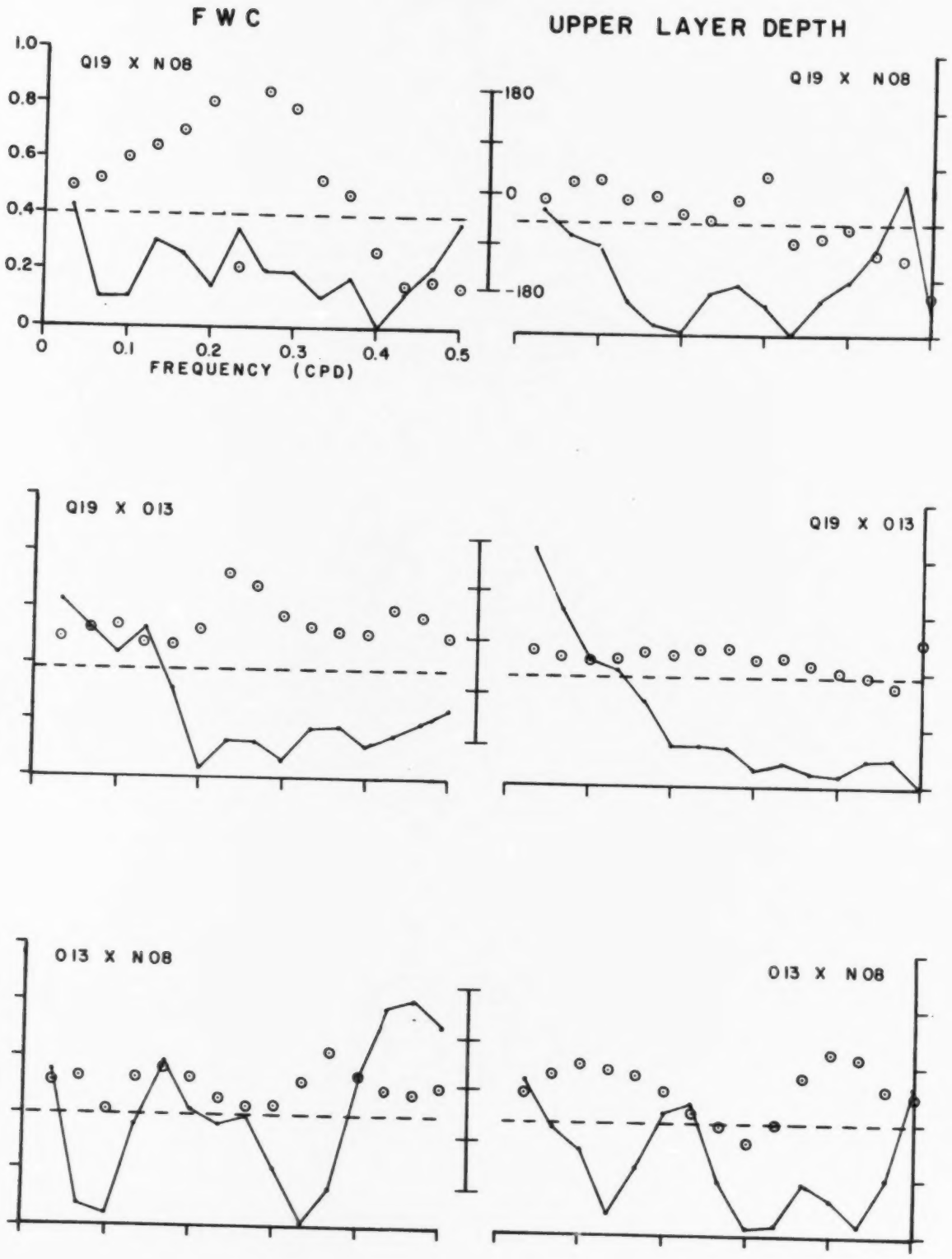
F W C
UPPER LAYER DEPTH
Q19 X N08
Q19 X N08
1.0
0.8
0.6
0.4
0.2
0
180
0
-180
0
0.1
0.2
0.3
0.4
0.5
FREQUENCY (CPD)
Q19 X 013
Q19 X 013
013 X N08
013 X N08

Figure D1

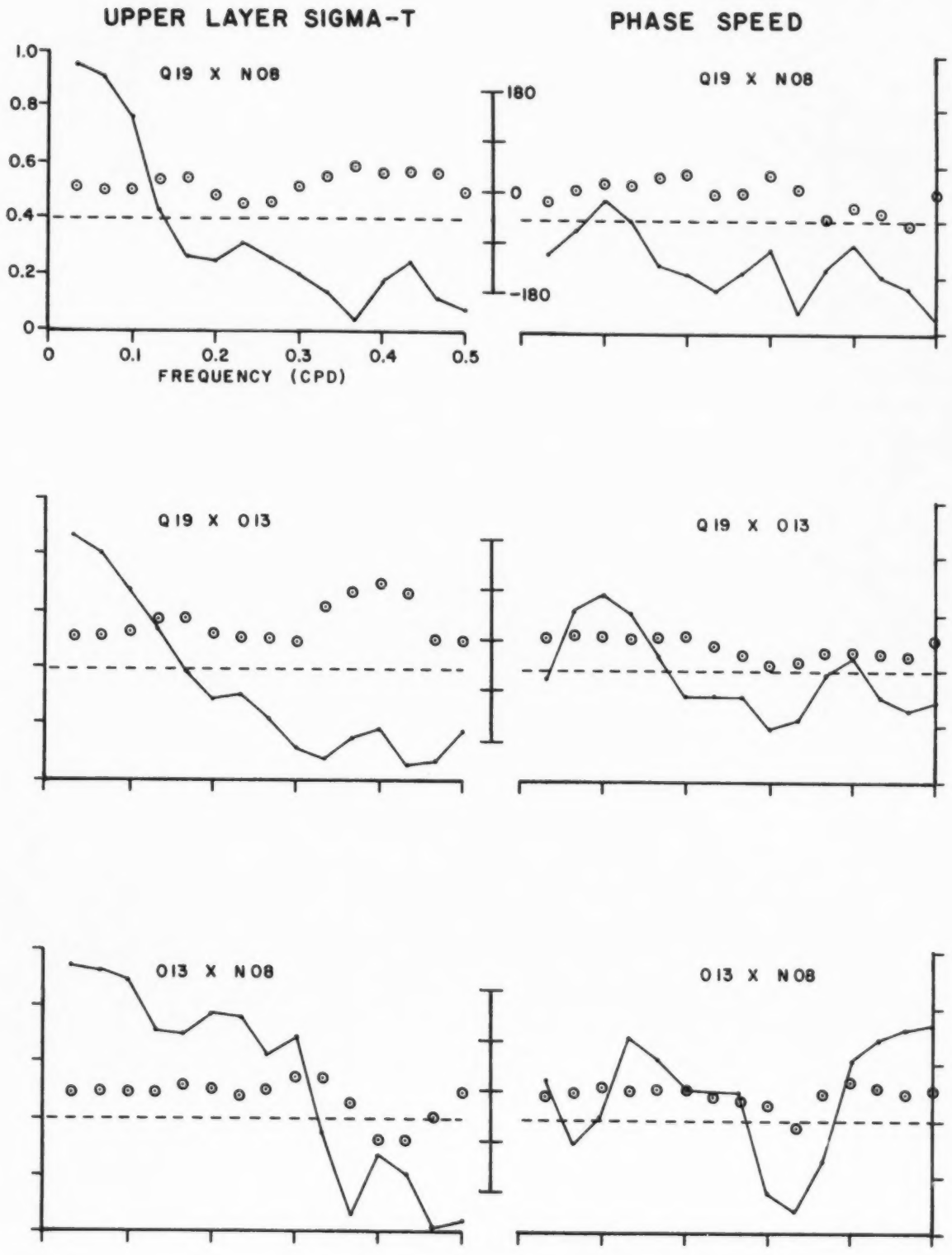
UPPER LAYER SIGMA-T
PHASE SPEED
Q19 X N08
Q19 X N08
1.0
0.8
0.6
0.4
0.2
0
180
0
-180
0
0.1
0.2
0.3
0.4
0.5
FREQUENCY (CPD)
Q19 X 013
Q19 X 013
013 X N08
013 X N08

Figure D2

APPENDIX E

Temperature-salinity diagrams for station Q19 from June 24 to September 6, 1981 at about 10 day intervals. Figures E1 to E8.

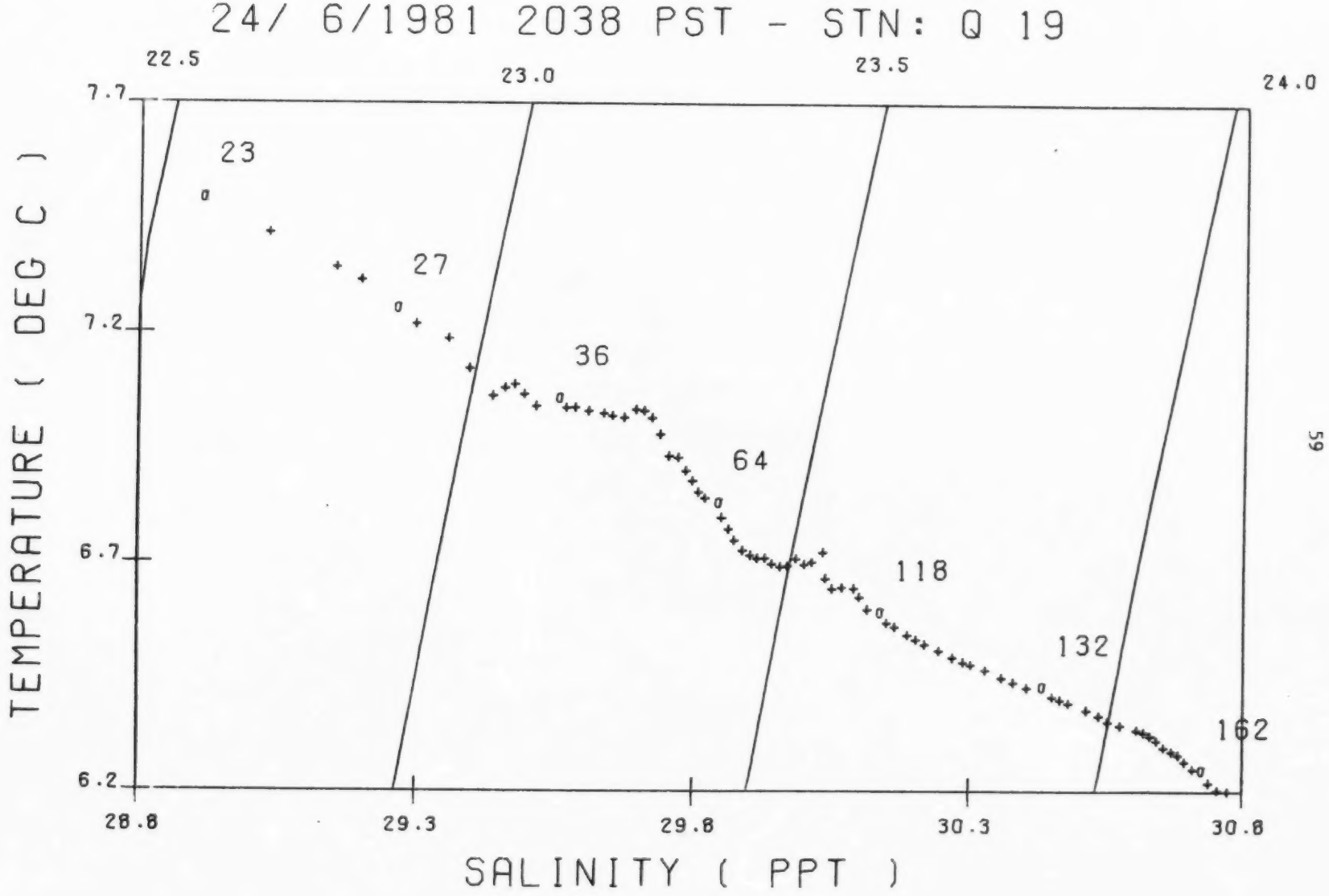
24/ 6/1981 2038 PST - STN: Q 19
22.5
23.0
23.5
24.0
7.7
7.2
6.7
6.2
TEMPERATURE (DEG C)
23
27
36
64
118
132
162
28.8
29.3
29.8
30.3
30.8
SALINITY (PPT)

Figure E1

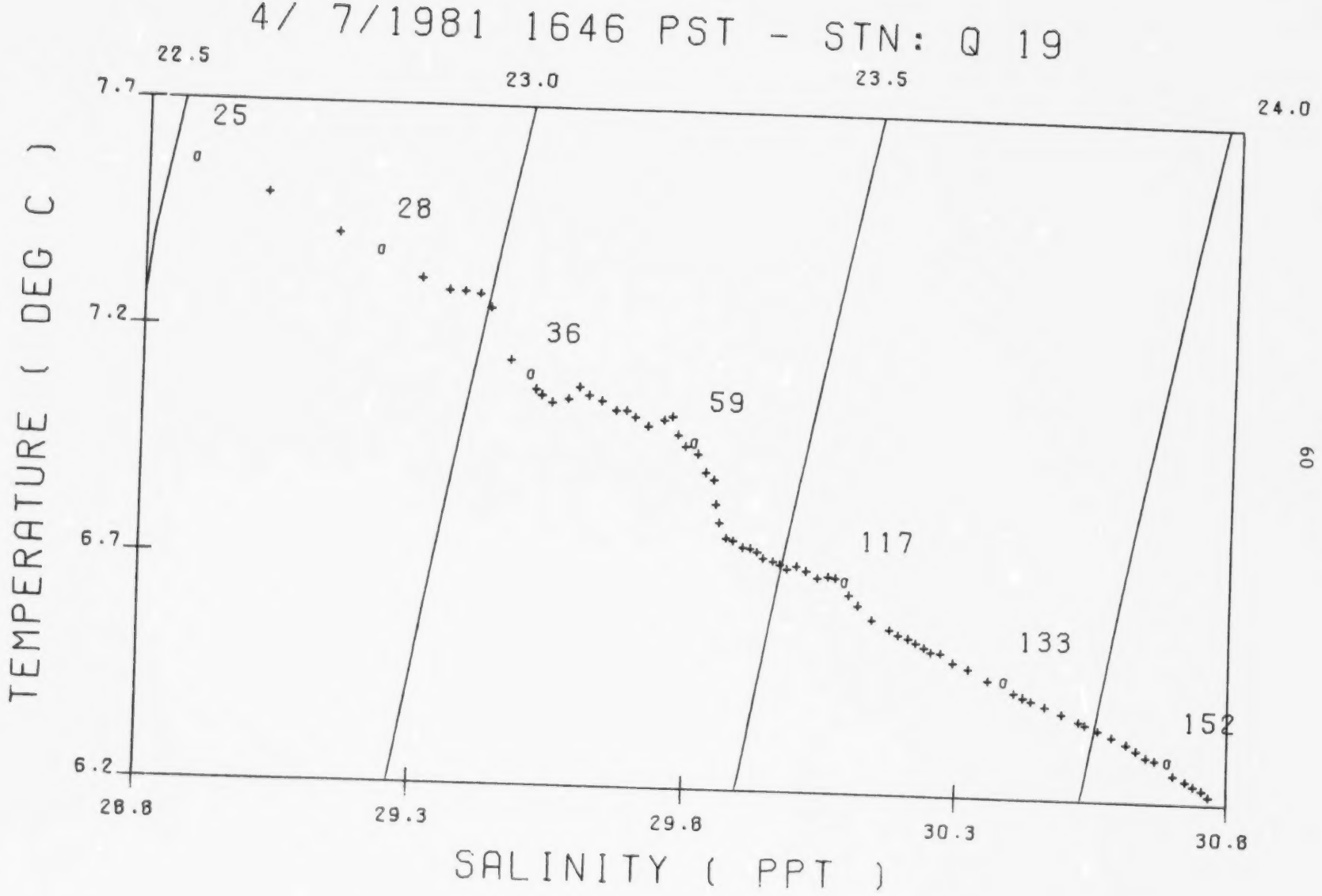
4/ 7/1981 1646 PST - STN: Q 19
22.5
23.0
23.5
24.0
7.7
7.2
6.7
6.2
25
28
36
59
117
133
152
TEMPERATURE (DEG C)
28.8
29.3
29.8
30.3
30.8
SALINITY (PPT)

Figure E2

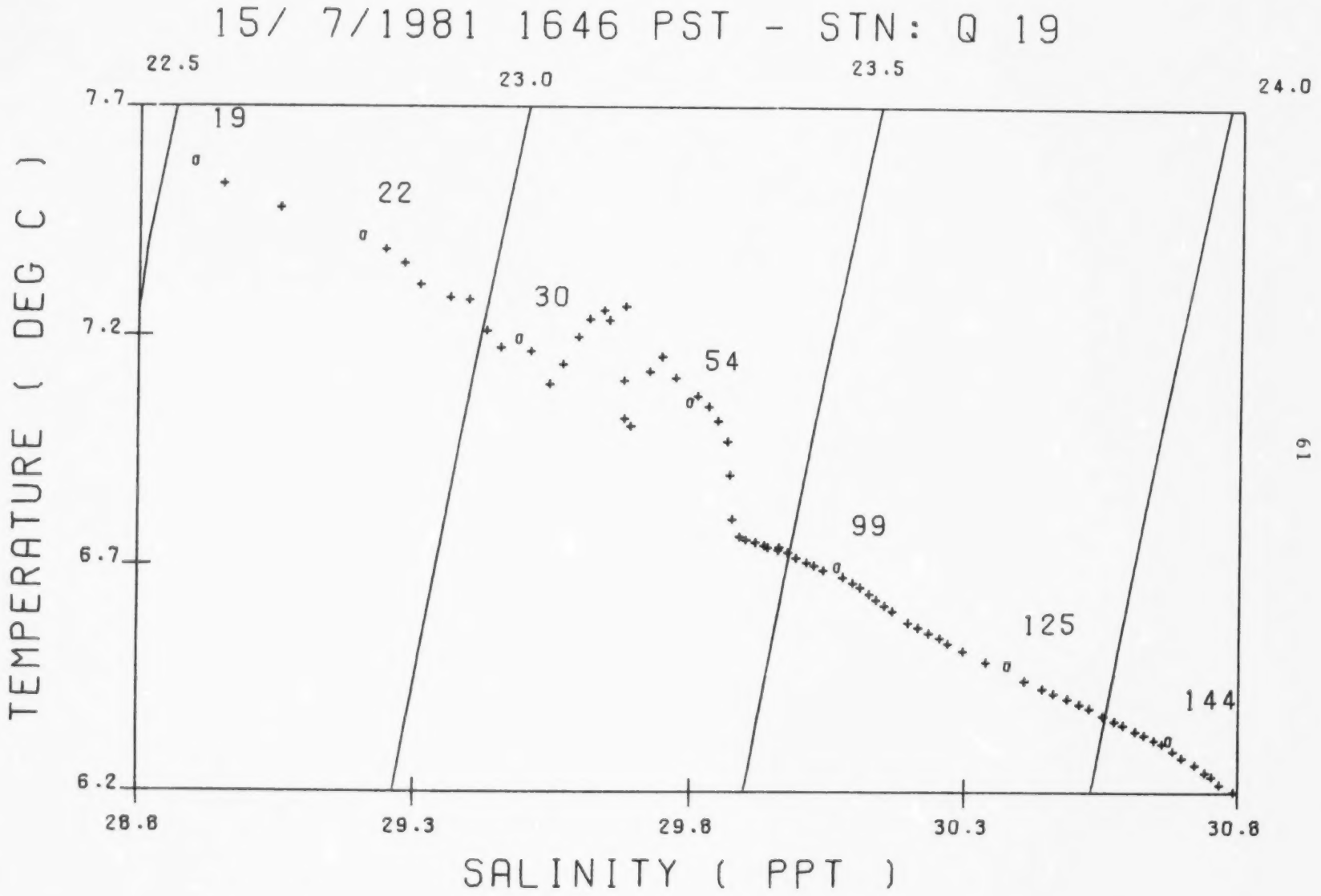
15/ 7/1981 1646 PST - STN: Q 19
22.5
23.0
23.5
24.0
7.7
7.2
6.7
6.2
19
22
30
54
99
125
144
TEMPERATURE (DEG C)
28.8
29.3
29.8
30.3
30.8
SALINITY (PPT)

Figure E3

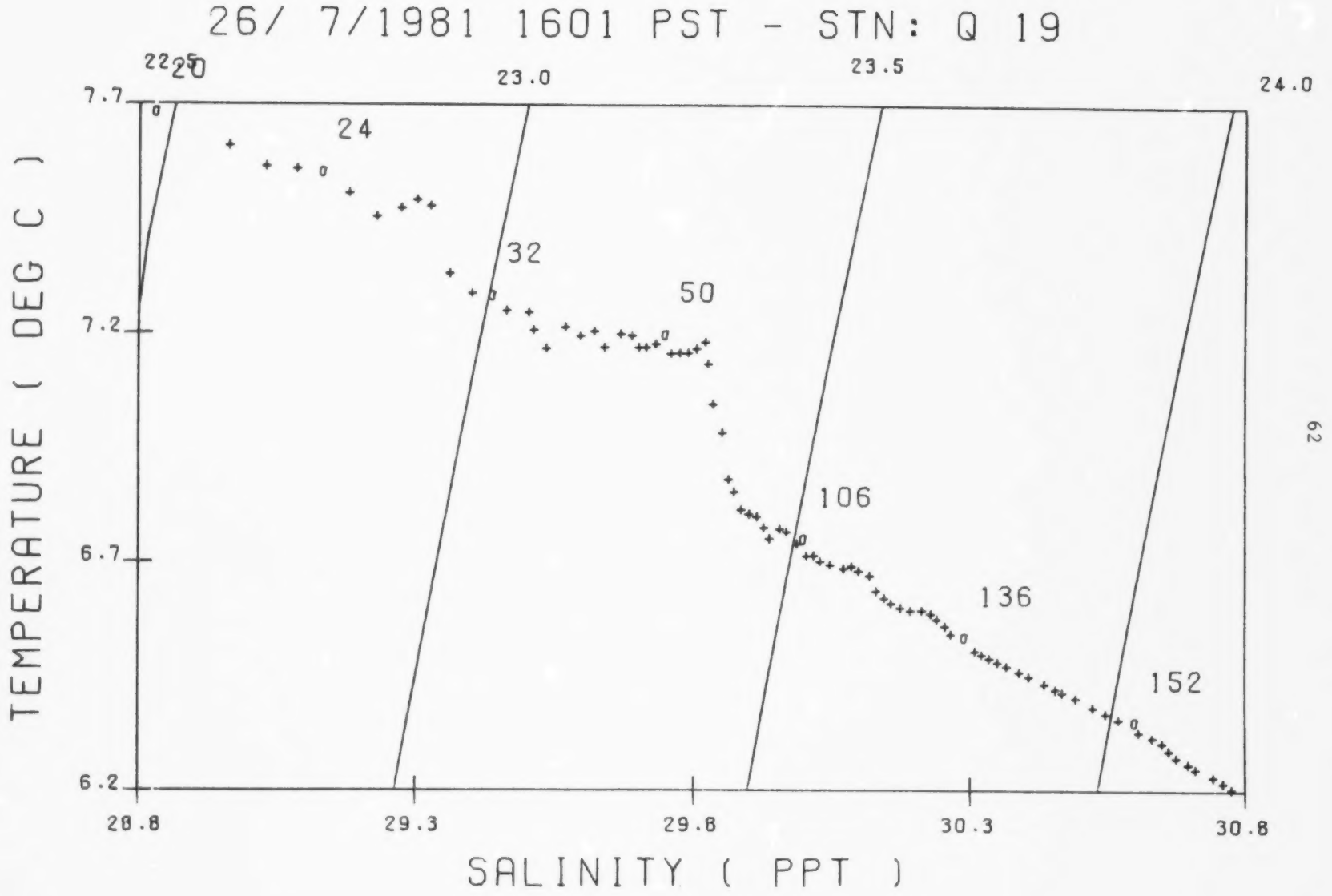
26/ 7/1981 1601 PST - STN: Q 19
22.5
23.0
23.5
24.0
7.7
7.2
6.7
6.2
TEMPERATURE (DEG C)
20
24
32
50
106
136
152
28.8
29.3
29.8
30.3
30.8
SALINITY (PPT)

Figure E4

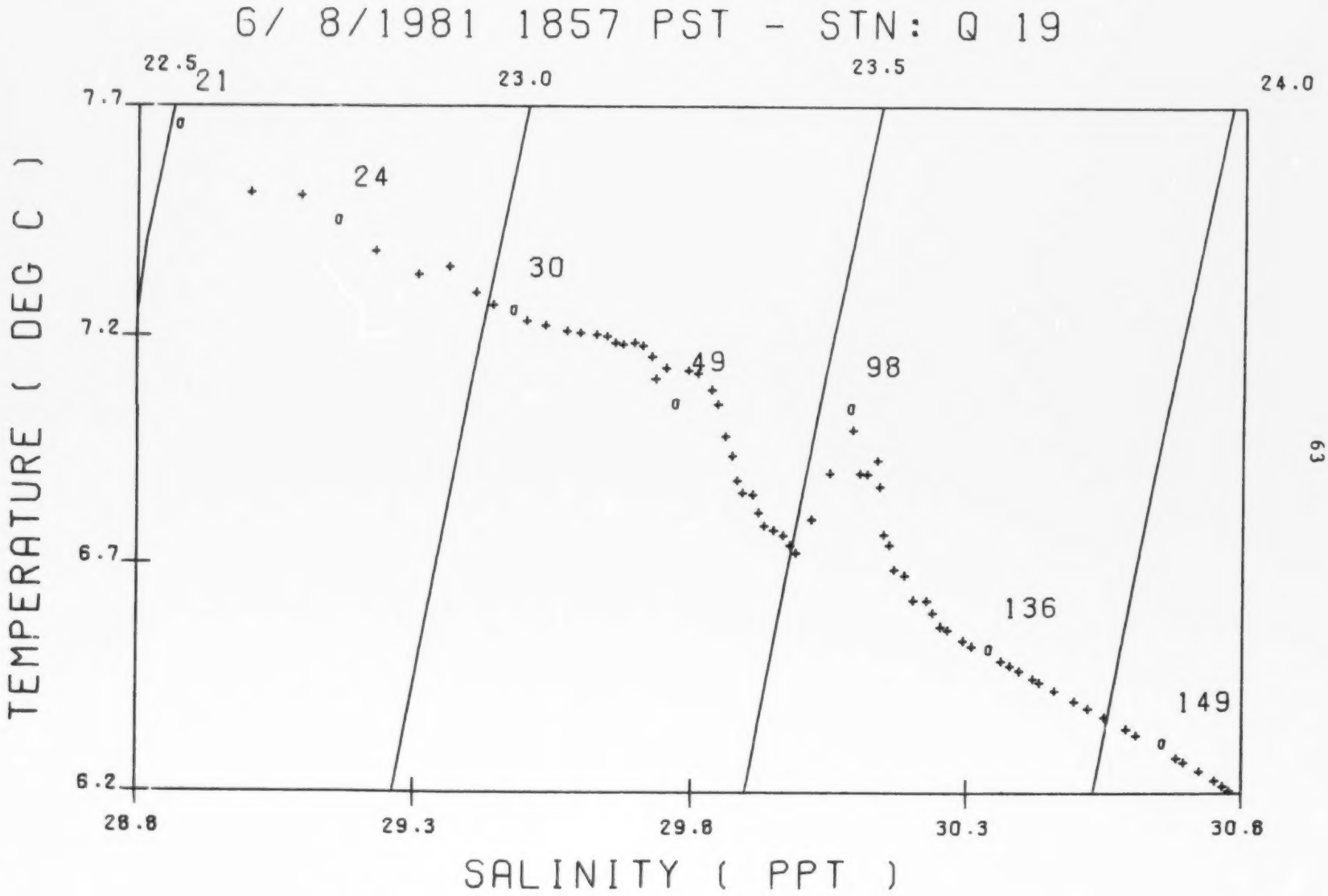
6/ 8/1981 1857 PST - STN: Q 19
22.5
23.0
23.5
24.0
21
24
30
49
98
136
149
7.7
7.2
6.7
6.2
TEMPERATURE (DEG C)
28.8
29.3
29.8
30.3
30.8
SALINITY (PPT)

Figure E5

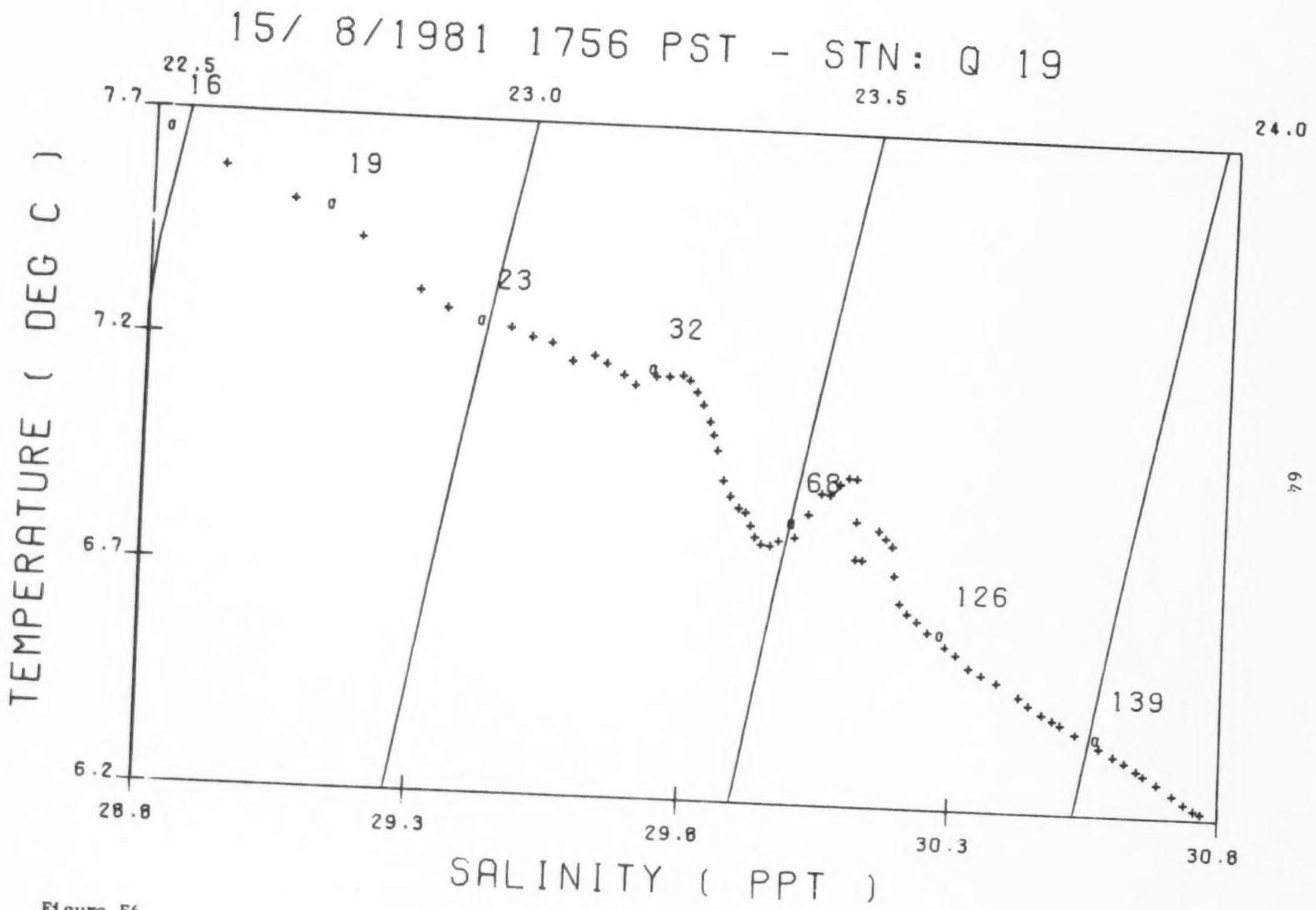
15/ 8/1981 1756 PST - STN: Q 19
22.5
16
7.7
23.0
23.5
24.0
19
23
7.2
32
68
6.7
126
139
6.2
28.8
29.3
29.8
30.3
30.8
TEMPERATURE (DEG C)
SALINITY (PPT)

Figure E6

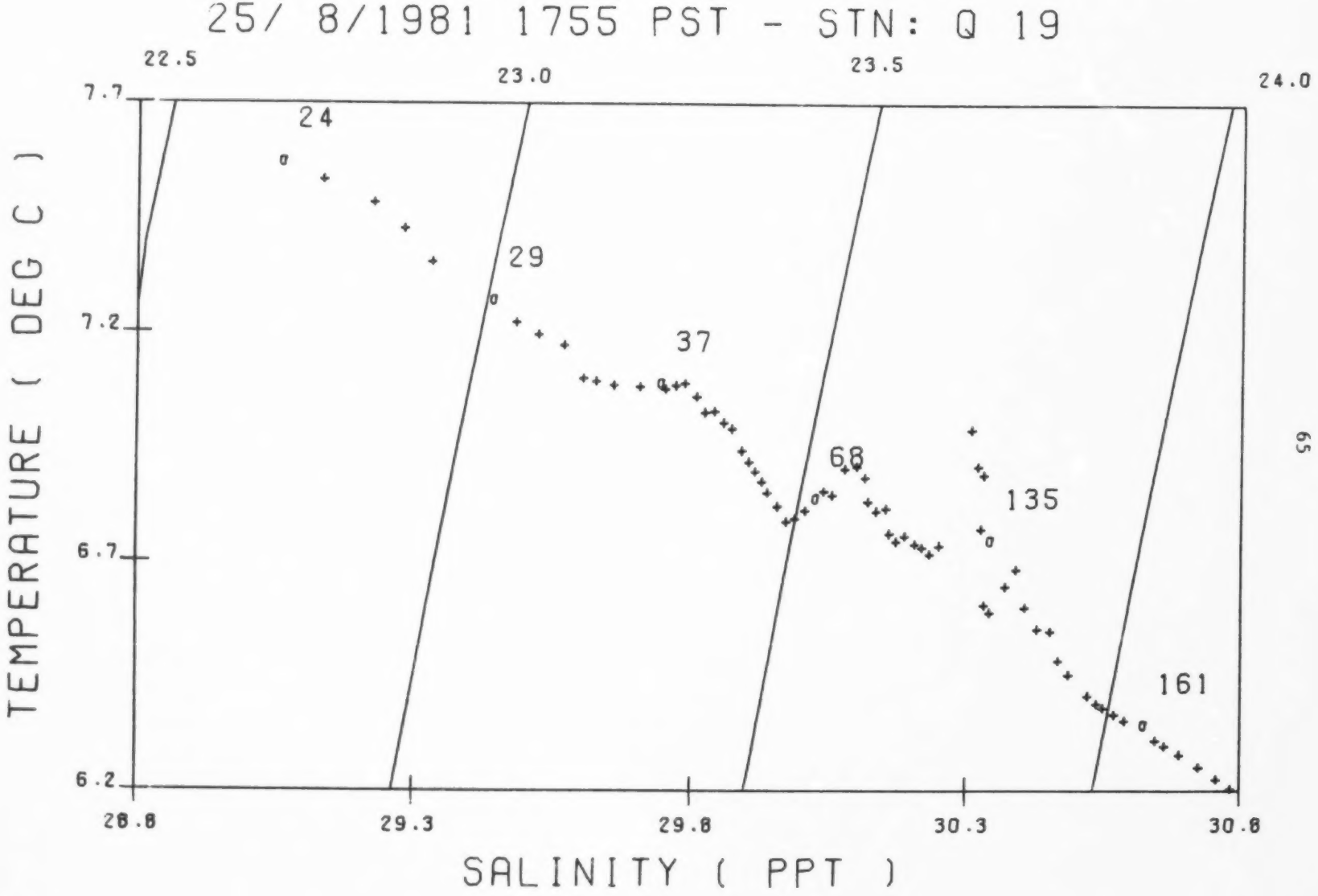
25/ 8/1981 1755 PST - STN: Q 19
22.5
23.0
23.5
24.0
7.7
7.2
6.7
6.2
24
29
37
68
135
161
TEMPERATURE (DEG C)
28.8
29.3
29.8
30.3
30.8
SALINITY (PPT)

Figure E7

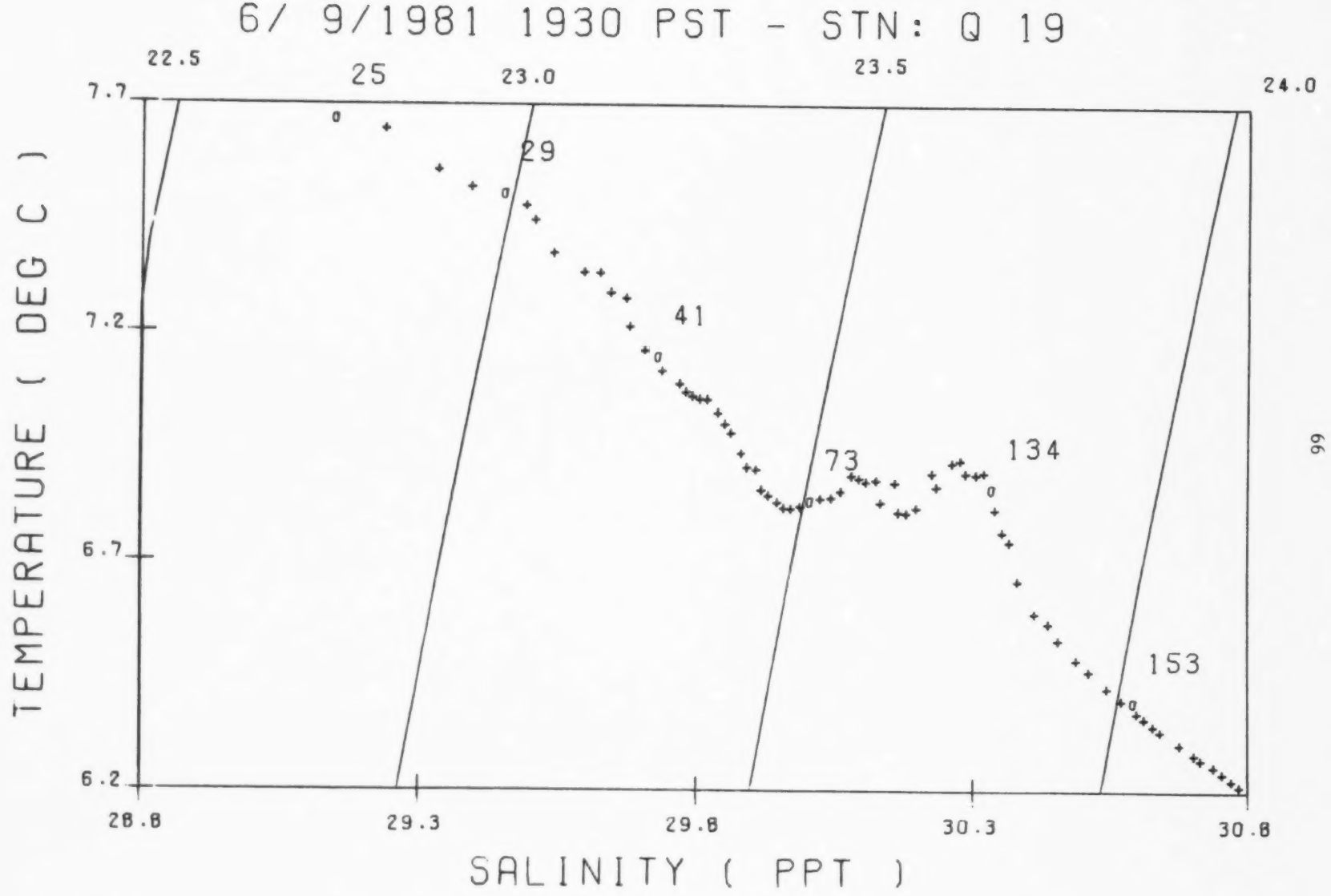
6/ 9/1981 1930 PST - STN: Q 19
22.5
25
23.0
23.5
24.0
7.7
7.2
6.7
6.2
29
41
73
134
153
TEMPERATURE (DEG C)
28.8
29.3
29.8
30.3
30.8
SALINITY (PPT)

Figure E8

POOR

QUALITY

ORIGINAL